Phenotypic and Molecular Characterization of Mice Deficient in Protein Kinase A Regulatory Subunit Type 1A (*Prkar1a*) and Catalytic Subunit A (*Prkaca*)

TSANG, Kit Man

A Thesis Submitted in Partial Fulfillment
of the Requirements for the Degree of
Doctor of Philosophy

in

Biochemistry (Medicine)

The Chinese University of Hong Kong

June 2010

Thesis/ Assessment Committee

Professor Siu-Kai Kong (Chair)
Professor Kwok-Pui Fung (CUHK Thesis Supervisor)
Dr. Constantine A. Stratakis (NIH Thesis Supervisor)
Professor Kwok-Nam Leung (Committee Member)

Abstract

A population of stromal cells that retains osteogenic capacity in adult bone (adult bone stromal cells or aBSCs) exists and is under intense investigation in relation to osteogenesis and relevant pathology. aBSCs may be different from their embryonic or neonatal counterparts, and are influenced by species-/age-specific and other factors. Mice heterozygous for a null allele of *prkar1a* (*Prkar1a*$^{+/-}$), a gene encoding for cyclic adenosine mono-phosphate (cAMP)-dependent regulatory subunit of protein kinase A (PKA), developed bone lesions that resembled fibrous dysplasia (FD) originated from cAMP-responsive osteogenic cells. *Prkar1a*$^{+/-}$ mice were crossed with mice heterozygous for catalytic subunit Cα (*Prkaca*$^{+/-}$), the main PKA activity-mediating molecule and generated mouse model with double heterozygosity for *prkar1a* and *prkaca* (*Prkar1a*$^{+/-}$*Prkaca*$^{+/-}$). Unexpectedly, *Prkar1a*$^{+/-}$*Prkaca*$^{+/-}$ mice developed a large number of osseous lesions starting at 2-3 months of age that varied from the rare chondromas in the long bones and the ubiquitous osteochondrodysplasia of tail vertebral bodies to the occasional sarcoma in older animals. Cells from these lesions were fibroblast- and FD-like, and almost always originated from an area proximal to the growth plate and adjacent to endosteal surface of the periosteum; they expanded gradually in the bone marrow space. These cells expressed osteogenic cell markers, showed higher PKA activity that was mostly type II (PKA-II) and display an alternate pattern of catalytic subunit expression, and surprisingly possessed higher cAMP levels. In addition, markers of bone synthesis and lysis were increased. Gene expression profiling not only confirmed an early (progenitor) osteoblastic nature for these cells but

also showed a signature that was indicative of mesenchymal-to-epithelial (MET) transition and increased *Wnt* signaling, particularly the *brachyury* expression. These studies show that a specific subpopulation of aBSCs can be stimulated in adult bone by PKA-II and altered Cα activity, generating the only available germline mutant mouse model of a disorder that has similarities to human FD. Along with previous data, these studies also suggest that the effects of cAMP signaling on osteogenesis and stromal cell maintenance and proliferation in mice are age-, bone-, site- but also PKA-type and catalytic subunit-specific.

Parts of the work have been published in Proceedings of the National Academy of Sciences of the United States of America 2010; 107(19):8683-8.

摘要

有成骨能力的基質細胞存在於成人骨骼中， 它們的功用及病變原因正是科學家們努力研究的範疇。 成人骨骼基質細胞 (aBSCs) 跟胚胎或新生的的幹細胞不同， 它們受到物種、 年齡、 人體結構上的位置等等所影響。 近年研究發現帶有雜合型 ***Prkar1a*** 轉基因老鼠 (***Prkar1a***$^{+/-}$)產生骨病變。 *Prkar1a* 基因編碼出蛋白激酶 A(Protein Kinase A) 的調節單位 (regulatory subunit) A， 它是一磷酸環腺(cAMP)的主要感受器， 亦是調節蛋白激酶 A 活性的主要單位。 這種骨病變源於對一磷酸環腺有反應的基質細胞， 而且病變組織跟骨纖維性結構不良症(Fibrous Dysplasia)非常相似。 為了探討基質細胞在缺少 ***prkar1a*** 而產生骨病變的過程及機制， 我們將雜合型 ***Prkar1a*** 轉基因老鼠與雜合型 ***Prkaca*** 轉基因老鼠 (***Prkaca***$^{+/-}$)交配， 製造出雙雜合型 ***prkar1a/prkaca*** 轉基因老鼠(***Prkar1a***$^{+/-}$ ***Prkaca***$^{+/-}$)。 *Prkaca*基因編碼出蛋白激酶 A 的主要催化亞單位 (catalytic subunit) 。意外地， ***Prkar1a***$^{+/-}$***Prkaca***$^{+/-}$雙雜合型轉基因老鼠相比 *Prkar1a* 轉基因老鼠更早產生骨病變， 大概開始於四個月大的成年老鼠。 在 ***Prkar1a***$^{+/-}$***Prkaca***$^{+/-}$雙雜合型轉基因老鼠身上有不同的骨病變， 包括長骨的軟骨瘤 (chondromas)， 尾椎骨的骨軟骨發育不良症 (osteochondrodysplasia)， 以及間中在年齡較大的老鼠中所發現的惡性毒瘤 (sarcoma)。 在這些骨病變中突變的細胞跟骨纖維性結構不良症中的成纖維細胞 (fibroblasts)相似， 突變的細胞通常源於近生長板

(growth plate) 的位置， 隨著時間突變細胞的數量在骨髓中的空間 (bone marrow space)增加。 這些突變細胞表達骨原細胞 (osteogenic)的標誌， 並擁有較高蛋白激酶 A 第二類型 (PKA-II) 的活性和一磷酸環腺的水平， 骨合成和分解的標誌基因也有所增加。 基因表達分析 (gene expression profiling)證實這些突變細胞帶有成骨細胞的特質， 並表達出間質-上皮轉變 (mesenchymal-to-epithelial transition) 和 Wnt 信號通路增加 (Wnt-signaling)的特徵。 總括而言， 這項研究識別出一種有成骨能力的成人基質細胞。 這些基質細胞受蛋白激酶 A 第二類型的刺激而激生。 另外, 讓我們製造出唯一的種系突變種（germline mutant）老鼠模式帶有跟骨纖維性結構不良症相似的骨病變。 同時， 這項研究也提出一磷酸環腺信號通路 (cAMP signaling)在成骨作用及維持基質細胞成長的效果是受到年齡、 骨種、 人體結構上的位置和蛋白激酶 A 類型的影響。

Acknowledgements

I would like to express my sincere thanks to my supervisors, Dr. Constantine A. Stratakis (NICHD, Bethesda, MD) for his supervision, guidance and advice and Professor Kwok-Pui Fung (CUHK, HK) for his unconditional supports during my PhD study. I am grateful to Dr. Matthew F Starost (DVS, Bethesda, MD), Dr. Pamela Robey (NIDCR, Bethesda, MD) and Dr. Micheal T. Collins (NIDCR, Bethesda, MD) for their kind support and crucial advice in various stages of this project.

I also would like to thank Dr. Sergei Leikin (NICHD, Bethesda, MD) and Dr. Edward L. Mertz (NICHD, Bethesda, MD) for their help in performing Raman microspectroscopy experiment; Dr. Chris Cheadle (John Hopkins University, Baltimore, MD) and Dr. Tonya Watkins (John Hopkins University, Baltimore, MD) for their assistance in performing microarray experiments; and Dr. Jean-Charles Grivel (NICHD, Bethesda, MD), Dr. Iusta Caminha (NIAID, Bethesda, MD) and Dr. Joao Bosco Oliveira (NIAID, Bethesda, MD) for their technical expertise in flow cytometry study.

I am thankful to Dr. Maria Nesterova, Dr. Sosipatros A. Boikos and Dr. Madson Q. Almeida for their supports and hand-on help; and Ms Brenda Hanning for editing the thesis.

Last but not least, I would like to express my heartfelt thanks to Professor Wai-Yee Chan (CUHK, HK), my family and my friends, especially Dr. Oscar K.T. Cheng for their unconditional support and spiritual encouragement.

This project is supported by U.S. National Institutes of Health, *Eunice Kennedy Shriver* National Institute of Child Health and Human Development intramural project Z01-HD-000642-04 (to Dr. C.A. Stratakis).

Content

List of Figures

List of Tables

Abbreviations

μCT	Microcomputed tomography
aBSCs	adult bone stromal cells
AC	adenylate cyclase
ACH	achondroplasia
Acp5	tartrate-resistant acid phosphatase 5
AKAP	A-kinase anchor protein
ALB	albumin
ALP	alkaline phosphatase
ALT	alanine aminotransferase
AST	aspartate aminotransferase
BAT	brown adipose tissues
BMP	bone morphogenetic protein
bp	base pair
BSCs	bone stromal cells
Ca	calcium
cAMP	cyclic adenosine mono-phosphate
CATK	cathepsin K
CHOL	cholesterol
CK	creatine kinase
CNC	Carney complex
CNCCs	cranial neural crest cells
CREB	cAMP response element-binding protein
CSF-1	colony-stimulating factor-1
DEAE	diethylaminoethyl

FD	fibrous dysplasia
FGF	fibroblast growth factor
FIAT	factor inhibiting activating transcription factor 4-mediated transcription
FMTC	familial medullary thyroid carcinoma
FOP	fibrodysplasia ossificans progressive
GDFs	growth and differentiation factors
GDNF	glial-derived neutrotrophic factor
GEO	Gene Expression Omnibus
GEP	gastro-entero-pancreatic tract
GH	growth hormone
GLU	glucose
GPCR	G protein-coupled receptor
Gs_{α}	stimulatory G-alpha protein
H&E	Haematoxylin and Eosin
HIF	hypoxia-inducible-factor
HMG	high-mobility-group
IHC	immunohistochemistry
IHH	Indian hedgehog
LCCSCT	primarily large-cell calcifying Sertoli cell tumor
LDH	lactate dehydrogenase
LOH	loss of heterozygousity
MAPK	mitogen-activated protein kinase
MEN	multiple endocrine neoplasia
MEN1	multiple endocrine neoplasia type 1
MEN2	multiple endocrine neoplasia type 2
MET	mesenchymal-to-epithelial
MMP9	matrix metalloproteinase 9

MTC	medullary thyroid carcinoma
NF1	neurofibromatosis type I
NMD	nonsense mRNA-mediated decay
OCM	osteochondromyxoma
OPG	osteoprotegerin
OSX	osterix
PCR	polymerase chain reaction
PDE	Phosphodiesterase
PHEO	phenochromocytoma
PHOS	inorganic phosphorus
PKA	cAMP-dependent protein kinase A
PKA-I	protein kinase A type I
PKA-II	protein kinase A type II
PKI	protein kinase inhibitor
PMS	pasmmomatous melanotic schwannoma
PPNAD	primary pigmented nodular adrenocortical disease
PRKAR1A	regulatory subunit α of the protein kinase A
PTH	parathyroid hormone
PTHrP	parathyroid hormone-related protein
RANKL	nuclear factor (NF)-κB ligand
RMS	Raman microspectroscopy
RT-QPCR	real-time quantitative real-time PCR
TD	thanatophoric dysplasia
TRAP	tartrate-resistant acid phosphatase
TRIG	triglycerides
VHL	Von Hippel-Lindau disease
WT	wild type

Chapter One

Introduction

1.1 Multiple endocrine neoplasia (MEN) syndromes

Multiple endocrine neoplasia (MEN) syndromes are defined as disorders with the presence of benign and/or malignant hormone-producing or hormone-secreting tumors in multiple endocrine tissues, including pituitary, parathyroid, adrenals, gastro-entero-pancreatic tract (GEP) and paraganglia. MEN can present by two coincidental tumors (non-hereditary) or certain patterns of tumor types. The classic MEN syndrome includes multiple endocrine neoplasia type 1 (MEN1) and multiple endocrine neoplasia type 2 (MEN2). However, Carney complex (CNC), Von Hippel-Lindau disease (VHL) and Neurofibromatosis type I (NF1) may also be considered in the category of MEN (1, 2). All these syndromes are inherited in autosomal dominant fashion.

MEN1 is characterized by various combinations of parathyroid adenomas, anterior pituitary adenomas, endocrine tumors of gastro-entero-pancreatic tract, adrenocrotical neoplasms and carcinoids. Some patients may also develop non-endocrine tumors, such as lipomas, angiofibromas, collagenomas and leiomyomas (3, 4). Inactivating germline mutations of *MEN1* genes have been identified in MEN1 patients. The *MEN1* gene consists of 10 exons and encodes a 610-amino acid protein called menin, which is a nuclear protein, participating in transcriptional regulation, DNA replication and repair and genome stability. The majority of the indentified mutations lead to truncated form of menin. MEN1 tumors also have loss of heterozygousity (LOH), resulting in the absence of menin in tumors, which indicates the tumor suppressor role of *MEN1*. No phenotype-genotype correlations have been identified for MEN1 (3, 5). However,

about 20% of MEN1 patient do not harbor mutations in *MEN1* gene (6-9), indicating the possible involvement of other mutations in unidentified predisposition genes. Recently, two *MEN1* mutation-negative patients, who present MEN1-like syndrome, were found to carry a germline nonsense mutation in *CDKN1B* gene (10, 11). *CDKN1B* gene encodes the cyclin-dependent kinase inhibitor p27 which regulates cell cycle by inhibiting cyclin/Cdk complexes. Homozygous germline mutation in Cdkn1b in rat led to MENX syndrome that has phenotypic features resembled human MEN1 and MEN2 (10, 11). This MEN1-like syndrome with *CDKN1B* mutation is now designated as MEN4 (OMIM#610755).

MEN2 is characterized by the presence of medullary thyroid carcinoma (MTC). Based on the risk and presence or absence of other clinical features, MEN2 can be divided into three clinical subtypes: MEN2A, MEN2B and familial MTC (FMTC). MEN2A is a syndrome of MTC, unilateral or bilateral phenochromocytoma (PHEO), and parathyroid cells hyperplasia or adenoma, which results in hyperparathyroidism. MEN2B is defined by MTC, PHEO, multiple neuromas and intestinal and mucosal ganglioneuromatosis, but not hyperparathyroidism. MEN2B is the most aggressive variant with higher morbidity and mortality rate. FMTC patients only develop MTC. At least four affected family members develop MTC but without the presence of PHEO and hyperparathyroidism should be considered to have FMTC (3, 12, 13). All MEN2 variants are caused by germline activating mutations in the *c-RET* proto-oncogene (14, 15). *c-Ret* encodes a membrane tyrosine kinase receptor called

RET, which consists of six extracellular domains (four cadherine-like domains, a calcium-binding domain and a cysteine-rich domain), one transmembrane domain and two distinct intracellular tyrosine kinase domains. RET functions as a signal transducer that binds to growth factors of glial-derived neutrotrophic factor (GDNF) family. Activation of RET induces cell growth and survival mediated by the mitogen-activated protein kinase (MAPK) signaling (3, 16). Unlike MEN1, MEN2 has a strong phenotype-genotype correlation. Missense mutations at the cysteine-rich domain are responsible for 90% of MEN2A and 80% of FMTC cases. MEN2B-associated mutations are mainly located in the intracellular tyrosine kinase receptor domains.

VHL is an inherited familial syndrome that predispose affected individual to a variety of begnin or malignant neoplasms of retina, cerebellar, central nervous system, renal cells and adrenal (OMIM#193300). VHL type 1 patients do not exhibit pheochromocytoma while type 2A is associated with it. In addition to pheochromocytoma, VHL type 2B patients also have renal cell carcinoma (17). The gene responsible for VHL, *VHL*, maps at 3*p*26-*p*25. *VHL* encodes a component of protein complex that possesses ubiquitin ligase E3 activity. It is involved in ubiquitination and degradation of hypoxia-inducible-factor (HIF) and thus, oxygen-sensing pathway (18).

NF1 is characterized by the presence of neurofibroma, gliomas, learning disability, bony abnormalities and café au lait spots (OMIM#162200) (19). It is caused by mutation in neurofibromin gene (*NF1*) on chromosome 17*q*11.2 (20).Neurofibromin is a negative regulator of *RAS* oncogene (21).

Carney complex (CNC), which considers as part of MEN, is discussed in the next section.

1.2 Carney complex (CNC)

Carney complex (CNC) is a familial multiple endocrine neoplasia (MEN) syndrome, inherited as an autosomal dominant manner, initially described by Dr. J.A. Carney at the Mayo Clinic in 1985 as "the complex of myxomas, spotty pigmentation and endocrine overactivity" (22). Currently, the criteria used for the diagnosis of CNC mainly include: A) spotty skin pigmentation; B) cutaneous and mucosal myxoma; C) cardiac myxoma; D) primary pigmented nodular adrenocortical disease (PPNAD); E) growth hormone (GH)-producing pituitary adenoma; F) thyroid carcinoma; G) testicular neoplasma [primarily large-cell calcifying Sertoli cell tumor (LCCSCT)]; and rarely include: H) pasmmomatous melanotic schwannoma (PMS); I) breast duct adenoma; J) bone tumor, osteochondromyxoma (22-31).

A diagnosis is made if the presence of two main components of the above criteria is proven by histology and/or biochemical testing or imaging; or if one of these manifestations is present and a familial pattern or inactivating mutations of the disease gene, regulatory subunit α of the protein kinase A (*PRKAR1A*), are also shown. CNC is a developmental disorder with some cases diagnosed at birth. Onset of the disease occurs commonly at a young age and the median age of diagnosis is 20 years (26).

1.3 Clinical manifestations of CNC

1.3.1 Skin pigmentary abnormalities

Skin lesions are the most common clinical manifestation of CNC. The patients get a specific type of skin freckles known as lentigines, which tend to be small, brown to black, round or irregular and typically increase in number around puberty. They are primarily located on the face, eyelids, ears and the vermilion border of the lips (Figure 1.1). Additional pigmented abnormalities include epithelioid blue nevi (large, blue to black, domed lesions), café-au-lait spots, and depigmented lesions (30, 32).

1.3.2 Myxomas

Heart and cutaneous myxomas are the clinical conditions on the basis of which most CNC patients are first diagnosed (33-35). Cardiac myxomas (Figure 1.2A) are the second most common tumor among CNC patients and are responsible for more than half of the CNC-related fatal complications (30). Unlike sporadic myxomas, they often present multicentrically in all heart chambers, without predilection for gender or age (36-38). The most typical cutaneous myxoma for CNC patients is trichofolliculoepithelioma that is usually found in external ear canal, eyelids and occasionally found in oropharynx and genital area of both sexes (37).

1.3.3 Endocrine tumors/overactivity

A) Primary pigmented nodular adrenocortical disease (PPNAD)

PPNAD (Figure 1.2B), a form of adrenocorticotropic hormone (ACTH)-independent Cushing syndrome, is the most frequent endocrine tumor observed in CNC, and occurs in about 25% of individuals. The disease usually involves micronodules of both adrenals. Pathological investigation reveals that adrenal glands from PPNAD patients have pigmented micronodular and some atrophy of surrounding cortex (28, 39, 40).

B) Growth hormone (GH)-producing pituitary adenoma

Somatomammotropic pituitary tumors are relatively rare in CNC. Most patients have pituitary tumors associated with growth hormone oversecretion and cause acromegaly. Acromegaly is the syndrome caused by the presence of excess growth hormone (GH) in the body. CNC patients have acromegaly due to diffuse enlargement and hyperplasia of the GH-producing cells of the pituitary, or, more rarely, due to GH-producing pituitary tumors. Occasionally, CNC patients may also have hyperprolactinemia; increased prolactin levels may be due to hyperplasia of the sommeto-memmo-tropic cells that also produce GH (41).

C) Testicular tumors (primarily large-cell calcifying Sertoli cell tumor, LCCSCT)

About one-third of males with CNC have large-cell calcifying sertoli cell tumors (LCCSCT) (Figure 1:2C). LCCSCT is always benign with only one case reported to have been malignant. LCCSCT may be hormone-producing and cause gynecomastia in prepubertal and peripubertal boys. Other testicular tumors observed in patients with CNC include Leydig cell tumors and adrenocortical rest tumors (27, 33, 42).

D) Thyroid adenoma or carcinoma

Thyroid gland abnormalities found in CNC patients are mostly benign non-hormone-secreting follicular adenomas. Thyroid carcinomas, both papillary and follicular, may develop in patients with a long history of multiple thyroid adenomas (43).

1.3.4 Psammomatous melanotic schwannoma (PMS)

PMS is a round dark tumor that may occur anywhere in the central and peripheral nervous system of patients with CNC. In CNC patients, PMS is most frequently found in the nerves of the gastrointestinal tract (esophagus and stomach) and paraspinal sympathetic chain. Primary tumors are often inoperable due to their location and may metastasize to lung, liver and brain (25, 44, 45).

1.3.5 Breast ductal adenoma (multiple)

Breast ductal adenoma is a benign tumor of the mammary gland duct (46, 47), that is frequently seen in women with CNC but rarely in the general population.

1.3.6 Osteochondromyxoma

Osteochondromyxoma, a form of bone tumor, is the most recently described tumor associated with CNC (27). Less than 10% of CNC patients have this tumor that usually involves long bones and rarely facial bones and sinuses. Microscopically, bone tumors feature benign-appearing polymorphic cells set in a myxomatous, cartilaginous, osseous, and hyaline fibrous matrix with low to

moderate cellularity (Figure 1.3). The proportion of multiple cell types and tissue matrices varies greatly from place to place even within an individual tumor. These tumors erode bone, e.g. by infiltrating between bony trabeculae. Complete resection of the tumor is curative; while incomplete excision results in local recurrence. To-date, no tumor metastasis has been found (25, 48).

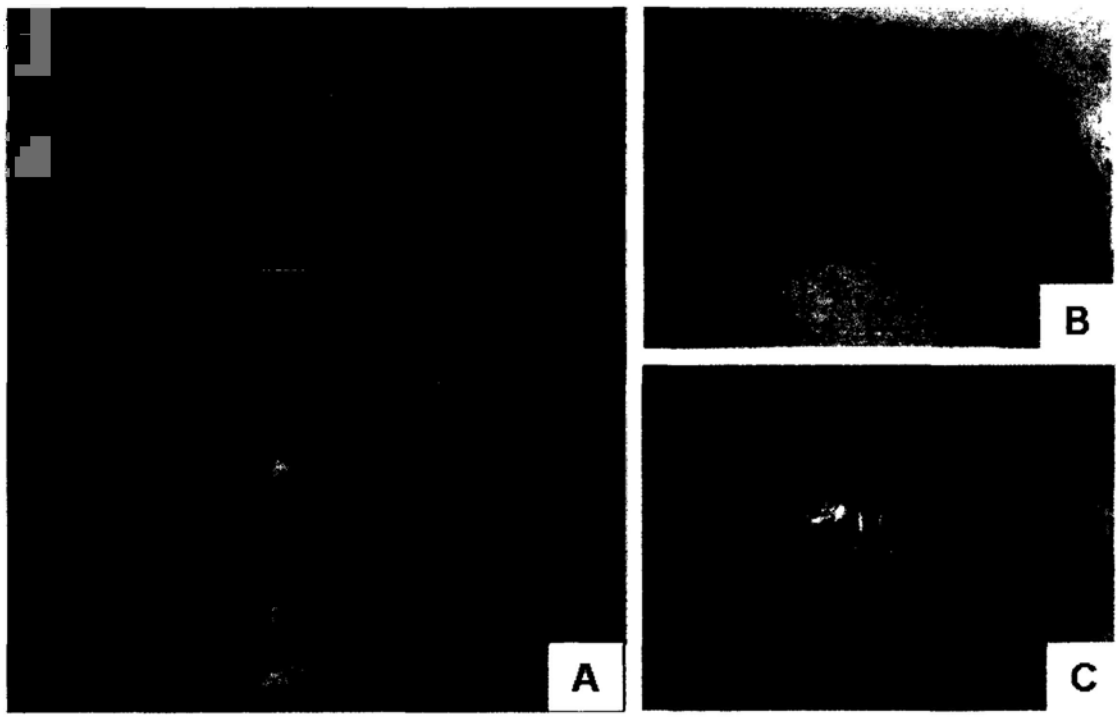

Figure 1.1 Lentigines in CNC patients who have intense pigmentation around the face (**A**), the eyes (**B**) and vermilion border of the lips (**C**). Pictures were taken and modified from Stergiopoulos and Stratakis, *FEBS*, 2003; Sandrini and Stratakis, *Molecular Genetics and Metabolism*, 2003.

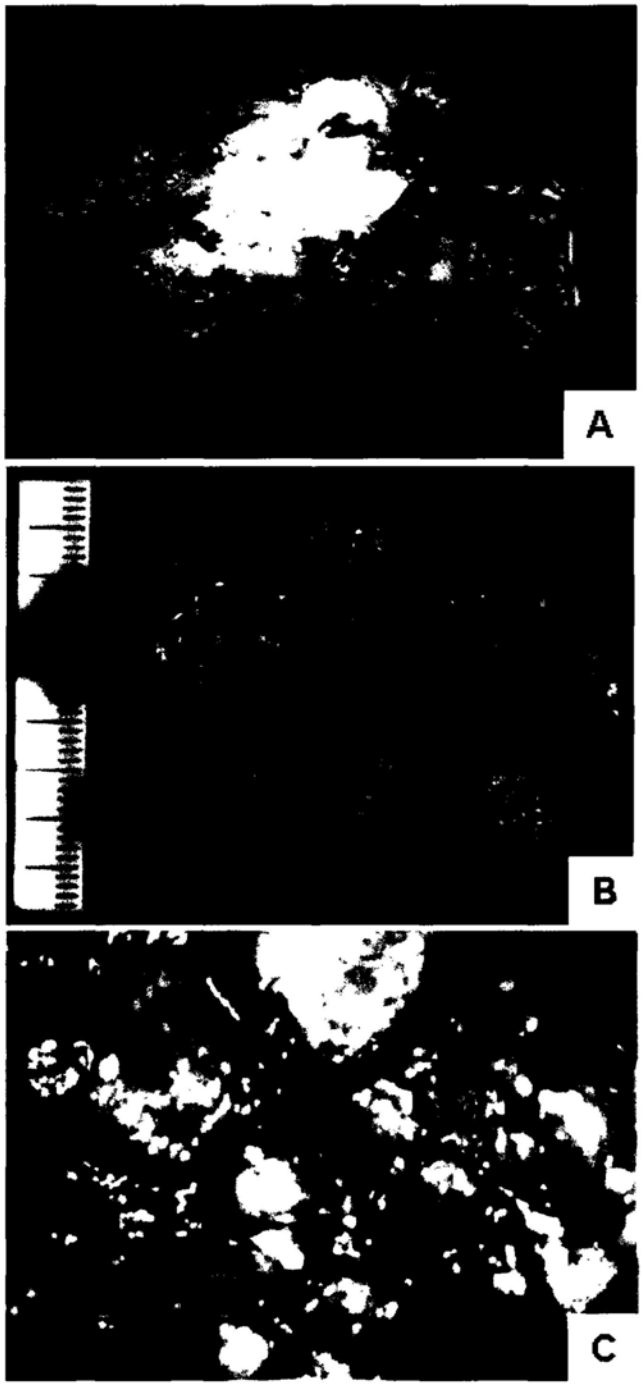

Figure 1.2 Cardiac myxoma (**A**), primary pigmented nodular adrenocortical disease (PPNAD) (**B**) and large-cell calcifying Sertoli cell tumor (LCCST) (**C**) from CNC patients. Pictures were taken and modified from Casey *et al.*, *Circulation*, 1998; Bertherat, *Orphanet Journal of Rare Diseases*, 2006; Stratakis, *Frontiers in Bioscience*, 2000.

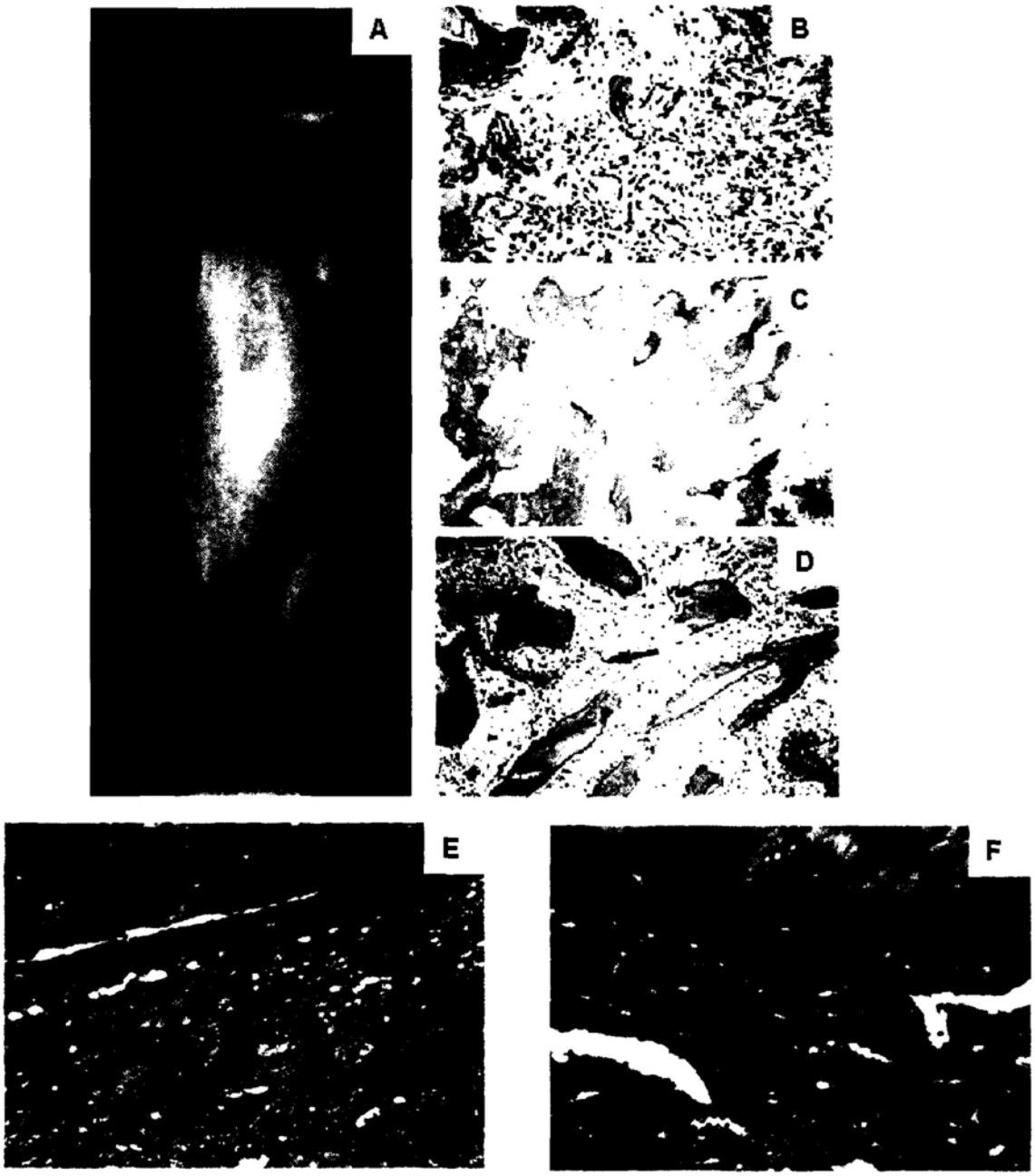

Figure 1.3 Bone lesions in CNC patients. (**A**) Mixed lucent and sclerotic lesions of the tibial diaphysis. (**B**) Moderately cellular tumor featuring eosinophilic hyaline bands (arrows). (**C**) Interconnected network of bone trabeculae with hypocellular tissue. (**D**) Moderately cellular tumor teatures immature cartilage (bottom half) and osteoid between bone trabeculae (arrow). (**E, F**) Representative hematoxylin and eosin stainings of bone lesions that were excised from two other, unrelated patients with CNC: (E) Zone of moderately cellular hyaline cartilage in a background of hypocellular vascularized myxoid tissue, characteristic of an osteochondromyxoma; (F) Two islands of hypocellular hyaline cartilage in a moderately cellular spindle cell stroma containing a few dilated blood vessels, characteristic of the cartilage component of the bone lesions seen in the context of CNC. Pictures were taken and modified from Carney *et al., The American Journal of Surgical Pathology*, 2001; Tsang *et al.,* unpublished data.

1.4 Identification of disease gene linked to CNC

Linkage analysis and use of loss of heterozygosity (LOH) by microsatellite markers and allelic loss (by fluorescent in situ hybridization) allowed Dr. Stratakis' group to identify *PRKAR1A* (17q22-24) as the gene mutated in more than 50% of patients with CNC or PPNAD. Genetic linkage analysis has also identified other genetic loci harboring a gene for CNC on chromosome 2 (2p16). However, the disease gene on 2p has not been identified.

PRKAR1A encodes for type 1 alpha regulatory subunit of cyclic adenosine monophosphate (cAMP)-dependent protein kinase (PKA), which is an important regulatory molecule in PKA signaling. This gene is composed of 11 exons and has a total length of at least 21kb. To date, 60 different *PRKAR1A* pathogenic mutations have been described (24, 49-52). Most mutations reported in the *PRKAR1A gene* of individuals with CNC are predicted to produce a truncated protein, in either a direct or indirect way. The most frequent *PRKAR1A* mutation in CNC is c.578delTG deletion, which results in frameshift in exon 4B of the gene. Exon 2 and 6 are the other two sites with frequent mutations. It is believed that the mutant mRNAs are degraded by nonsense mRNA-mediated decay (NMD) and so most mutations cause complete inactivation of *PRKAR1A* at tissue level by NMD and LOH. Because of this, it is believed that *PRKAR1A* may act as a tumor-suppressor gene in CNC as well as in sporadic adrenal and thyroid tumors.

1.5 Cyclic adenosine monophosphate (cAMP)-dependent protein kinase (PKA)

PKA exists as a holoenzyme that consists of a homodimer (and rarely heterodimer) of regulatory subunits and two inactive catalytic subunits, each bound to one of the regulatory subunits of the dimer (53). Four main regulatory subunit isoforms [*PRKAR1A* (RIα), *PRKAR1B* (RIβ), *PRKAR2A* (RIIα) and *PRKAR2B* (RIIβ)] and four catalytic subunit isoforms [*PRKACA* (Cα), *PRKACB* (Cβ) and *PRKACG* (Cγ) and Prkx] have been identified (53, 54). The holoenzyme of two molecules of catalytic subunits with dimers of R1α or R1β has been identified as "PKA type I isozyme (PKA-I)" while the complex with either RIIα or RIIβ is known as the "PKA type II isozyme (PKA-II)" (53-55). PKA-I and –II have different cellular localizations, functions, and affinity to cAMP (54, 55), but in general the mechanism of their activation is the same: ligand-induced activation of G protein-coupled receptor (GPCR) leads to subsequent activation of an adenylate cyclase (AC) which produces cAMP. The sequential binding of two cAMP molecules to each regulatory subunit "activates" PKA by leading to dissociation of the tetramer and release of catalytic subunits which, in turn, phosphorylate serine-threonine residues of downstream targets (55). PKA catalytic subunits can also phosphorylate cAMP response element-binding protein (CREB) in the nucleus, resulting in activation of DNA transcription of cAMP-responsive element-containing genes (56).

1.6 Mouse models

1.6.1 *Prkar1a* knockout and heterozygous mice (*Prkar1a*$^{-/-}$ and *Prkar1a*$^{+/-}$)

As mentioned above, CNC is caused by inactivating mutations in *PRKAR1A*. To better understand the disease-causing mechanism, *Prkar1a* homozygous and heterozygous knockout mice have been developed (57, 58). Homozygous mutant mice (*Prkar1a*$^{-/-}$) die early in embryonic life and are severely growth retarded. *Prkar1a*$^{-/-}$ mice show developmental defects starting from E7.5 when compared to wild type littermates. They fail to develop functional heart tubes at E8.5 and are resorbed at around E10.5. Although the *Prkar1a*$^{-/-}$ embryos develop an apparent anterior-posterior axis, two-thirds of mesoderm cells fail to exit the streak and to move laterally and anteriorly, resulting in a reduced trunk. Moreover, *Prkar1a*$^{-/-}$ embryos have increased basal PKA activity and the defects can be rescued by crossing *Prkar1a*$^{-/-}$ mutants to mice carrying targeted disruption in *Prkaca* gene. These findings indicate that dysregulated PKA activity is responsible for the abnormal phenotype (58).

Due to embryonic lethality of *Prkar1a*$^{-/-}$ mice, Dr. Stratakis' group has created a heterozygous mouse model with conventional null allele of *Prkar1a* (*Prkar1a*$^{+/-}$), which provides a better understanding of the effect of 50% germline *Prkar1a* reduction in adult mice (57). *Prkar1a*$^{+/-}$ mice have normal body weight and survive to adulthood. However, at around 6 – 8 months of age, they start to develop various degrees of nonpigmentated schwannomas, bone tumors and thyroid neoplasms which are also observed in CNC patients (57). Haploinsufficiency of *Prkar1a* in mice also leads to upregulation of PKA activity in

male meiotic and postmeiotic germ cells, resulting in structural defects in mature sperm and, in turn, reduction in fertility (59).

1.6.2 *Prkar2a* knockout and heterozygous mice (*Prkar2a*$^{-/-}$ and *Prkar2a*$^{+/-}$)

The generation of *Prkar2a*$^{+/-}$ and *Prkar2a*$^{-/-}$ mice leads to the expected Mendelian ratio, indicating that the null mutation does not cause any embryonic lethality. Both mutants exhibit normal growth and appear healthy. In *Prkar2a*$^{-/-}$ mice, the levels of R1α protein are increased while Cα protein is decreased in adult skeletal muscle. With reduction in Cα protein, as expected, the total kinase activity is decreased. A particular study in *Prkar2a*$^{-/-}$ skeletal muscle cells reveal that the upregulated R1α protein is able to bind to the same A-kinase anchor protein (AKAP) associated with or near the L-type Ca2+ channel as to RIIα protein, suggesting that R1α is able to compensate for the function of RIIα in a localized manner (60).

1.6.3 *Prkar2b* knockout and heterozygous mice (*Prkar2b*$^{-/-}$ and *Prkar2b*$^{+/-}$)

RIIβ protein is highly expressed in brown and white adipose tissue and brain. Mice lacking *Prkar2b* (*Prkar2b*$^{-/-}$) exhibit 50% reduction in white adipose tissue despite normal food intake. They are also resistant to diet-induced obesity. Similar to the findings from *Prkar2a*$^{-/-}$ mice, brown adipose tissues (BAT) have compensatory increase in R1α protein and basal PKA activity, suggesting that PKA dysregulation results from type II to type I isoform switch in BAT, rather than from dysregulation of catalytic subunits. RIIβ mutants are otherwise normal and fertile (61).

1.6.4 *Prkaca* knockout and heterozygous mice (*Prkaca*$^{-/-}$ and *Prkaca*$^{+/-}$)

It has been demonstrated that a null mutation of *Prkaca* generated in mice leads to early postnatal lethality in 70% of *Prkaca*$^{-/-}$ mice. The remaining 30% survive to adulthood, probably due to the compensatory kinase activity derived from the *Prkacb* gene. However, the surviving *Prkaca*$^{-/-}$ mice are growth-retarded with normal circulating growth hormone (GH) levels but reduction in GH-dependent molecules, IGF-1 and MUPs. This suggests that *Prkaca*$^{-/-}$ mice are partially GH resistant. Loss of *Prkaca* results in 90% reduction in kinase activity in most tissues, except in brain in which expression of *Prkacb* is increased by posttranscriptional stabilization for compensation. *Prkaca*$^{-/-}$ mice also have a reduction of both RI and RII subunits in skeletal muscle, heart and sperm. Despite a loss of more than 95% of total PKA activity in *Prkaca*$^{-/-}$ testis, spermatogenesis remains unaffected, maintained by the remaining *Prkacb* activity. However, the mature sperm exhibit a near-total loss of forward velocity that indicates the incapability of *Prkaca*$^{-/-}$ mice in successful fertilization (62). There is no significant difference between wild-type and *Prkaca*$^{+/-}$ mice in total body weight or in visceral organ weights.

1.6.5 *Prkacb* knockout and heterozygous mice (*Prkacb*$^{-/-}$ and *Prkacb*$^{+/-}$)

Prkacb encodes three different isoforms of Cβ subunits, Cβ1, Cβ2 and Cβ3. Cβ1 is relatively more ubiquitously expressed; while expression of Cβ2 and Cβ3 is restricted to brain (63). Mice lacking all three isoforms of Cβ have no abnormalities with fertility and development. And *Prkacb*$^{-/-}$ mice are shown to have normal locomotor response to novel environment that, at least in part, is

due to the functional substitution by Cα. Despite a compensatory increase in Cα protein, basal PKA activity is reduced by 26% in the brains of *Prkacb*$^{-/-}$ mice. Since Cβ subunits are highly expressed in amygdale and hippocampus, which play an important role in learning and memory, *Prkacb*$^{-/-}$ mice were subjected to fear conditioning studies to evaluate the effect of the absence of Cβ in brain. The study found that cued fear conditioning was disrupted in *Prkacb*$^{-/-}$ mice on C57BL/6/129 background, but had no significant defect in *Prkacb*$^{-/-}$ mice on a 98% C57BL/6 genetic background, suggesting that this phenotype was sensitive to strain-specific genetic modifiers (64).

1.7 Skeletogenesis

The vertebrate skeleton is an organ with high complexities. In general, there are four different types of bone that compose the adult human skeleton; they are: 1) long bones like humeri, radii, femurs, tibiae etc.; 2) short bones like carpal and tarsal bones; 3) flat bones including skull, mandible and ribs; and 4) irregular bones like vertebrae and sacrum. Long bones of the limbs and elements of the axial skeleton are formed by a combination of endochondral and intra-membraneous ossification, whereas flat bones of the skull are formed by intra-membraneous ossification only. The skeleton developmental process starts from condensation of mesenchymal cells, also known as osteochondral progenitors, that give rise to either chondrocytes to form cartilaginous templates in endochondral ossification or osteoblasts to form bone directly in intra-membraneous ossification (65, 66).

1.7.1 Intra-membranous bone formation

The mesenchyme that is mostly derived from cranial neural crest cells (CNCCs) develops into mesenchymal blastemas. Blastema, a mass of undifferentiated cells with osteogenic potential, is the precursor of the bones of cranial vault (67-69). During intra-membranous ossification of bones of the craniofacial area, mesenchymal cells directly differentiate into osteoblast progenitors and then into osteoid, which produce mature osteoblasts without any cartilage formation. The osteoblasts then deposit extracellular matrix consisting mainly of type I collagen, other bone-related proteins, like osteocalcin, and proteoglycans, followed by mineralization. As the ossification proceeds, the borders of each cranial bone come closer and initiate the formation of sutures in which bone expansion happens during postnatal craniofacial growth. Under pressure from the expanding brain, sutures, the unossified bone growth site, allow the formation of new bone at the edges of the bone fronts; while the cells within the sutures remain undifferentiated. This process allows the cranial vault to increase in size to accommodate the enlarging brain, while at the same time, keeping the sutures as the bone growth sites (69).

This intra-membranous bone growth site is tightly regulated by different signaling pathways. Premature fusion of these sutures leads to craniosynostosis. Thus, it is important to elucidate the factors that are involved in regulating suture morphogenesis, suture patency and suture fusion.

In vivo mouse studies have demonstrated that, in intra-membranous ossification, upregulation of Wnt/β-catenin signaling in mesenchymal progenitors is essential to inhibit *Sox9* expression and promote *Runx2* expression, leading to mesenchyme differentiation into osteoblast lineage but not chondrocytes (70). Moreover, Bmp signaling is also an important factor in regulating suture morphogenesis and function. Previous studies have shown that *BMP-2, BMP-4* and *BMP-7* are expressed in osteogenic bone fronts during the early stages of suture morphogenesis. *Gdf6* (*Bmp-13*) knockout mice fail to develop coronal sutures, leading to craniosynostosis (71).

The importance of *FGFR-1*, *-2* and *-3* and transcription factors, *TWIST1* and *MSX2* in suture development is supported by the discovery of mutations in these genes that are associated with craniosynostosis syndromes in the human, such as Apert syndrome (OMIM#101200), Crouzon syndrome (OMIM#123500), Pfeiffer syndrome (OMIM#101600), Jackson-Weiss syndrome (OMIM#123150) craniosynostosis type 1 (OMIM#123100), craniosynostosis type 2 (OMIM#604757) (66, 72-75).

1.7.2 Endochondral bone formation

During endochondral bone formation, the osteochondral progenitors within the condensation centers are programmed to differentiate into chondrocytes, forming a cartilaginous template called growth plate; surrounding chondrocytes become perichondrium, a part of which give rise to periosteum, containing osteoblast precursors (76) and the other part of which remain as perichondrial cells. Chondrocytes in the center of the growth plate transform into early chondrocytes and start to proliferate. Both round and flat (more differentiated proliferative chondrocytes) proliferative chondrocytes secrete a matrix rich in collagen type II, collagen type XI and aggrecan. Signaling molecule, parathyroid hormone-related protein (PTHrP), secreted by perichondrial cells acts on these chondrocytes to keep them proliferating. Since PTHrP is only secreted by perichondrial cells and early chondrocytes near the end of bones, the chondrocytes distant from perichondrium receive a very weak PTHrP signal which makes them stop proliferating and become prehypertrophic chondrocytes. Prehypertrophic chondrocytes synthesize Indian hedgehog (IHH) proteins, which act on perichondrial cells for the synthesis of PTHrP. IHH-stimulated PTHrP expression keeps the chondrocytes in the proliferative pool and results in the delay of IHH production. The indirect ability of PTHrP to repress IHH expression establishes a negative feedback loop, which determines the length of columns of proliferative chondrocytes (77, 78). IHH is also able to accelerate the differentiation of round proliferative chondrocytes into flat chondrocytes in a PTHrP-independent pathway (79).

Prehypertrophic chondrocytes undergo further genetic changes and differentiate into post-mitotic hypertrophic chondrocytes that produce collagen type X and direct the mineralization of the surrounding matrix. Hypertrophic chondrocytes play a seminal role in bone development as they provide a scaffold for new bone formation (80). Hypertrophic chondrocytes eventually die through apoptosis. Concurrently, they trigger the invasion of blood vessels and osteoblast precursors, which are differentiated from perichondrium next to the region of prehypertrophic and hypertrophic chondrocytes under the stimulation by IHH signals, to form the primary spongiosa, the precursor of trabecular bone. While the chondrocytes continue to proliferate and lengthen the bone, the osteoblasts of primary spongiosa form trabecular bone and osteoblasts of bone collar form cortical bone. The secondary ossification center also forms after cycles of chondrocyte hypertrophy and vascular invasion.

1.7.3 Chondrogenesis

The cellular events involved in chondrogenesis, and subsequent osteogenesis/bone formation, are very complex. Thus, tight regulation by different signals should be present to generate a biomechanically strong bone structure. Besides PTHrP and IHH signaling, not surprisingly, different signaling pathways and transcription factors are also involved in regulating the proliferation, differentiation and apoptosis of chondrocytes in growth plates.

- Fibroblast growth factor (FGF) signaling

Several FGF and FGF receptor genes have been identified to be expressed during endochondral bone formation. *FGFR3* is expressed in proliferating chondrocytes; *FGFR1* is expressed in prehypertrophic/hypertrophic chondrocytes; whereas *FGFR2*, *FGF7*, *FGF8*, *FGF9*, *FGF17* and *FGF18* are expressed in perichondrium (81).

The identification of activating mutations in fibroblast growth factor receptor 3 (*FGFR3*) from patients with achondroplasia (ACH), a form of short-limbed dwarfism (82-84)and thanatophoric dysplasia (TD) (85, 86) points to the importance of FGF signaling in chondrocytes proliferation and differentiation. Mice lacking *Fgfr3* accelerate the rate of proliferation of chondrocytes, which results in overgrowth of long bones and vertebrae (87, 88). These findings provide the evidence for the negative regulation of chondrocyte proliferation by *FGFR3*. *In vivo* evidence from other studies suggested that *Fgfr3* inhibits bone growth by inhibiting chondrocyte differentiation via the mitogen-activated

protein kinase (MAPK) pathway and by inhibiting chondrocyte proliferation through activator of transcription-1 (Stat1) (89).

Knockout of *Fgf18* in mice leads to an increase in chondrocyte proliferation that closely resembles the bone phenotype of *Fgfr3*$^{-/-}$ mice, but in a more severe way. This severe phenotype suggests that *Fgf18* may also act on *Fgfr1* to delay terminal differentiation of hypertrophic chondrocytes and on *Fgfr2* to delay osteoblast development (90, 91).

- Bone morphogenetic protein (BMP) signaling

Bone morphogenic proteins (BMPs), also called growth and differentiation factors (GDFs), are members of the TGFβ family of secreted signaling molecules that can activate the corresponding receptors with serine/threonine kinase activity (80). Bmp signaling acts in both early and late stages of cartilage development. Type 1B Bmp receptor (*BMPR1B*) is expressed in mesenchymal condensation; while type 1A Bmp receptor (*BMPR1A*) is expressed throughout the growth plate with higher expression in prehypertrophic and hypertrophic chondrocytes (66). Expression of *BMP2, -3, -4, -5* and *-7* are found in the perichondrium; *BMP2* and *-6* are expressed in hypertrophic chondrocytes; *BMP7* is expressed in proliferating chondrocytes (80). *In vivo* gain and loss-of-function studies of *Noggin*, a BMP antagonist, in mice suggest that BMP signaling is required for chondrogenic mesenchymal cell condensation and maintenance of chondrocyte lineage (92). Application of exogenous BMPs to *in vitro* limb-culture increases the proliferation of

chondrocytes, while addition of NOGGIN inhibits proliferation (93, 94). Conditional removal of *Bmpr1a* in chondrocytes decreases *Ihh* expression and expands hypertrophic zone due to delayed terminal hypertrophic differentiation (95). As discussed in the previous section, FGF signaling decreases chondrocyte proliferation and accelerates the terminal hypertrophic differentiation while BMP signaling acts in an opposite manner. Because of this opposing effect, these two pathways have been suggested as antagonizing each other (80, 93).

- *Sox9* transcription factor

The Sox family of transcription factors, which contains the high-mobility-group (HMG) DNA-binding domain, is the master regulator of early chondrogenesis. Loss of function studies on mouse have shown that *sox9* is essential for condensation and proliferation of chondrocytes and the expression of collagen type II, collagen type XI and aggrecan, the matrix in the proliferating zone of growth plate (96-99). *Sox9* is expressed in proliferating chondrocytes but not in hypertrophic chondrocytes. Several studies have shown that *Sox9*, cooperating with the large Sox5 isoform (*L-Sox5*) and *Sox6*, is an indispensable transcription factor for the determination of chondrocyte cell fate and proliferation by activating cartilage-specific enhancer (77, 98, 100-103).

- Runx2 transcription factor

RUNX2, also known as *CBFA1*, belongs to a family of transcription factors that share the DNA-binding domain of the Drosophila pair rule gene *runt*. *RUNX2* was first characterized as an important transcription factor for osteoblast differentiation from mesenchymal progenitors, which is supported by the loss of osteoblast differentiation in *Runx2* knockout (*Runx2*$^{-/-}$) mice (104-107). Loss of *Runx2* in mice also leads to delays in chondrocyte maturation since most bones have a decreased number of hypertrophic chondrocytes (108, 109). Additoinal studies revealed that *Runx2* is expressed in prehypertrophic and hypertrophic chondrocytes but not in proliferating chondrocytes. These findings support the conclusion that *Runx2* plays a role in chondrocyte hypertrophy. Moreover, *RUNX2* is expressed in perichondrial cells and inhibit the proliferation of chondrocytes indirectly by regulating *FGF18* expression (110). In chondrocytes, *RUNX2* is also involved in IHH-PTHrP pathway by controlling the expression of *IHH*. *In vivo* studies find that *Runx2*, partly involves *Runx3*, positively regulates the expression of *Ihh* in prehypertrophic chondrocytes (111). *IHH* upregulation indirectly delays chondrocyte hypertrophy through the induction of *PTHrP* production; whereas *Runx2* upregulation leads to acceleration of chondrocyte hypertrophy (112). The dual antagonistic role of *Runx2* in chondrocytes, acting individually or integrating with other signaling pathways, is present to coordinate chondrocyte proliferation and hypertrophic so as to prevent premature chondrocyte maturation.

1.7.4 Osteoblastogenesis

Osteoblasts are responsible for bone formation, matrix deposition and osteoclast differentiation in both intra-membranous and endochondral ossification. Different genetic and *in vivo* studies have demonstrated that *Runx2* is the master regulator of osteoblast differentiation. In endochondral bone formation, *RUNX2* expression is absolutely required for osteoblast differentiation in osteochondral progenitors of perichondrium and of the bone collar after mesenchymal condensation; in intra-membranous bone formation, *RUNX2* in expressed in condensed mesenchymal anlagen (113). Forced *RUNX2* expression in mesenchymal cells of non-osteoblastic lineage induces the expression of osteoblast-specific genes, like osteocalcin and type I collagen, indicating the ability of *RUNX2* to regulate the expression of osteoblast-specific genes during osteoblastogenesis (105). Transcription factors *SOX8*, *MSX2*, *DLX5* and *BAPX1* have been suggested to be the regulators of *RUNX2* expression (114-118). A second osteoblast-specific transcription factor, osterix (OSX), which acts both downstream of *RUNX2* or independent of *RUNX2*, is required for the transition of uncommitted to commited osteoblast progenitors (119).

After the establishment of cell fate, osteoblast progenitors mature into type I collagen and matrix producing osteoblasts. At this stage, *ATF4*, a transcription factor accumulates mainly in osteoblast partly due to lack of proteasomal degradation, is expressed that favors the synthesis of type I collagen (120, 121). *ATF4* activity in early osteoblasts is inhibited through protein-protein interaction

with *FIAT* (factor inhibiting activating transcription factor 4-mediated transcription) (122). Moreover, *ATF4* has been shown to be involved in regulating the expression of osteocalcin and a gene encoding an osteoclast differentiation factor (123).

1.7.5 Osteoclastogenesis

Osteoclast, a cell type resorbing mineralizaed bone matrix, belongs to monocyte/macrophage cell lineage (113, 124) and is the key participant in bone remodeling. *Pu.1*, an ETS-domain-containing transcription factor (125, 126), is the earliest known factor essential for the differentiation of macropahges into preosteoclasts (113). Receptor activator of nuclear factor (NF)-κB ligand (RANKL) and colony-stimulating factor-1 (CSF-1), produced by bone stromal cells (BSCs) and osteoblasts, are necessary to induce expression of genes, including tartrate-resistant acid phosphatase (TRAP), cathepsin K (CATK), that lead to the differentiation of mature osteoclasts (124, 127, 128). RANKL interacts with its receptor RANK on osteoclasts and activates MAPK, PI-3K/Akt pathways and components of NF-κB complex (127, 129). One of the downstream targets of RANKL/RANK pathway is *c-fos,* a member of AP-1 family (127). Overexpression of *c-fos* in transgenic mice leads to osteosarcoma (130). Mice lacking *c-fos* develop osteopetrosis and exhibit hematopoietic defects, leading to large number of macrophages (131). These studies indicate that *c-fos* is necessary for osteoclastogenesis by directing precursors to form osteoclasts instead of macrophages. Besides activating the differentiation of osteoclasts, *RANKL* can also activate mature osteoclasts, leading to internal structural changes which prepare the osteoclasts to resorb bone (124). The studies on RANKL-deficient mice, which develop severe osteopetrosis (132), further support the essential role of *RANKL* in the control of osteoclast differentiation and function.

A balance in bone remodeling is essential to maintiain a rigid bone structure. Any excess in osteoclasts activity favors bone resorption, leading to adult skeletal diseases, like osteoporosis, rheumatoid arthritis etc. In normal circumstance, RANK signaling is negatively regulated by osteoprotegerin (OPG), a soluble "decoy receptor" secreted by osteoblasts to compete with RANK for RANKL (133). Accordingly, *Opg* knockout mice have increased osteoclast activity, leading to osteoporosis (134). Thus, OPG and RANKL are coordinated to regulate osteoclasts activity via RANK and in turn, bone resorption.

Upon initiation of bone remodeling, osteoclast cell body is polarized. Hyrodgen ions exported from mature osteoclasts acidify the resorption compartment, causing the exocytosis of CATK and TRAP which digest the proteinaceous matrix. Degradated products are processed by osteoclasts and released to circulation (65, 124).

1.8 Significance of study

Previous studies have shown that *prkar1a* heterozygous mice (*Prkar1a*$^{+/-}$) develop various tumors, which include schwannomas, thyroid neoplasias and tail bone lesions, in a spectrum that overlaps with that observed in CNC patients (57). R1α haploinsufficiency leads to increased total PKA activity in response to cAMP and an increased PKA-II to PKA-I ratio (135-139). Dysregulation of the catalytic subunits appears to be the most important mechanism for an increase in cAMP-responsive, total, PKA activity (140). Previous studies in mice and human cell lines have all suggested that coordinated inhibition of the catalytic subunit is the most important function of the PKA regulatory subunits (24, 141-143). Accordingly, we hypothesized that *Prkar1a*$^{+/-}$ deficiency in the background of *prkaca* haploinsufficiency (*Prkaca*$^{+/-}$) would abrogate most if not all of the tumors that developed in the former, since Cα is the main PKA catalytic subunit in both humans and mice (55, 135, 140, 143).

The present study reports the results of this experiment. Unlike *Prkar1a*$^{+/-}$ animals, the *Prkar1a*$^{+/-}$*Prkaca*$^{+/-}$ mice did not develop any thyroid tumors or schwannomas, indicating that indeed reduction of Cα can abrogate the development of tumors by thyroid follicular and Schwann cells. Unexpectedly, however, the *Prkar1a*$^{+/-}$*Prkaca*$^{+/-}$ mice not only continued to develop bone lesions but also demonstrated a significant increase in both the number and the severity of the lesions, as well as a reduction in the age of first appearance of any bone abnormality. Biochemical characterization showed an overall increase in PKA

activity and protein expression studies showed an increase in type-II regulatory subunits and alternate PKA catalytic subunits in cells derived from the lesions.

Like in *Prkar1a*$^{+/-}$ animals (144), histological analysis of bone from *Prkar1a*$^{+/-}$ *Prkaca*$^{+/-}$ mice showed that lesions had similarity to tumors from humans with CNC (48) and some resemblance (but also differences) from humans and mice with (FD) (145, 146). *Prkar1a*$^{+/-}$ and *Prkar1a*$^{+/-}$*Prkaca*$^{+/-}$ mouse lesions always involved a particular sub-population of cells that could be identified as belonging to the osteoblastic lineage and resembled BSCs (147).

These studies showed that genetic manipulation of the PKA pathway in mice, revealed a particular population of BSCs in adult animals (adult BSCs or aBSCs) that are responsive to cAMP signaling mediated mainly by PKA-II and alternate catalytic subunits; it is noteworthy that these PKA alterations did not affect embryonic or early postnatal skeletal development. These data have implications for the understanding of bone marrow subgroups of cells and their potential pharmacological manipulation through the cAMP signaling pathway.

Chapter Two

Materials and Methods

2.1 Generation of *Prkar1a*$^{+/-}$*Prkaca*$^{+/-}$ double heterozygous mice

Prkar1a heterozygous mice (*Prkar1a*$^{+/-}$), which contain one null allele of *Prkar1a*$^{\Delta 2}$, were previously generated in our laboratory (57). *Prkaca* heterozygous mice (*Prkaca*$^{+/-}$), which have a neomycin resistance cassette to replace exons 6-8 of the *prkaca* gene (62), were purchased from Mutant Mouse Regional Resource Centers (MMRRC, strain name: B6; 129X1-Prkaca^{tm1Gsm}/Mmnc). *Prkar1a*$^{+/-}$ and *Prkaca*$^{+/-}$ mice were interbred to generate *Prkar1a*$^{+/-}$*Prkaca*$^{+/-}$ double heterozygous mice, which were maintained on a mixed C57BL/6 129Sv/B6 hybrid background. All animal work in this study was carried out under animal protocol 06-033 (Building10A Animal Facility, NIH, Bethesda, MD).

2.2 Generation of *Prkar1a*$^{+/-}$*Prkar2b*$^{+/-}$ double heterozygous mice

The same *Prkar1a* heterozygous mice (*Prkar1a*$^{+/-}$) used in *Prkaca* crosses was interbred with *Prkar2b* heterozygous mice (*Prkar2b*$^{+/-}$); which have a neomycin resistance cassette to insert into exons 1 of the *prkar2b* gene (61), to generate *Prkar1a*$^{+/-}$*Prkar2b*$^{+/-}$ double heterozygous mice. *Prkar2b*$^{+/-}$ mice were purchased from Mutant Mouse Regional Resource Centers (MMRRC, strain name: B6.129X1-*Prkar2b*^{tm1Gsm}/Mmmh). *Prkar1a*$^{+/-}$*Prkar2b*$^{+/-}$ mice were maintained on a mixed C57BL/6 129Sv/B6 hybrid background. All animal work in this study was carried out under animal protocol 06-033 (Building10A Animal Facility, NIH, Bethesda, MD).

2.3 Genotyping analysis

Initial genotyping of founders was by polymerase chain reaction (PCR) that was then used to genotype our mice containing one null allele (*Prkar1a*$^{\Delta 2}$) and those with the NEO cassette within *Prkar1a* gene: Three primers (5'-AGCTAGCTTGGCTGGACGTA-3', 5'-AAGCAGGCGAGCTATTAGTTTAT-3' and 5'- CATCCATCTCCTATCCCCTTT-3') were used for *prkar1a* genotyping: the WT allele generated a 250 base pair (bp) fragment and the null allele generated an 180 bp product.

Genotyping of *Prkaca* was done with two pairs of primers: the first pair (5'-CTGACCTTTGAGTATCTGCAC-3' and 5'- GTCCCACACAAGGTCCAAGTA-3') amplified the WT allele with a product of 250 bp; the second pair (5'-AGACTACTGCTCTATCACTGA-3' and 5'-GTGGTTTGTCCAAACTCATCAATGT-3') identified the neo-inserted allele with a product of 250 bp.

Genotyping of *Prkar2b* was also done with two pairs of primers: the first pair (5'- GCAGGATGAGCATCGAG-3' and 5'- TTCGAGAGTGAGGCGGA-3') amplified the WT allele with a product of 330 bp; the second pair (5'-AGGAGCTGGAGATGCTGCCAA-3' and 5'-GTGGTTTGTCCAAACTCATCAATGT-3') identified the neo-inserted allele with a product of 194 bp.

	Temperature	Time	Cycles
Prkar1a genotyping	94°C	5 minutes	1
	94°C	30 seconds	
	54°C	30 seconds	35
	72°C	1 minutes	
	72°C	5 minutes	1
	4°C	∞	
Prkaca WT allele genotyping	94°C	5 minutes	1
	94°C	30 seconds	
	58°C	45 seconds	35
	72°C	1 minutes	
	72°C	5 minutes	1
	4°C	∞	
Prkaca neo-inserted allele genotyping	94°C	5 minutes	1
	94°C	30 seconds	
	58°C	30 seconds	35
	72°C	40 seconds	
	72°C	5 minutes	1
	4°C	∞	
Prkar2b WT allele genotyping	94°C	3 minutes	1
	94°C	30 seconds	
	65℃ (-0.5°C per cycle)	50 seconds	24
	72°C	45 seconds	
	94°C	30 seconds	
	53°C	50 seconds	24
	72°C	45 seconds	
	72°C	5 minutes	1
	4°C	∞	
Prkar2b neo-inserted allele genotyping	94°C	5 minutes	1
	94°C	30 seconds	
	67℃ (-0.5°C per cycle)	50 seconds	16
	72°C	45 seconds	
	94°C	30 seconds	
	59°C	50 seconds	30
	72°C	45 seconds	
	72°C	5 minutes	1
	4°C	∞	

Table 2.1 The PCR conditions for *Prkar1a*, *Prkaca* and *Prkar2b* genotyping

2.4 Loss of heterozygosity (LOH) analysis

The presence of *Prkar1a* and *Prkaca* allele was detected in both peripheral and tumor DNA by PCR. *Prkar1a* allele was detected by primers 5'-ATTCCCTGGGAATTGTGAGT-3' and 5'-TAGGCTCAGAAAGTCACTGCA-3'; while *prkaca* allele was detected by primers 5'-AAACTCACACACACAGAGACAACA-3' and 5'- GCCCCAGTGTGACTAAGGAG-3'.

2.5 Mouse numbers, necropsies, phenotyping

A total of 84 *Prkar1a*$^{+/-}$*Prkaca*$^{+/-}$, 126 *Prkar1a*$^{+/-}$, 114 *Prkaca*$^{+/-}$, and 96 control (wild-type, WT) littermate mice were handled for the purposes of this project over three years. For this experiment, complete phenotyping that included all aspects of bone development at various ages (up to 18 months of age) received 42 *Prkar1a*$^{+/-}$*Prkaca*$^{+/-}$, 34 *Prkar1a*$^{+/-}$, 8 *Prkaca*$^{+/-}$, 23 *Prkar2b*$^{+/-}$, 39 *Prkar1a*$^{+/-}$ *Prkar2b*$^{+/-}$ mice and 24 WT mice from the corresponding litters, as determined after genotyping.

2.6 X-ray

Radiographs of the tail were taken using the Faxitron x-ray system (Model MX-20). The X-ray tube was set at 40 seconds 30kv. Kodak, Portal Pack, PPL film

(SourceOne Healthcare Technology, San Diego, CA) and was placed at the bottom of unit and the carcass in the plastic tray was put 4 inches above the film.

2.7 Microcomputed tomography (µCT)

µCT analysis of caudal vertebrae at 8µm resolution was performed using a GE Medical Systems eXplore Locus SP µCT scanner (GE Medical Systems, London, ON, Canada). Tissue mineral density (TMD) was calculated on a 1.52 mm thick cortical slice of the diaphysis using GE Health Care MicroView ABA 2.2 software (GE Medical Systems, London, ON, Canada).

2.8 Raman microspectroscopy (RMS)

Longitudinal, radial cryo-sections (15 µm) of affected and unaffected caudal vertebrae from 6 months old *Prkar1a*$^{+/-}$*Prkaca*$^{+/-}$ mouse were hydrated in sub-saturating CsCl, 10mM HEPES, pH7.4, placed between quartz slides and examined in a confocal Raman microscope (Senterra, Bruker Optics Inc.). Bright-field and polarized transmission images were collected with a 10X/0.3NA objective. Raman spectra were collected from 2x2 µm spots at extracellular matrix with 10-15cm^{-1} resolution using a 40X/0.95NA objective, 50 µm pinhole, and 532 nm / 9 mW depolarized excitation laser. The mineral/matrix ratio was evaluated from the ratio of spectral peaks of $v_1PO_4^{3-}$stretching vibration of mineral phosphate (922-983cm^{-1}) and CH stretching vibrations in organic

molecules (2820-3020 cm^{-1}) after subtracting baseline, water, and quartz contributions.

2.9 Haematoxylin and Eosin (H&E) staining

Bone tissues were removed from mice and fixed in 4% paraformaldehyde for 48 hours then transferred to 8% formic acid solution (Decalcifier I, Surgipath Medical Industries, Inc., Richmond, IL) for 24-48 hours. After that, they were rinsed in tap water for 10 minutes and processed through a series of alcohol and xylene and embedded in paraffin. 5μm bone sections were cut from paraffin-embedded blocks. The slides were subjected to deparaffinization, followed by washing with distilled water. The slides were stained with hematoxylin and eosin.

2.10 Primary cultures of mouse bone tumors

Tumors or vertebral bones were removed from mice and minced into small fragments. These fragments were incubated with collagenase A (Sigma, St. Louis, MO) at 37°C for 15 minutes. The digested fragments were then centrifuged at 360xg for 5 minutes and washed twice with PBS. The pelleted cells and fragments were cultured in a 25cm^2 flask with DMEM supplemented with 20% fetal bovine serum (Hyclone, Logan, UT) and 1x antibiotic-antimycotic (Invitrogen, Carlsbad, CA). Medium was refreshed at 3 day intervals. After 10 days, primary tumors cells attached to the flask were harvested and plated in

75cm^2 flask. The primary cells were then used for protein extraction and FACS study.

2.11 Microarray and real-time quantitative real-time PCR (RT-QPCR) analysis

mRNA was isolated from normal caudal vertebrae of WT, *Prkaca*$^{+/-}$ mice and caudal vertebrae lesions of *Prkar1a*$^{+/-}$ and *Prkar1a*$^{+/-}$*Prkaca*$^{+/-}$ mice by Trizol extraction (Invitrogen, Carlsbad, CA). The quality of total RNA samples was assessed using an Agilent 2100 Bioanalyzer (Agilent Technologies, Palo Alto, CA). Microarray experiments were performed as described (148). Briefly, 0.5μg of total RNA from each sample was amplified and transcribed to cDNA, which was then used to generate single strand biotin-labeled cRNA. A total of 0.85μg of cRNA was hybridized to Illumina MouseRef-8 v2.0 Expression BeadChips (Illumina, San Diego, CA). The hybridized biotinylated cRNA was detected with streptavidin-Cy3 and quantitated using Illumina's Bead-Station 500GX Genetic Aalysis System scanner. Array data was analyzed as previously described (149). The raw and normalized array data have been deposited in National Center for Biotechnology Information's Gene Expression Omnibus (GEO) and are accessible through GEO Series accession number GSE20984. For RT-QPCR analysis, total mRNA (750ng) was reverse-transcribed using High Capacity RNA-to-cDNA Kit (Applied Biosystems, Foster City, CA). RT-QPCR was performed using Applied Biosystems 7500 real-time PCR system. *Runx2* mRNA expression

level was detected by using Power SYBR® Green PCR Master Mix (Applied Biosystems, Foster City, CA) and primers 5'-AGCGGACGAGGCAAGAGTTT-3' and 5'-TGGGTTCTGAGGCGGGACA-3'. Adenylate cyclases mRNA expression levels were detected using Taqman Gene Expression Assay (Applied Biosystems, Foster City, CA): *Adcy1* (Mm01187829_m1), *Adcy6* (Mm00475772_m1), *Adcy9* (Mm00507743_m1). Gene expression data on Wnt and osteogenesis pathway were performed using Wnt-signaling pathway PCR array (SABiosciences, Frederick, MD) and osteogenesis pathway PCR array (SABiosciences, Frederick, MD). The relative expression of each transcript against WT tail tissue was calculated using *Gapdh* (Taqman Rodent Gapdh control, Applied Biosystems, Foster City, CA) as standard and $2^{-\Delta\Delta CT}$ method (150).

2.12 Western blot analysis

Tissue lysates were extracted by homogenization in T-PER tissue protein extraction reagent (Thermo Fisher Scientific, Rockford, IL), containing protease inhibitor cocktail I (EMD Biosciences, La Jolla, CA) with subsequent centrifugation at 10,000rpm for 10 minutes at 4°C. Protein concentration was determined by BCA protein assay (Thermo Fisher Scientific, Rockford, IL). Twenty micrograms of protein diluted in deionized water were mixed with NuPAGE® 4X LDS sample buffer (Invitrogen, Carlsbad, CA), and then boiled for 10 min at 70°C, and run on NuPAGE®Novex® Bis-tris gel (Invitrogen, Carlsbad,

CA). Protein was transferred onto a 0.45-μm nitrocellulose membrane. The membrane was blocked with TBS containing 5% nonfat dried milk and 1% Tween 20. Proteins were detected with primary antibodies against the target proteins (Table 2) and horseradish peroxidase–conjugated secondary antibodies against rabbit IgG (1:4000) (Thermo Fisher Scientific, Rockford, IL). All antibodies were diluted in 1% nonfat dried milk in TBS-Tween 20. Bands were detected by enhanced chemiluminescence reagent (PerkinElmer, Waltham, MA).

2.13 Immunohistochemistry

All immunohistochemistry was performed at Histoserve, Inc. (Germantown, MD). Briefly, 5μm bone sections were cut from paraffin-embedded blocks. The slides were subjected to deparaffinization, followed by washing with distilled water. The slides were then pretreated at 85°C for 20 minutes with subsequence hydrogen peroxidase and bovine serum albumin blocking. Our target proteins were detected with corresponding primary and secondary antibody (Table 2) from which the signal was developed by binding with horseradish peroxidase–conjugated streptavidin.

2.14 Immunofluorescence

Immunofluorescence was performed after dewaxing, rehydration and permeabilization; in control sections, rabbit IgG was used instead of primary

antibody. The bone sections were detected using anti-Runx2 antibody at 1:100 dilution and Alexa488-tagged anti-rabbit secondary antibody (Invitrogen, Carlsbad, CA), and the section was then mounted with hard set mounting media (Vector Lab, Burlingame, CA). Images were collected using a Leica SP2 Confocal microscope and Leica LSC acquiring software (Leica Microsystems Inc, Deerfield, IL).

2.15 Flow cytometry

Primary cells from bone tumors (1x 10^5) were collected from cultures and fixed using BD Cytofix/Cytoperm™ Fixation/Permeabilization Solution Kit (BD biosciences, San Jose, CA). The fixed cells were then washed with wash buffer. After that, primary antibody (Suppl. Table 4) was used for staining at 4°C for 30 minutes. The cells were washed again and stained with FITC-tag secondary antibody (1:250) at 4°C for 30 minutes.The stained cells were ready for flow cytometry analysis. The cells were stained with vimentine, foxo1, c-fos, c-kit, runx2, collagen 1. MC3T3 (ATCC CRL-2593), which is a preosteoblast cell line, was used as control cell. For staining with cd44, cd45, cd90 and vcam, the cells were collected and washed with staining buffer (phosphate-buffered saline supplemented with 2% normal mouse serum; Gemini Bioproducts, West Sacramento, CA). After that, the cells were stained with APC, PE or FITC-tagged primary antibodies (Table 2). The cells were washed again and then were ready for analysis. Data were acquired on an LSRII flow cytometer (BD Biosciences)

equipped with 355, 407, 488, 532, and 638 nm laser lines using DIVA 6.1.2 software (BD Biosciences), and analyzed with FlowJo version 8.7.3 (Tree Star, Ashland, OR) (151).

2.16 Serum Matrix Metalloproteinase 9 (Mmp9) level measurement

Mouse Mmp9 concentration in serum was measured by using Quantikine Mouse MMP-9 (total) Immunoassay kit (R&D system, Minneapolis, MN). The assay was performed according to the manufacturer's instructions. Briefly, diluted serum samples were incubated in Mmp9 pre-coated microplate for 2 hours at room temperature. The samples were then removed and each well was washed four times with the wash buffer provided. After washing, an enzyme-linked polyclonal antibody specific for mouse Mmp9 was added and incubated for 30 minutes at room temperature. A substrate solution was then added for color development. Optical density at 450nm of each well was measured.

2.17 PKA activity

PKA enzymatic activity was measured by a method described previously (152). The assays were carried out in a total volume of 50 μL for 15 minutes at 37°C in the reaction mixture containing 50 mmol/L Tris-HCl (pH 7.5), 5 mmol/L DTT, 10 mmol/L $MgCl_2$, 60 μmol/L Kemptide (a phosphate acceptor peptide; Leu-Arg-Arg-Ala-Ser-Leu-Gly), 20 μmol/L [γ-32P]ATP (25 Ci/mmol), with or without 5 μmol/L

cAMP and 10 μL of the tissue extracts. After incubation, the reaction mixtures were spotted onto 0.23-mm phosphocellulose discs and washed three times in 0.5% phosphoric acid. Filters were air dried and counted by liquid scintillation counter. Total kinase activity represented enzymatic activity after stimulation with cAMP. Statistical analysis of comparisons between groups was undertaken using a two-sample t-test; differences were considered significant at $P < 0.05$.

2.18 cAMP assay

Levels of cAMP were determined by ^{3}H Biotrak Assay System (Amersham Biosciences, Piscataway, NJ). All procedures were carried out according to the manufacturer's instructions. The presented values represent the average of three independent experiments.

2.19 PDE activity

Phosphodiesterase activity was assayed with [H^3]-cAMP by the method described previously (153) with modifications. Incubation mixture (total volume 200 ml) contained 10 mM Tris-HCl (pH 7.5), 10 mM $MgCl_2$, 0.1 mM cAMP (2.5 mCi/mmol). Incubations were performed at 37°C for 30 minutes. Reactions were stopped by cooling rapidly down to 5°C, with subsequent addition of 100 mL of 0.17 M $ZnSO_4$ and 100 mL of 0.15 M $Ba(OH)_2$. In this procedure, precipitation of adenosine, inosine, hypoxantine and inorganic phosphate was achieved by 97%

and cAMP did not precipitate. Precipitate was removed by centrifugation (6,000xg, 5 min) and 100 mL of supernatant, which contained cAMP, was placed in scintillation liquid and counted.

2.20 DEAE-cellulose chromatography

This experiment was performed as described (154). Briefly, primary cells derived from either normal tissues or lesions were homogenized in 5mL of lysis buffer (10 mM Tris/HCl, 1 mM EDTA, 1 mM dithiothreitol and protease inhibitor cocktail I (EMD Biosciences, La Jolla, CA)) and then kept on ice for 10 minutes. The lysates were centrifuged at 10,000g for 10 minutes. Protein concentration of the supernatants was determined by measuring the absorbance at 280nm. A total of 2.5 mg of protein from each sample was loaded on the pre-equilibrated DEAE column with 10 mM Tris/HCl, pH7.1, containing 1 mM EDTA and 1 mM phenylmethylsulfonly fluoride. The column was developed with 0 to 350mM NaCl gradient at a flow rate of 15 mL/hr. 2-ml fractions were collected on ice and assayed for protein kinase activity as described above.

2.21 Statistical analysis

Statistical analysis on bone tumor frequency was performed using a log rank test. A two-sample t-test was done for the rest of the experiments. Experiments were

done at least in triplicate and a mean was calculated and presented. A $P < 0.05$ was considered significant.

Antibody	Company	Dilution
Acp5	Abnova (H00000054-D01P)	1:100 (IHC)
Adcy1	Abcam (ab69597)	1:1000 (WB)
Adcy6	Abcam (ab14781)	1:1000 (WB)
Adcy9	Abcam (ab14783)	1:1000 (WB)
Brachyury	Abcam (ab20680)	5μg/ml (IHC)
Cathepsin K	Abcam (ab19027)	1:100 (IHC)
Cd44/APC	eBioscience (17-0441)	1:200 (Flow cytometry)
Cd45/PE	Miltenyi (130-091-610)	1:200 (Flow cytometry)
Cd90/FITC	Abcam (ab25672)	1:200 (Flow cytometry)
c-fos	Santa Cruz (sc-253)	1:100 (IHC); 1μg (Flow cytometry)
c-kit	Abcam (ab5506)	1μg (Flow cytometry)
Collagen 1	Abcam (ab34710)	1μg (Flow cytometry)
Cytokeratin 18	Abcam (ab32118)	1:100 (IHC)
Cα	Santa Cruz (sc-903)	1:2500 (WB); 1:100 (IHC)
Cβ	Santa Cruz (sc-904)	1:1000 (WB); 1:100 (IHC)
Cγ	Santa Cruz (sc-905)	1:1000 (WB); 1:100 (IHC)
E-cadherin	Abcam (ab53033)	1/250 (IHC)
Foxo1	Abcam (ab39670)	1:100 (IHC); 1μg (Flow cytometry)
Gapdh	Abcam (ab9485)	1:10000 (WB)
Mmp2	Santa Cruz (sc-10736)	1:1000 (WB)
Mmp9	Santa Cruz (sc-10737)	1:1000 (WB)
N-cadherin	Abcam (ab12221)	10μg/ml (IHC)
Osteocalcin	Santa Cruz (sc-30045)	1:100 (IHC)
Pde4d	Abcam (ab14613)	1:1000 (WB)
Pde7a	FabGennix (PD7A-100P)	1:1000 (WB)
Pde11a	Abcam (ab14624)	1:1000 (WB)
p-RII	Epitomics (1151-1)	1:1000 (WB)
Prkx	Gift from Dr. Robert M. Kotin (NHLBI, NIH, Bethesda, MD)	1:1000 (WB); 1:100 (IHC)
RIα	Abcam (ab38936)	1:1000 (WB); 1:100 (IHC)
RIIα	Santa Cruz (sc-909)	1:2500 (WB); 1:100 (IHC)
RIIβ	Santa Cruz (sc-25424)	1:1000 (WB); 1:100 (IHC)
Runx2	Santa Cruz (sc-10758)	1:1000 (WB) 1μg (Flow cytometry)
Vcam-1/Alexa 647	eBioscience (51-1061)	1:200 (Flow cytometry)
Vimentin	Abcam (ab45939)	1:700 (IHC); 1μg (Flow cytometry)

Table 2.2 List of antibodies used in the present study.

Chapter Three

Phenotypic Characterization of Mice Deficient in Protein Kinase A Regulatory Subunit Type 1A (*prkar1a*) and Catalytic Subunit A (*prkaca*)

3.1 Generation of *Prkar1a$^{+/-}$Prkaca$^{+/-}$* double heterozygous mice

All mice were bred into a mixed C57BL/6x129Sv/B6 hybrid background, because the C57BL/6 background favored the reproduction and survival of *Prkaca$^{+/-}$* mice (62). Genomic DNA extracted from tail tips were used for genotyping that helped to confirm the generation of *Prkar1a$^{+/-}$Prkaca$^{+/-}$* double heterozygous mice. Genotypings were performed by polymerase chain reaction (PCR) using the conditions described in the Materials and Methods chapter. The products of PCR were analyzed in 1% DNA agarose gel (Figure 3.1).

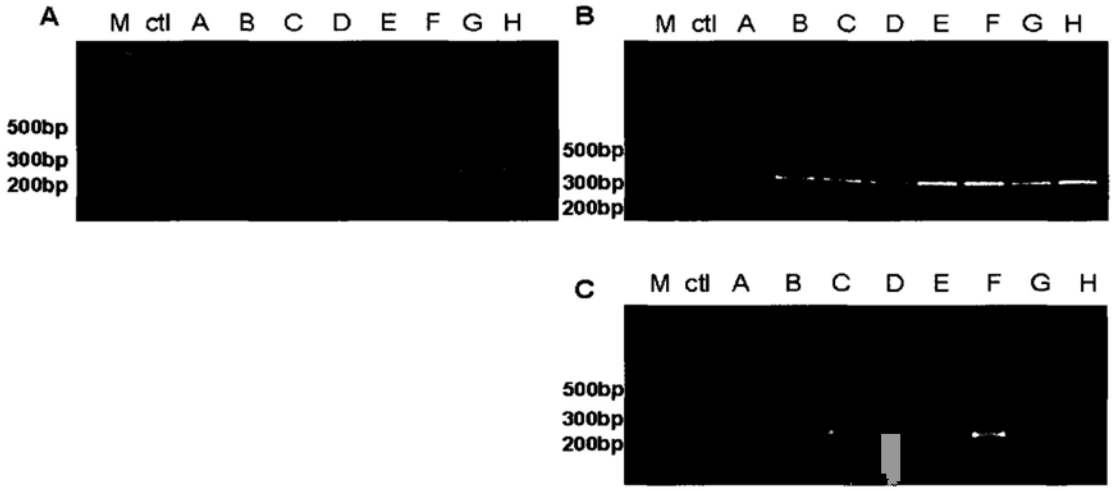

Figure 3.1 Genomic PCR experiments were used for the genotyping of *prkar1a* and *prkaca* genes in mice. (**A**) Genotyping of *prkar1a*, (**B**) Genotyping of *prkaca* WT allele and (**C**) Genotyping of *prkaca* KO allele in animal A-H using the primers described in Material and Methods. Taken together, Animal A had the genotype *prkar1a$^{+/+}$/prkaca$^{+/+}$*; Animal B had the genotype *prkar1a$^{+/-}$/prkaca$^{+/+}$*; Animal C had the genotype *prkar1a$^{+/-}$/prkaca$^{+/-}$*; Animal D had the genotype *prkar1a$^{+/-}$/prkaca$^{+/+}$*; Animal E had the genotype *prkar1a$^{+/-}$/prkaca$^{+/+}$*; Animal F had the genotype *prkar1a$^{+/-}$/prkaca$^{+/-}$*; Animal G had the genotype *prkar1a$^{+/+}$/prkaca$^{+/+}$*; Animal H had the genotype *prkar1a$^{+/+}$/prkaca$^{+/-}$*. M, 100bp ladder; ctl, negative control.

3.2 Phenotypic analysis of *Prkar1a$^{+/-}$Prkaca$^{+/-}$* double heterozygous mice

After the confirmation of genotypes, 34 *Prkar1a$^{+/-}$*, 8 *Prkaca$^{+/-}$* and 42 *Prkar1a$^{+/-}$Prkaca$^{+/-}$* mice at various ages (up to 18 months of age) were subjected to complete phenotyping. 24 control (wild-type, WT) mice were used from the same litter and were matched for age.

None of the *Prkar1a$^{+/-}$Prkaca$^{+/-}$* mice showed schwannomas or thyroid tumors that were found, as previously reported (57), in the *Prkar1a$^{+/-}$* mice. In the population of mice from the present study, *Prkar1a$^{+/-}$* (32.4%) also had eosinophilic cellular alteration (Figure 3.2A, B) in the liver; and two 18 month-old *Prkar1a$^{+/-}$* mice developed hepatocellular adenoma (Figure 3.2C, D) that were not found in *Prkar1a$^{+/-}$Prkaca$^{+/-}$* mice.

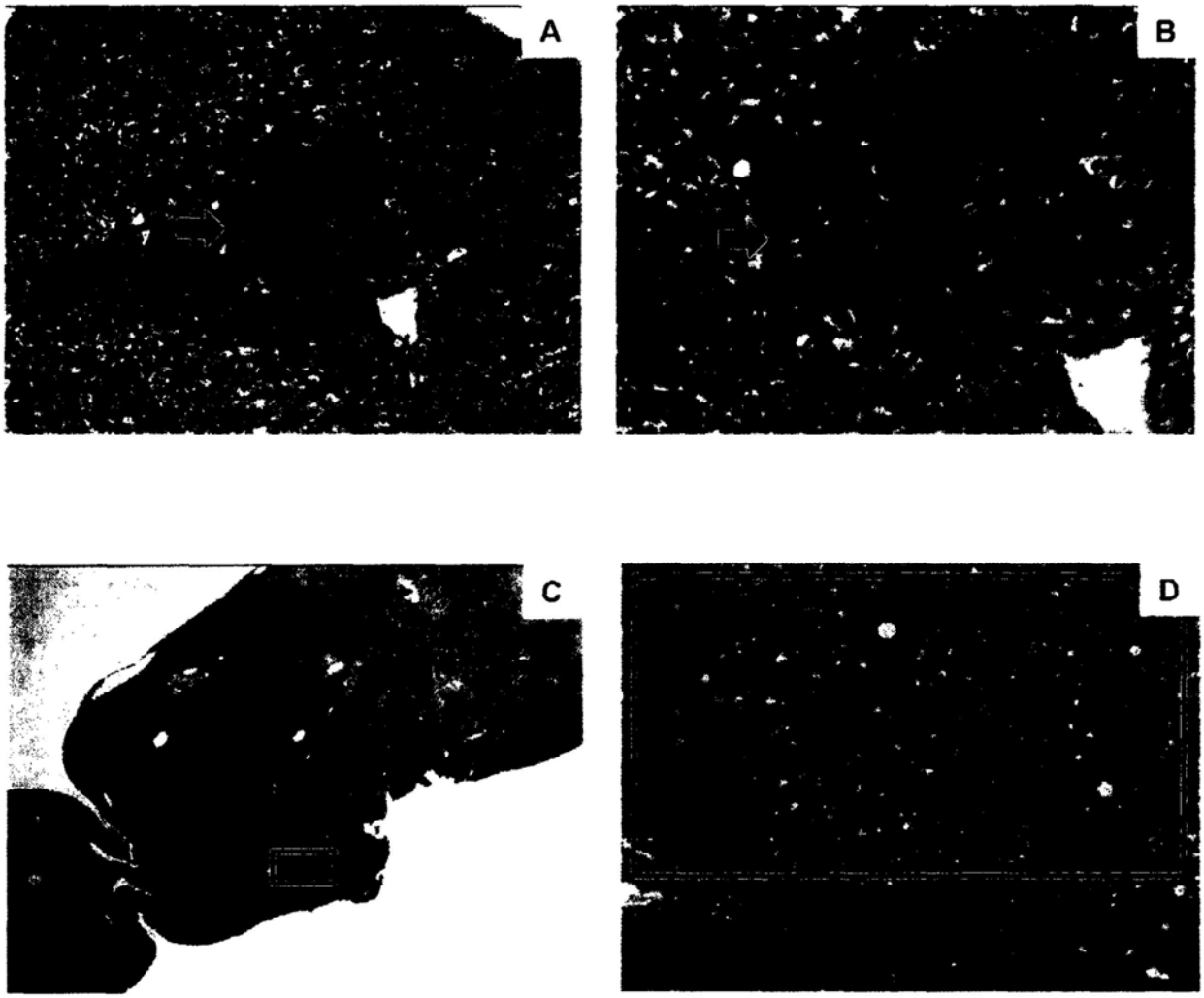

Figure 3.2 Representative views of liver eosinophilic cellular alteration and hepatocellular adenoma in *Prkar1a*$^{+/-}$ mice. (**A,B**) Haematoxylin and eosin (H&E) staining of sections of liver from 14-month old *Prkar1a*$^{+/-}$ mouse. Black arrow denote the presence of eosinophilic focus. (A) Original magnification, 20x. (B) Original magnification, 40x. (**C,D**) H&E staining of sections of liver from 18-month old *Prkar1a*$^{+/-}$ mouse. (C) Area under square was looked under high magnification and showed in panel D. (Original magnification, 2x). (D) Square indicates the presence of hepatocellular adenoma. (Original magnification, 20x).

Twenty out of 42 *Prkar1a$^{+/-}$Prkaca$^{+/-}$* mice (47.6%) and 15 out of 34 *Prkar1a$^{+/-}$* mice (44.1%) developed subcapsular hyperplasia (Figure 3.3) in adrenal when compared to 7 out of 24 (29.1%) WT mice. This phenotype associated with WT mice was age-related incidental finding. This indicates that *prkar1a* haploinsufficiency is sufficient to increase the frequency of adrenal hyperplasia in mice.

Prkar1a$^{+/-}$Prkaca$^{+/-}$ mice developed *pars distalis* cysts (Figure 3.4A, B) in pituitary (14.3%) that were only found in three *Prkar1a$^{+/-}$* mice (8.8%). One of the *Prkar1a$^{+/-}$Prkaca$^{+/-}$* mice at 12 months of age also developed *pars intermedia* hyperplasia (Figure 3.4C, D) in pituitary, indicating that, instead of obrogating the development of tumors, reduction of Cα induces the development of pituitary hyperplasia.

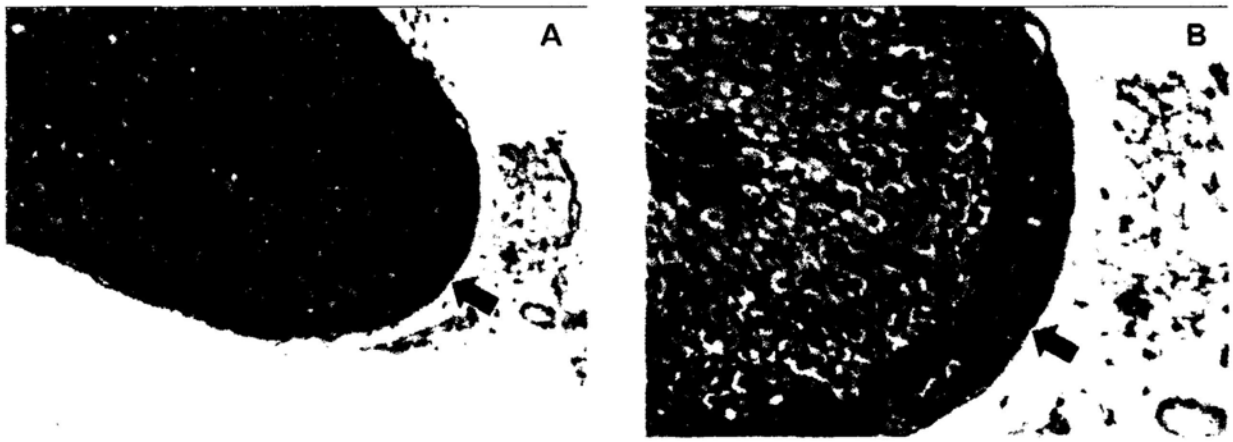

Figure 3.3 Representative views of adrenal subcapsular hyperplasia. (**A,B**) H&E staining of the sections of adrenal from 9-month old *Prkar1a$^{+/-}$Prkaca$^{+/-}$* mouse. Black arrows denote the presence of subcapsular hyperplasia. (A) Original magnification 20x. (B) Original magnification 40x.

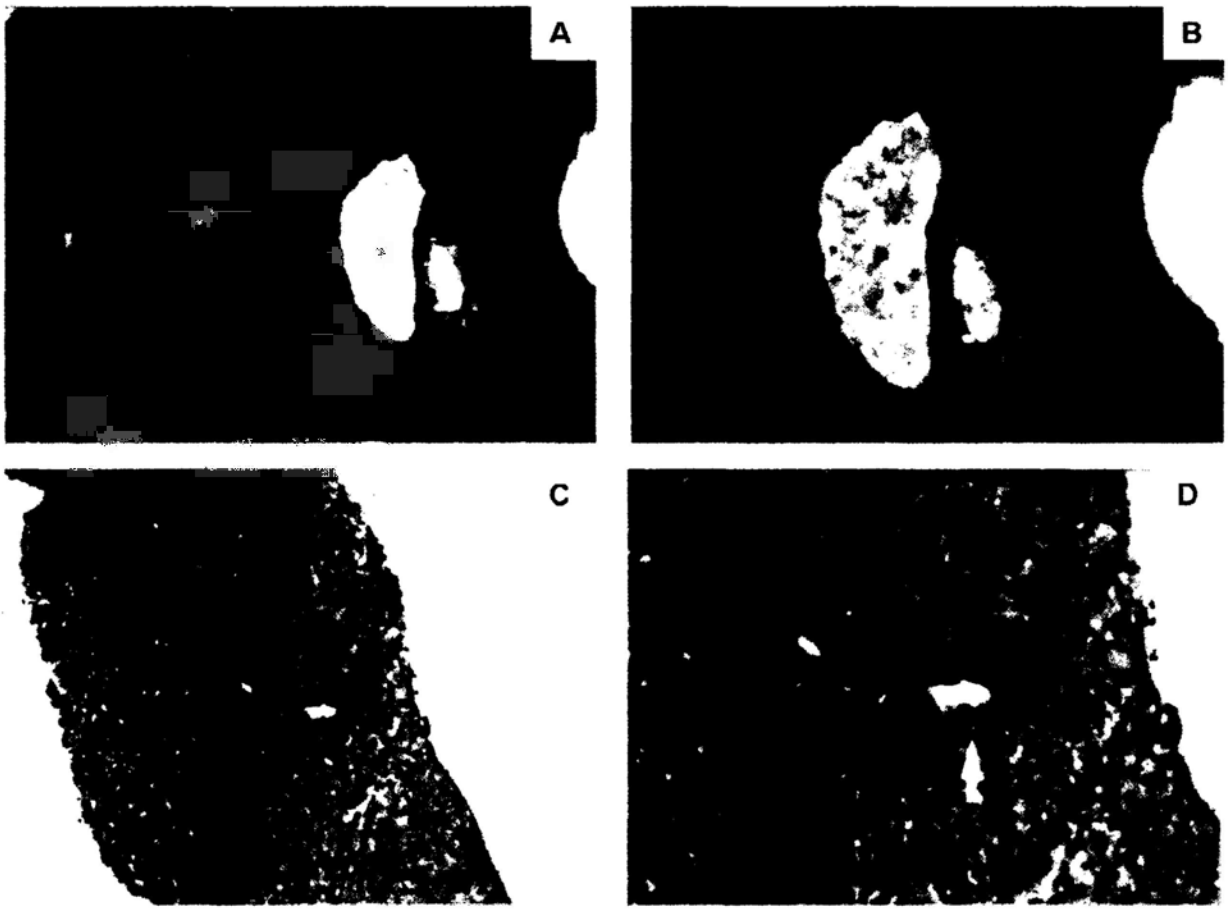

Figure 3.4 Representative views of pars distalis cysts and pituitary hyperplasia. (**A, B**) H&E staining of the section of pituitary from 9-month old *Prkar1a$^{+/-}$Prkaca$^{+/-}$* mouse, showing a typical pars distalis cysts. (A) Original magnification 40x. (B) Original magnification 60x. (**C, D**) H&E staining of the section of pituitary from 12-month old *Prkar1a$^{+/-}$Prkaca$^{+/-}$* mouse, showing a typical pituitary hyperplasia. (C) Original magnification 20x. (D) Original magnification 40x.

Previous data showed that about 50% of *Prkar1a*$^{+/-}$ mice in the 129Sv/B6 background developed osteomyxomas in the caudal vertebrae (tail bone) by 8 months of age, a number that increased to 100% by one year (57, 144). This number was apparently lower in the mixed C57BL/6x129Sv/B6 background for the *Prkar1a*$^{+/-}$ mice (Figure 3.5A), indicating that the intensity of this phenotype varies with the genetic background. Multiple bone lesions (osteomyxomas) were also observed in *Prkar1a*$^{+/-}$*Prkaca*$^{+/-}$ mice and they first appeared at 4-5 months of age. Ninety percent of *Prkar1a*$^{+/-}$*Prkaca*$^{+/-}$ mice exhibited these lesions by 6 months, and 100% by 9 months. Radiographs of the tails showed radiolucent masses that suggested that non-ossified lesions were growing into normal bone (Figure 3.5B). *Prkar1a*$^{+/-}$*Prkaca*$^{+/-}$ mice not only developed these lesions earlier but also showed an increased number of lesions when compared to the age-matched *Prkar1a*$^{+/-}$ mice (Figure 3.5A).

Interestingly, *Prkar1a*$^{+/-}$*Prkaca*$^{+/-}$ mice also developed other types of bone lesions that were less frequently found in *Prkar1a*$^{+/-}$ mice. First, a single, male 3 month-old *Prkar1a*$^{+/-}$*Prkaca*$^{+/-}$ mouse developed a tibial chondroma (Figure 3.6), a tumor analogous to what is seen in CNC patients (48); more than 26 *Prkar1a*$^{+/-}$ mice have been phenotyped at the ages of 2-3 months and there were never any tumors or any other bony lesions at this age. Second, four out of 30 *Prkar1a*$^{+/-}$ *Prkaca*$^{+/-}$ mice (13%) (*vs* 1 out of 34 *Prkar1a*$^{+/-}$ mice) developed osteochondromyxoma (OCM) (Figure 3.7A, B), a tumor that was histologically similar to the bony lesions that have been reported in association with CNC (48). Third, cartilaginous hyperplasia, chondromas and osteochondrodysplasia were

observed in marrow cavities of about 1/3 of the long bones (femur, tibia) (Figure 3.7C, D) and in most of the vertebral bodies (up to 23% of the spinal column) (Figure 3.7E, F) of the *Prkar1a*$^{+/-}$*Prkaca*$^{+/-}$ mice (*vs* 2 out of 34 *Prkar1a*$^{+/-}$ mice).

Three metastatic chondrosarcomas developed in *Prkar1a*$^{+/-}$ mice that were 6 and 16 month-old, and one *Prkar1a*$^{+/-}$*Prkaca*$^{+/-}$ mouse that was 14 month-old; in all cases the most likely primary sites were hind-limb masses, and metastases were renal and lung, respectively (Figure 3.8).

Like in the previous studies from Dr. Stratakis' laboratory (57, 144), we did not observe any gender differences in the incidence of bone lesions. Blood cell counts and biochemical values (i.e. total and ionized calcium, phosphate, and others) were within normal range, with the exception of elevated alkaline phosphatase (ALP) level in *Prkar1a*$^{+/-}$*Prkaca*$^{+/-}$ mice (Table 3.1 and Figure 3.9).

These data suggested that the reduction of *prkar1a* under p*rkaca* haploinsufficiency background can obrogate the development of tumors from thyroid follicles and Schwann cells; unexpectedly, however, *prkar1a* and *prkaca* haploinsufficiency has prominent effects on adult bone development, although not on prenatal skeleton development. The following studies aimed at identifying the origin and type of abnormal cells contributing to the growth of bone tumors.

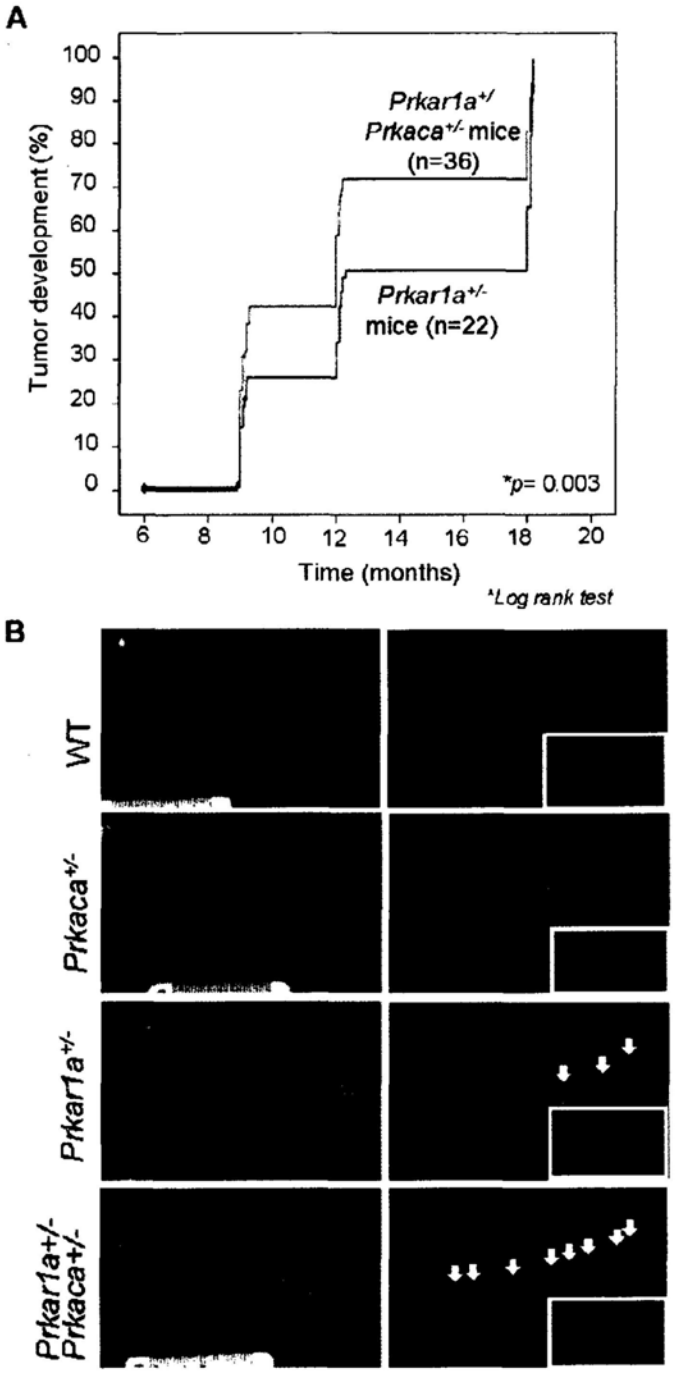

Figure 3.5 Development of vertebral bone lesions of the caudal vertebrae from *Prkar1a*$^{+/-}$ and *Prkar1a*$^{+/-}$*Prkaca*$^{+/-}$ mice. (**A**)) Kaplan Meier curve shows the number of tail masses found in various ages of *Prkar1a*$^{+/-}$ and *Prkar1a*$^{+/-}$*Prkaca*$^{+/-}$ mice. (**B**) Left panel, comparison of tails from WT, *Prkaca*$^{+/-}$, *Prkar1a*$^{+/-}$ and *Prkar1a*$^{+/-}$*Prkaca*$^{+/-}$ mice at 12 month-old. Right panel, X-ray radiographs of caudal vertebrae of WT, *Prkaca*$^{+/-}$, *Prkar1a*$^{+/-}$ and *Prkar1a*$^{+/-}$*Prkaca*$^{+/-}$ mice at 12 month-old. White arrows point to the lesions.

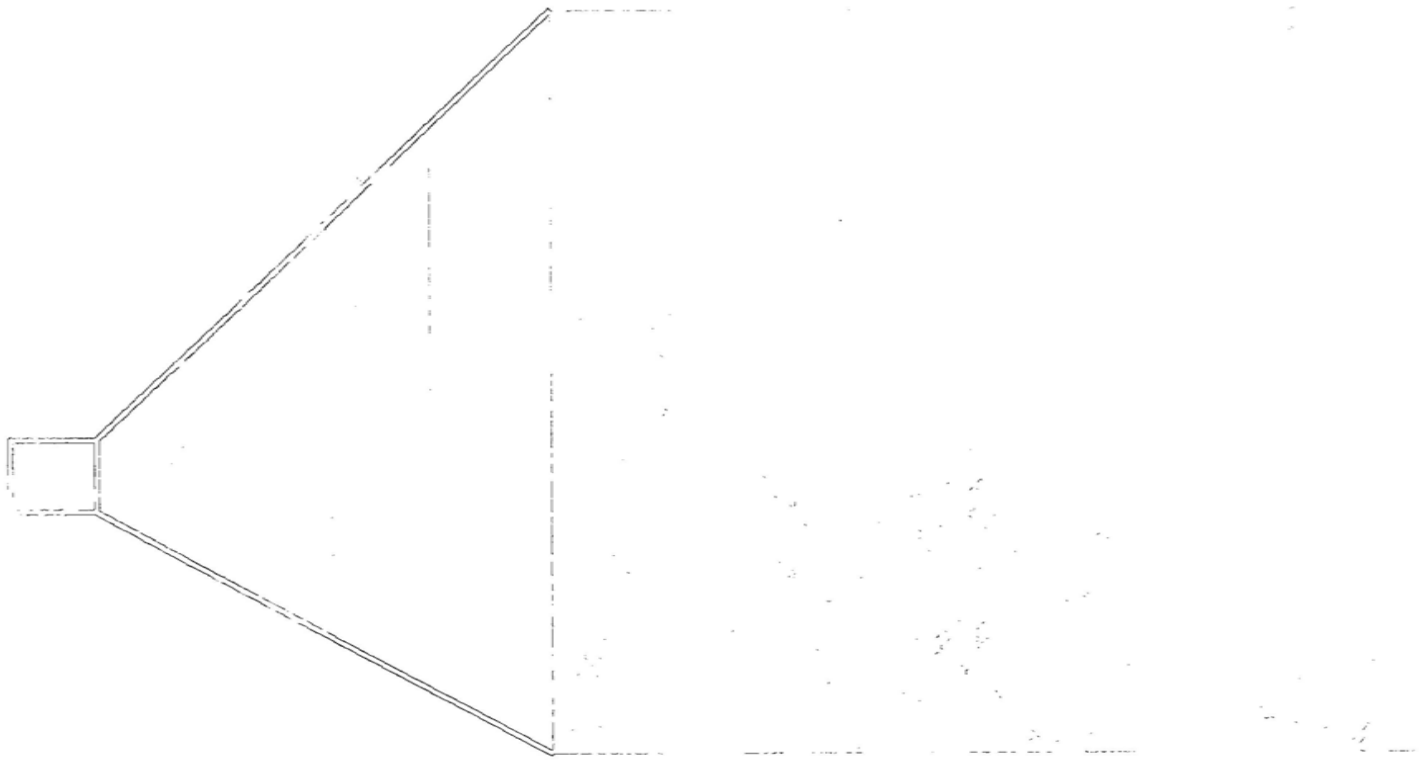

Figure 3.6 Tibial chondroma in a 3 month-old *Prkar1a$^{+/-}$Prkaca$^{+/-}$* mouse. H&E staining of longitudinal sections of tibia. Left panel, original magnification 2x. Right panel, original magnification 20x.

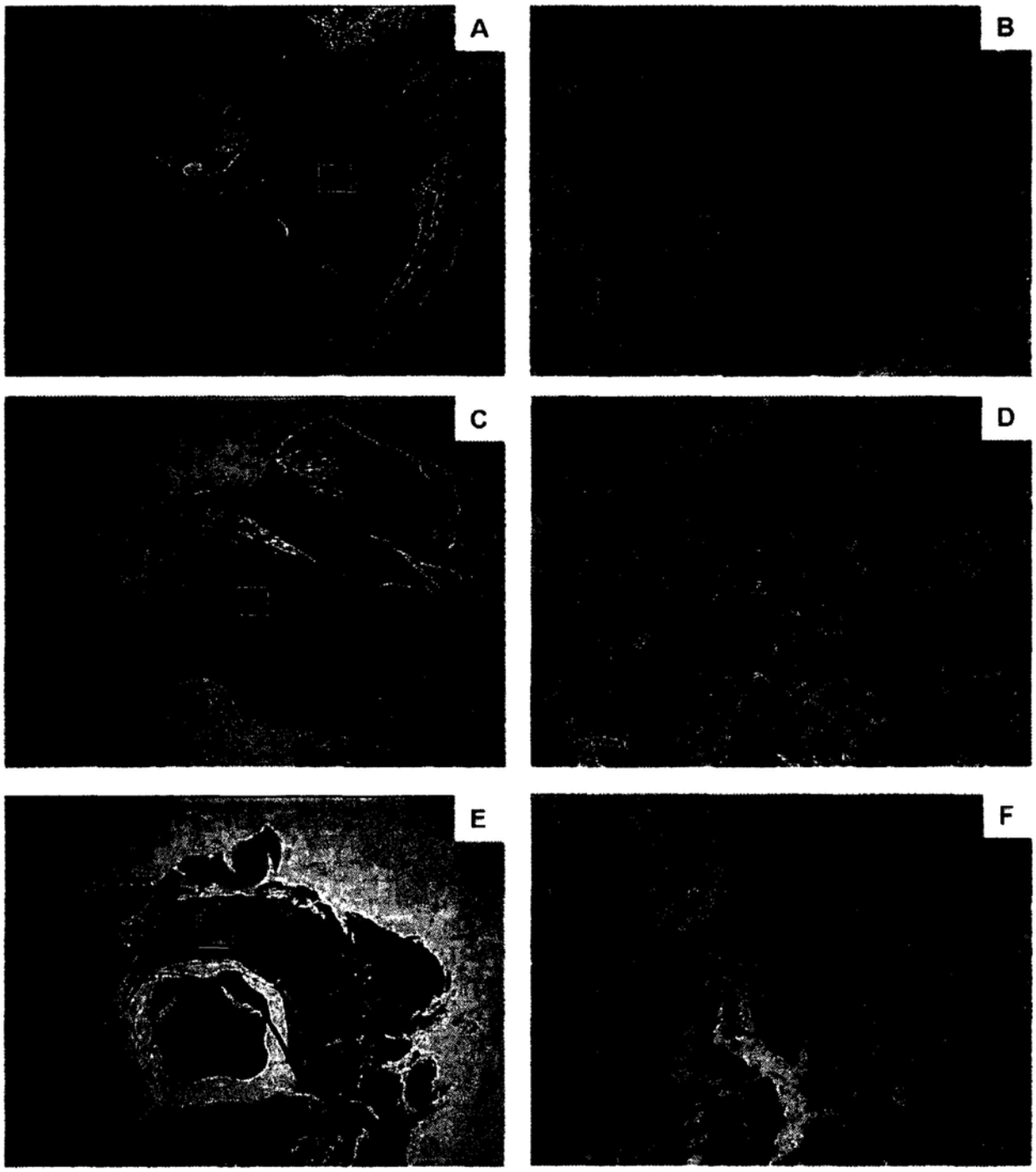

Figure 3.7 Representative views of osteochondromyxoma from caudal vertebrae and chondromas from long bone and spinal column. (**A, B**) H&E staining of longitudinal sections of caudal vertebrae from an 18 month-old *Prkar1a$^{+/-}$Prkaca$^{+/-}$* mouse, showing a typical osteochondromyxoma in *Prkar1a$^{+/-}$Prkaca$^{+/-}$* mouse. (**C, D**) H&E staining of longitudinal sections of femur from an 18 month-old *Prkar1a$^{+/-}$Prkaca$^{+/-}$* mouse, showing a typical chondroma. (**E, F**) H&E staining of longitudinal sections of vertebral bone from an 18 month-old *Prkar1a$^{+/-}$Prkaca$^{+/-}$* mouse, showing a typical chondroma. (A, C, E) Original magnification, 2x. Areas under squares were looked under high magnification and showed in panel B, D and F respectively. (B, D, F) Original magnification, 20x.

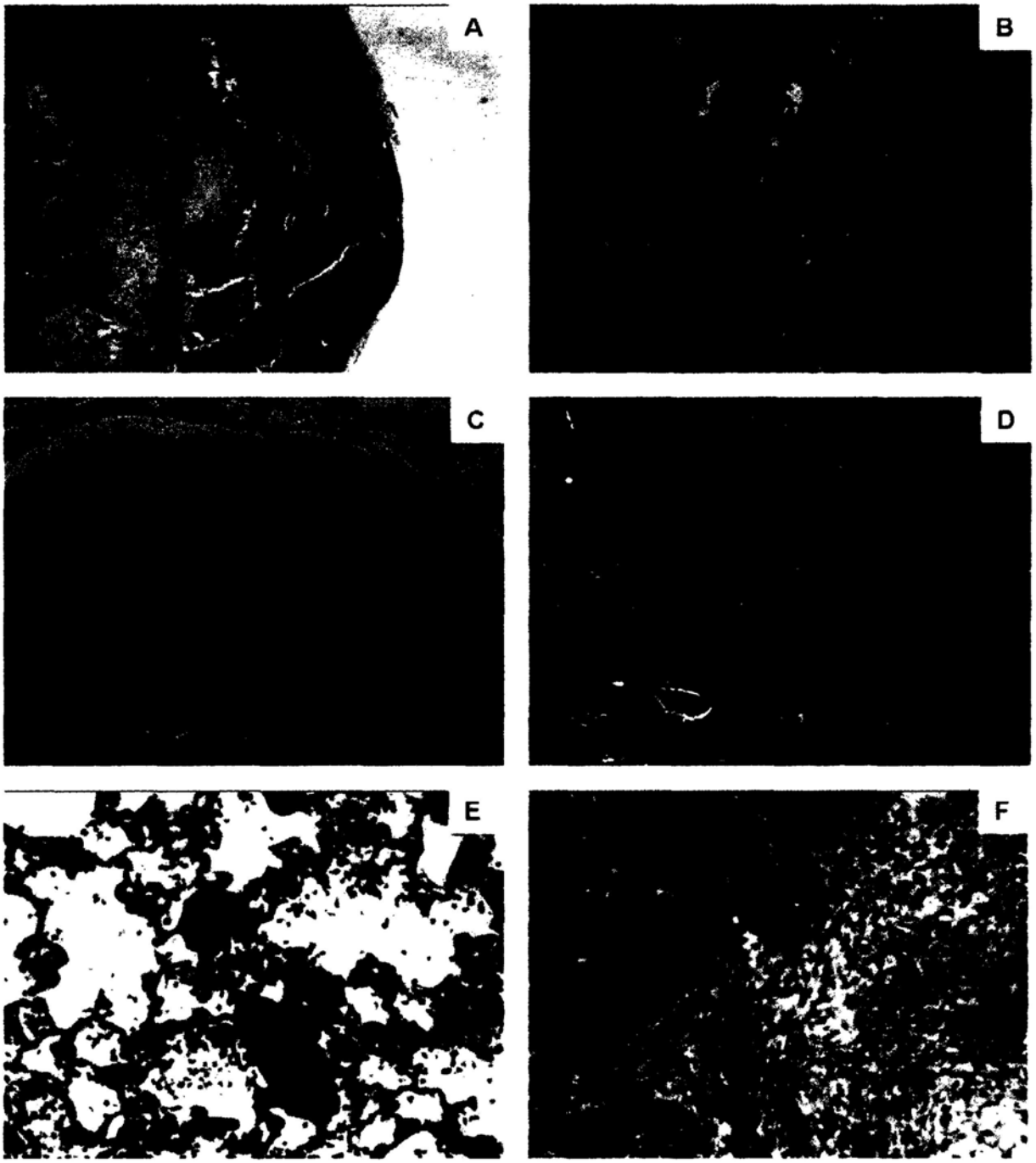

Figure 3.8 Representative views of metastatic sarcoma in *Prkar1a$^{+/-}$* and *Prkar1a$^{+/-}$ Prkaca$^{+/-}$* mouse. (**A, B**) H&E staining of the section of forelimb from a 6 month-old *Prkar1a$^{+/-}$* mouse, showing a chondrosarcoma. (A) Original magnification 2x. (B) Original magnification 40x. (**C, D**) H&E staining of the section of caudal vertebra from a 14 month-old *Prkar1a$^{+/-}$Prkaca$^{+/-}$* mouse, showing a sarcoma. (C) Original magnification 10x. (D) Original magnification 20x. (**E**) H&E staining of the section of lung from a 6 month-old *Prkar1a$^{+/-}$*mouse, showing the metastasis to lung. Original magnification 40x. (**F**) H&E staining of the section of kidney from a 14 month-old *Prkar1a$^{+/-}$ Prkaca$^{+/-}$* mouse, showing the metastasis to kidney. Original magnification 40x.

Genotype	Sex	GLU*	CHOL*	TRIG*	ALB*	Ca*	PHOS*	ALP*	ALT*	AST*	LDH*	CK*	Creatinine
		mg/dL	mg/dL	mg/dL	g/dL	mg/dL	mg/dL	U/L	U/L	U/L	U/L	U/L	mg/dL
WT	M	229	99	74	3	10.2	7	58	32	113	260	-	-
WT	M	269	91	65	2.8	9.2	7.3	72	81	290	752	-	-
WT	M	240	89	57	2.6	10.1	7.3	72	42	74	353	219	0.2
WT	M	190	41	69	2.8	8.8	0.6	10	11	56	16	21	0.2
WT	F	229	64	46	2.8	9.5	7.2	90	29	52	124	51	0.2
WT	F	219	80	59	2.9	10.6	5.4	115	28	157	229	-	-
WT	F	236	93	132	3	13.5	5.7	82	51	76	346	226	0.3
Prkaca$^{+/-}$	M	282	108	91	2.7	10.4	6.9	52	45	56	160	-	-
Prkaca$^{+/-}$	M	197	103	102	2.7	10.7	0	72	49	74	447	-	-
Prkaca$^{+/-}$	M	249	100	104	2.8	8.6	5.7	99	67	168	450	736	0.3
Prkaca$^{+/-}$	F	298	75	130	2.9	9.2	7.1	53	39	61	155	59	0.4
Prkaca$^{+/-}$	F	188	77	118	2.9	12.6	5.7	134	45	198	395	-	-
Prkar1a$^{+/-}$	M	217	94	67	3	10.4	0.1	93	69	93	254	-	-
Prkar1a$^{+/-}$	M	173	68	56	2.4	9.2	6.5	41	30	142	291	762	0.3
Prkar1a$^{+/-}$	F	243	89	61	1.7	-	6.4	77	-	-	-	77	0.2
Prkar1a$^{+/-}$	F	263	57	52	2.7	11.1	6.6	111	35	145	365	673	0.4
Prkar1a$^{+/-}$	F	200	85	73	3	10.5	6	68	49	69	305	142	0.3
Prkar1a$^{+/-}$	F	222	87	68	3	10	0	120	30	79	228	-	-
Prkar1a$^{+/-}$	F	221	66	67	2.6	10.8	6.4	71	24	93	498	283	0.3
Prkar1a$^{+/-}$ Prkaca$^{+/-}$	M	243	127	84	3.1	11.7	7.1	139	65	95	253	-	-
Prkar1a$^{+/-}$ Prkaca$^{+/-}$	M	214	88	46	2.7	10.5	7.5	95	47	212	638	-	-
Prkar1a$^{+/-}$ Prkaca$^{+/-}$	M	256	107	99	3	9.2	5.3	111	66	62	217	108	0.2
Prkar1a$^{+/-}$ Prkaca$^{+/-}$	M	251	110	62	3	9.2	6.1	195	49	85	204	251	0.4
Prkar1a$^{+/-}$ Prkaca$^{+/-}$	M	253	87	75	2.6	9.9	6.8	147	37	117	591	397	0.3

Genotype	Sex	GLU*	CHOL*	TRIG*	ALB*	Ca*	PHOS*	ALP*	ALT*	AST*	LDH*	CK*	Creatinine
		mg/dL	mg/dL	mg/dL	g/dL	mg/dL	mg/dL	U/L	U/L	U/L	U/L	U/L	mg/dL
Prkar1a$^{+/-}$ Prkaca$^{+/-}$	M	230	120	48	2.8	9.1	8.1	138	52	171	451	676	0.3
Prkar1a$^{+/-}$ Prkaca$^{+/-}$	F	217	67	79	2.7	8.4	5.8	109	38	66	241	114	0.3
Prkar1a$^{+/-}$ Prkaca$^{+/-}$	F	239	95	120	2.9	8.8	6	69	49	67	148	64	0.4
Prkar1a$^{+/-}$ Prkaca$^{+/-}$	F	283	56	48	2.8	8.5	6.3	85	34	61	181	95	0.3
Prkar1a$^{+/-}$ Prkaca$^{+/-}$	F	187	63	45	3	11.3	6.7	210	36	162	478	598	0.4
Prkar1a$^{+/-}$ Prkaca$^{+/-}$	F	228	80	89	2.7	9	5.3	196	40	58	226	65	0.4
Prkar1a$^{+/-}$ Prkaca$^{+/-}$	F	214	98	126	2.9	10.3	6.6	179	34	77	349	212	0.4
Prkar1a$^{+/-}$ Prkaca$^{+/-}$	F	230	65	46	2.7	10.8	5.5	225	28	71	467	196	0.3
Prkar1a$^{+/-}$ Prkaca$^{+/-}$	F	211	58	48	2.6	9.1	7	125	31	56	223	121	0.2
Prkar1a$^{+/-}$ Prkaca$^{+/-}$	F	259	53	67	2.6	9.7	5.7	124	31	135	332	508	0.3
Prkar1a$^{+/-}$ Prkaca$^{+/-}$	F	280	80	66	2.8	11.6	7.8	85	34	75	193	-	-
Prkar1a$^{+/-}$ Prkaca$^{+/-}$	F	253	71	90	2.9	9.7	4.9	128	37	115	313	-	-
Prkar1a$^{+/-}$ Prkaca$^{+/-}$	F	221	103	110	3	11.7	5.2	76	43	97	429	-	-
Prkar1a$^{+/-}$ Prkaca$^{+/-}$	F	206	92	52	2.8	11.5	6.3	87	36	105	371	-	-
Prkar1a$^{+/-}$	F	168	78	58	2.9	11.3	0	148	33	54	192	-	-

Genotype	Sex	GLU*	CHOL*	TRIG*	ALB*	Ca*	PHOS*	ALP*	ALT*	AST*	LDH*	CK*	Creatinine
		mg/dL	mg/dL	mg/dL	g/dL	mg/dL	mg/dL	U/L	U/L	U/L	U/L	U/L	mg/dL
Prkaca$^{+/-}$													
Prkar1a$^{+/-}$ Prkaca$^{+/-}$	F	263	85	99	2.9	10.6	0	156	38	69	404	-	-
Prkar1a$^{+/-}$ Prkaca$^{+/-}$	F	166	75	67	2.9	11	0.1	152	36	126	337	-	-
***p*-value**		0.98	0.59	0.85	0.86	0.80	0.75	**0.001**	0.81	0.41	0.66	0.26	0.024

*GLU, glucose; CHOL, cholesterol; TRIG, triglycerides; ALB, albumin; Ca, calcium; PHOS, inorganic phosphorus; ALP, alkaline phosphatase; ALT, alanine aminotransferase; AST, aspartate aminotransferase; LDH, lactate dehydrogenase; CK, creatine kinase. # *p*-value was calculated with Student T-test. *p*-value was comparing WT and *Prkar1a$^{+/-}$Prkaca$^{+/-}$* mice and less than 0.05 were considered significant which are shown in Figure 3.9.

Table 3.1 Serum chemistries of 1-year old WT, *Prkaca$^{+/-}$*, *Prkar1a$^{+/-}$* and *Prkar1a$^{+/-}$Prkaca$^{+/-}$* mice.

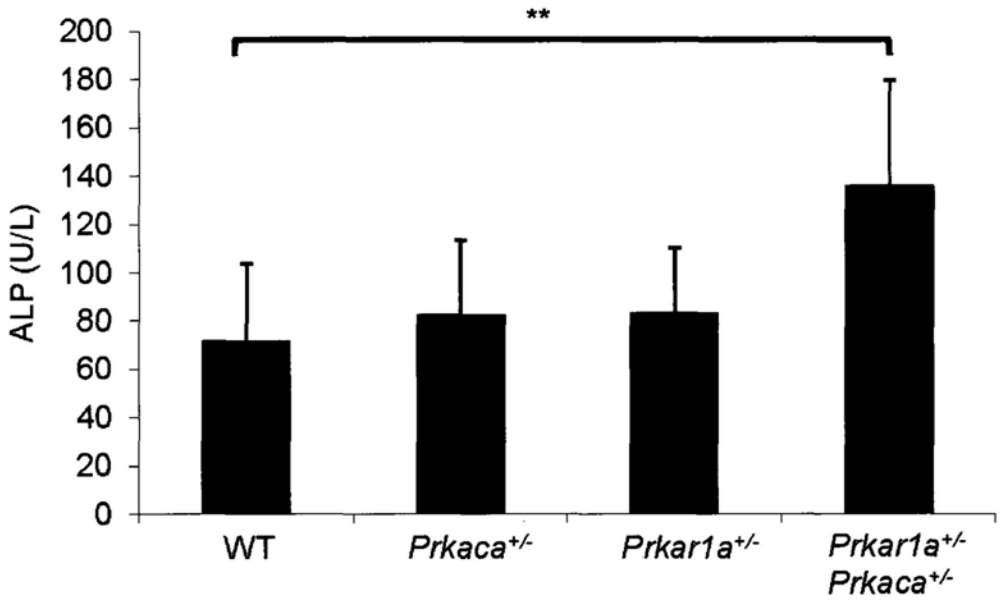

Figure 3.9 Increased serum alkaline phosphatase (ALP) in *Prkar1a$^{+/-}$Prkaca$^{+/-}$* mice. Average of serum ALP level in WT, *Prkaca$^{+/-}$*, *Prkar1a$^{+/-}$* and *Prkar1a$^{+/-}$ Prkaca$^{+/-}$* mice. **P<0.01. Error bars represent means ± SD.

3.3 Evolution of bone lesions in *Prkar1a$^{+/-}$Prkaca$^{+/-}$* mice

By studying the histology of the bone lesions from different ages of *Prkar1a$^{+/-}$Prkaca$^{+/-}$* mice (Figure 3.10A, B), we observed that the lesions always started from the same location in the diametaphyseal region: immediately under the growth plate, from the endosteal surface of the proximal periosteum and nearby trabecular bone (Figure 3.10C, D). In younger *Prkar1a$^{+/-}$Prkaca$^{+/-}$* mice (starting at 4-5 months of age), osteoblast-like cells lined along the trabecular bone and then gradually, with advancing age, filled the bone marrow with loosely arranged collagenous connective tissue and fibroblastoid cells (Figure 3.10D, E). Progression included an increase in active fibroblasts arranged in a uniform array parallel to the axis of the vertebrae. Abundant amounts of loosely arranged collagenous connective tissue continued to fill the marrow spaces (Figure 3.10E, F). As the marrow spaces were being filled, some of the trabeculae were being digested by activated osteoclasts (Figure 3.10G). During this stage, formation (osteoblasts), as well as destruction (osteoclasts) of bone was observed with multiple "cement" lines (Figure 3.10H). As the extracellular matrix increased, the marrow spaces became wider. At this point (usually after 6 months of age) swelling of the affected vertebrae was visible macroscopically compared to adjacent unaffected vertebrae (Figure 3.10I). As the collagenous matrix expanded, ground substances accumulated in several lesions giving them a myxomatous appearance (Figure 3.10J). As the new bone formation continued, it effaced the cartilaginous growth plate and eventually coalesced with adjacent masses encasing the joint space (Figure 3.10K). As the lesions continued to

expand, islands of hyaline cartilage started to form, usually in the center of a population of fibroblasts; in time, hyaline cartilage could fill up the marrow where previously only cells or collagenous matrix was (Figure 3.10L).

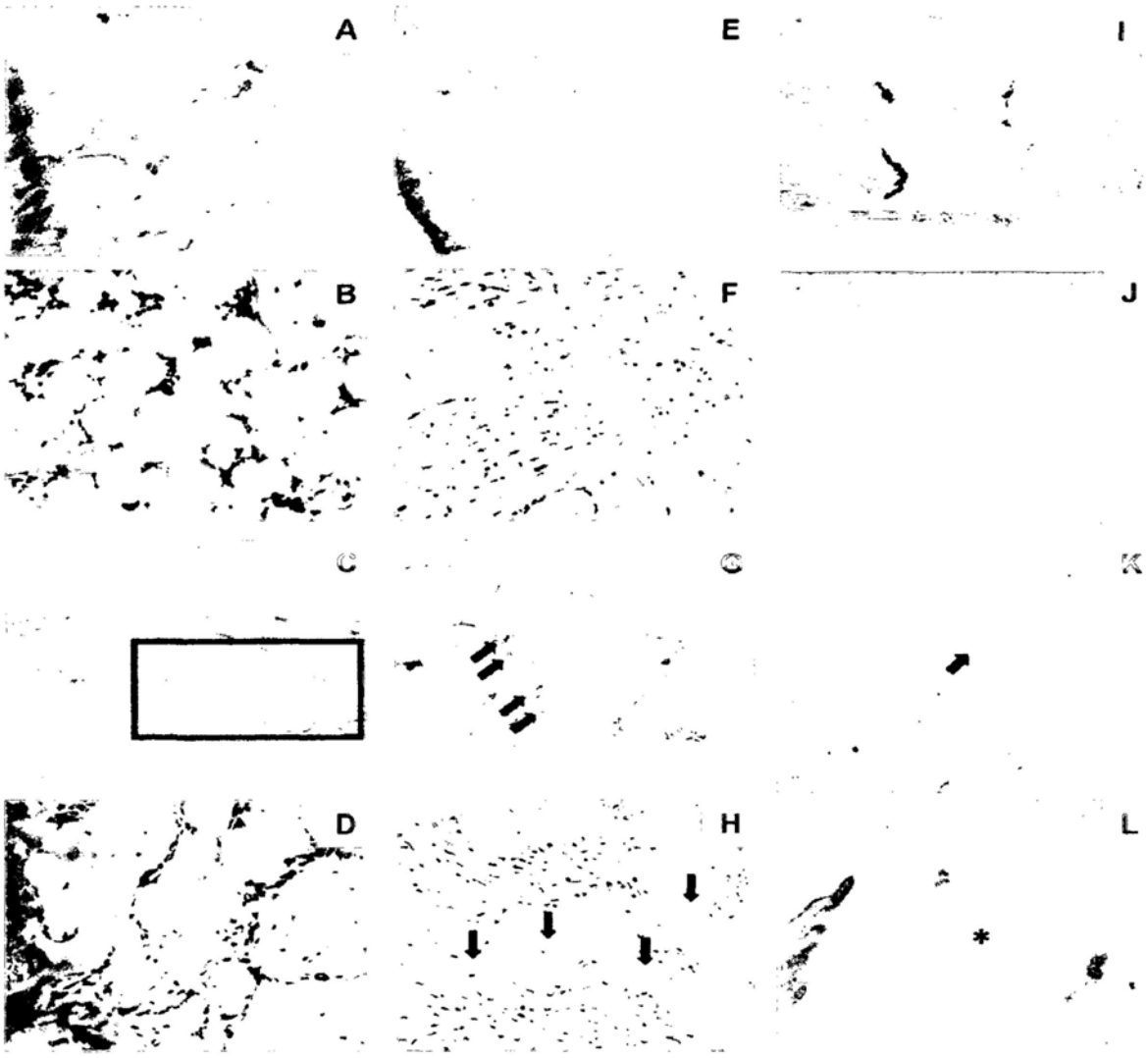

Figure 3.10 The progression of bone lesions in *Prkar1a*$^{+/-}$*Prkaca*$^{+/-}$ mice. H&E staining of caudal vertebrae from *Prkar1a*$^{+/-}$*Prkaca*$^{+/-}$ mice. (**A, B**) Unaffected vertebra. (A) Original magnification, 20x. (B) Original magnification, 40x. (**C, D**) Start of the development of a lesion in diametaphyseal region under the growth plate. (C) square indicates the start of the lesion (original magnification, 20x). (D) Start of the accumulation of fibroblastoid cells inside the bone marrow cavity (original magnification, 20x). (**E, F**) Continuous accumulation of active fibroblasts. (E) Original magnification, 10x. (F) Original magnification, 40x. (**G**) Black arrows denote the presence of osteoclasts within the abnormal fibroblasts (original magnification, 20x). (**H**) Black arrows denote the presence of cement lines. (original magnification, 20x). (**I**) The tumor was macroscopically visible usually after 6 months of age (original magnification, 2x). (**J**) Accumulation of ground substances inside the collagenous matrix. (original magnification, 20x). (**K**) Black arrow denotes the destroyed cartilaginous growth plate and joint space (original magnification, 2x). (**L**) Asterisk denotes the presence of cartilage island within the active fibroblasts (original magnification, 20x).

Although the bone lesions from *Prkar1a*$^{+/-}$ and *Prkar1a*$^{+/-}$*Prkaca*$^{+/-}$ mice were similar, there were also differences beyond the timing (earlier) and the number (increased): Upper spine vertebrae, tibia and femurs were more frequently involved in *Prkar1a*$^{+/-}$*Prkaca*$^{+/-}$ mice. The lesions from *Prkar1a*$^{+/-}$ *Prkaca*$^{+/-}$ mice were also hyper-cellular and contained more, albeit irregular, cartilage or bone islands (Figure 3.11A). Successive vertebrae were affected in the *Prkar1a*$^{+/-}$*Prkaca*$^{+/-}$ mice, whereas this was unusual in *Prkar1a*$^{+/-}$ mice; engorgement of the affected vertebrae was macroscopically visible by 6-12 months in most of the caudal vertebrae of all *Prkar1a*$^{+/-}$*Prkaca*$^{+/-}$ mice (Figure 3.10I and Figure 3.11B). In all cases, as the main lesions grew larger, new lesions were starting from collections of the same fibroblastoid cells within the bone marrow space that was now gradually encircled by the newly formed bone (Figure 3.12A).

Moreover, the periosteum of affected bones was also abnormal. First, occasionally, active proliferating cells from lesions from *Prkar1a*$^{+/-}$*Prkaca*$^{+/-}$ mice (but not from *Prkar1a*$^{+/-}$ animals) invaded and crossed the periosteum into the extraosseous space (Figure 3.12B, C). Second, *Sharpey* fibers, characteristic of FD lesions (155), were present at various sites along the affected periosteum (Figure 3.12D). An increased number of apoptotic bodies within the rapidly proliferating cells was evident (Figure 3.12E), and osteocytes were mostly abnormal within the newly formed osteoid (arrows in Figure 3.12C, D, E).

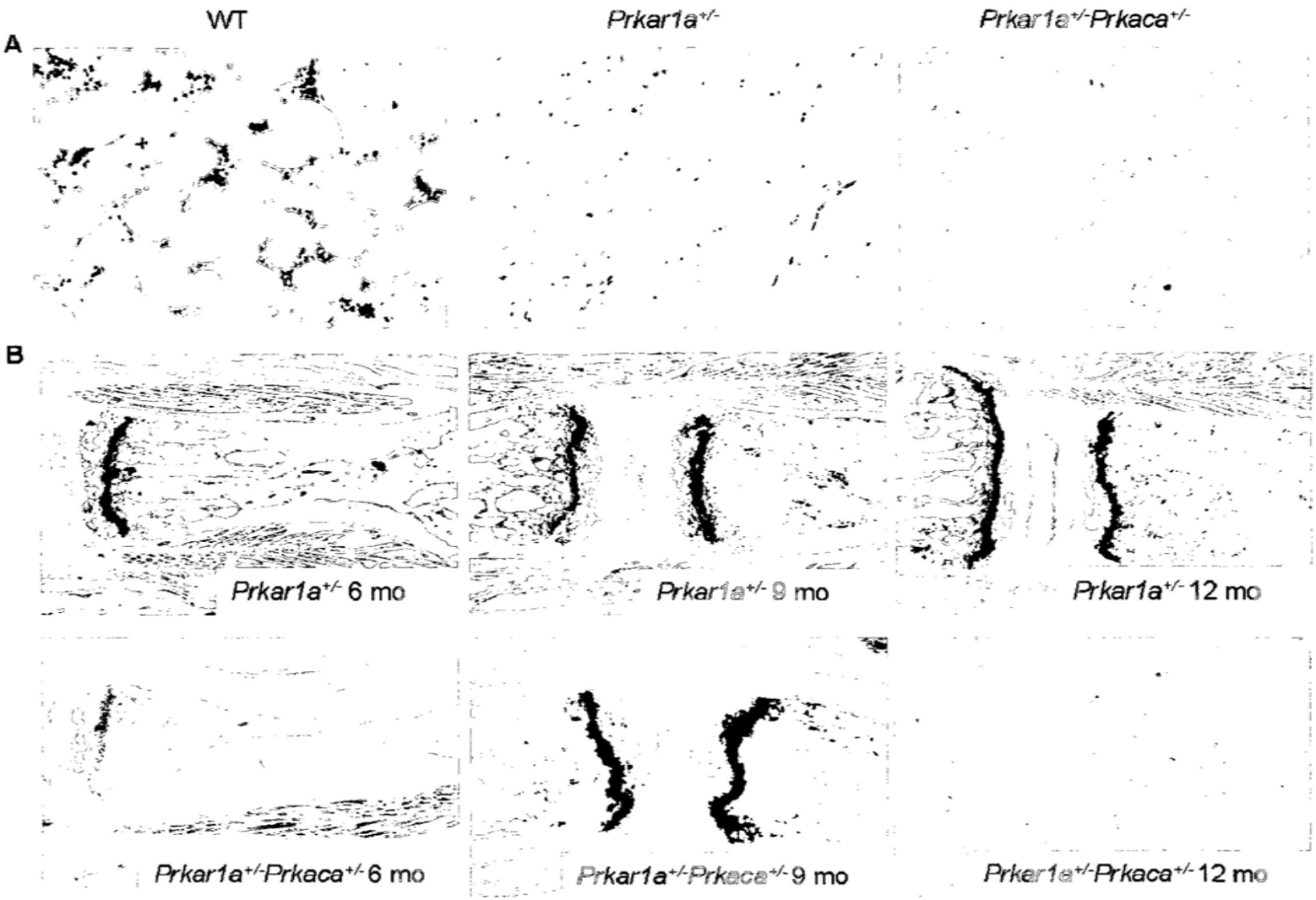

Figure 3.11 Lesions from *Prkar1a$^{+/-}$Prkaca$^{+/-}$* mice were more cellular and aggressive. (**A**) Representative images of H&E staining of caudal vertebrae from WT, *Prkar1a$^{+/-}$* and *Prkar1a$^{+/-}$Prkaca$^{+/-}$* mice at 9 month-old (original magnification, 40x). (**B**) Representative images of H&E staining of caudal vertebrae from *Prkar1a$^{+/-}$* and *Prkar1a$^{+/-}$Prkaca$^{+/-}$* mice at various ages (6, 9 and 12 month-old) which show the increase of aggressiveness in *Prkar1a$^{+/-}$Prkaca$^{+/-}$* mice (original magnification, 2.5x).

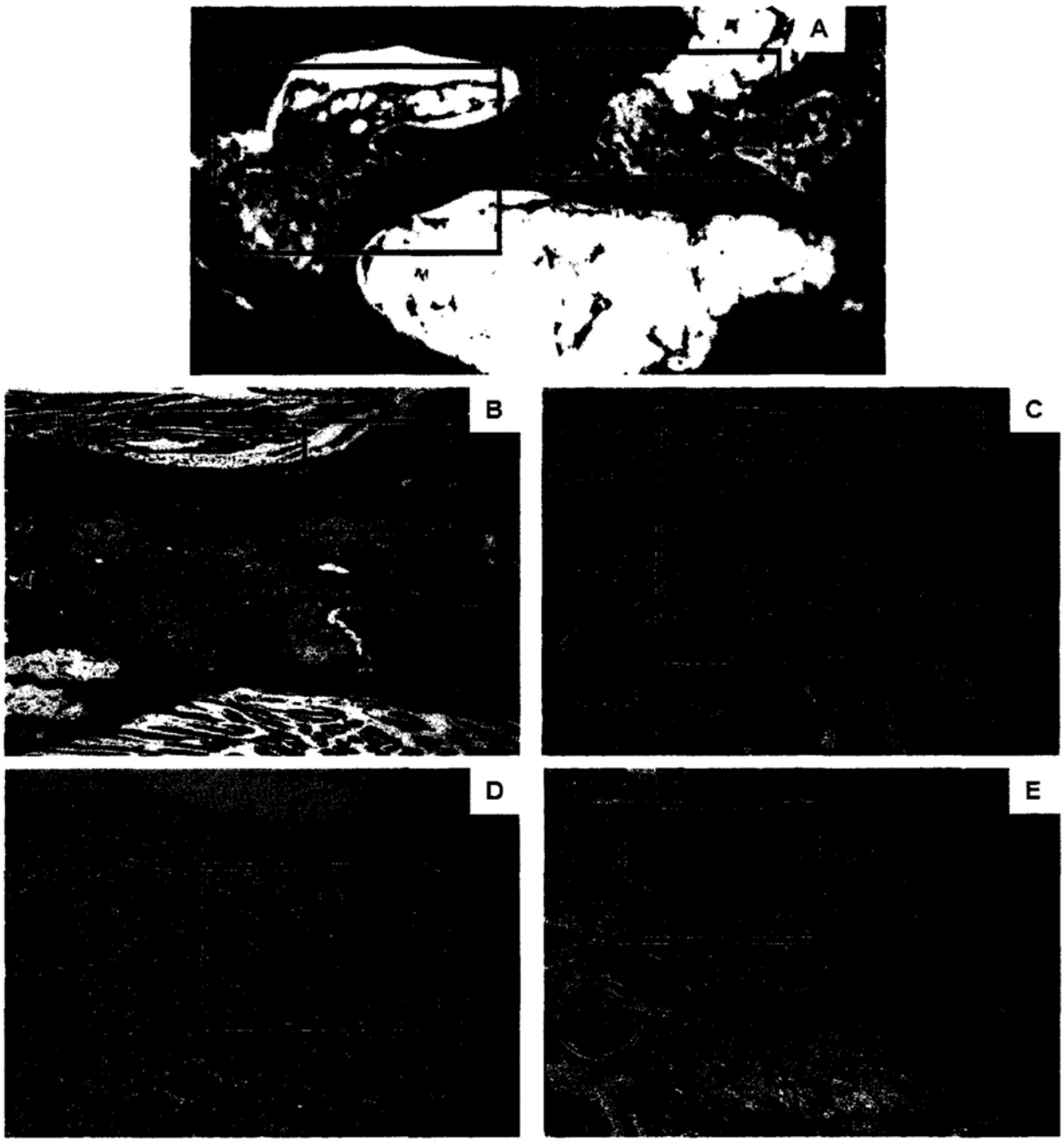

Figure 3.12 Abnormal periosteum and bone marrow space in affected bone from *Prkar1a$^{+/-}$ Prkaca$^{+/-}$* mice. H&E staining of caudal vertebrae of 9 month-old *Prkar1a$^{+/-}$Prkaca$^{+/-}$* mice. (**A**) Squares show the start of two new lesions in different locations of the bone marrow space (original magnification, 20x). (**B**) Arrows denote the abnormal periosteum; square shows the invasion of lesions into extraosseous space (original magnification, 5x). (**C**) Arrows denote the abnormal osteocytes; the square covers the region with invasion of cells from lesions into extraosseous space (original magnification, 20x). (**D**) Arrows denote the abnormal osteocytes; square indicates the presence of *Sharpey* fibers (original magnification, 20x). (**E**) Arrows denote the abnormal osteocytes; note the increased number of apoptotic bodies within the active proliferating cells (indicated within the square) (original magnification, 20x).

3.4 Altered mineralization pattern in bone lesions from caudal vertebra of *Prkar1a$^{+/-}$Prkaca$^{+/-}$* mice

Micro-computed tomography (μCT) and Raman microspectroscopy (RMS) were used to reveal the mineralization pattern within the bone lesions. μCT is a nondestructive imaging technique that produces high resolution three-dimensional images of bone structure by collecting the projections of X-rays and applying tomographic principles (156). RMS allows acquisition of spatially resolved spectra, with micron scale resolution. And characteristic spectra can be obtained for the mineral and protein components of bone tissues (157).

μCT analysis of caudal vertebrae (Figure 3.13) revealed that the overall bone mineralization density of caudal vertebrae from *Prkar1a$^{+/-}$* and *Prkar1a$^{+/-}$ Prkaca$^{+/-}$* mice were significantly lower when compared to WT: thus, despite active proliferation and new bone formation there was an overall undermineralization in both *Prkar1a$^{+/-}$* and *Prkar1a$^{+/-}$Prkaca$^{+/-}$* that was further pronounced in the latter (Figure 3.13B). While the single heterozygote, *Prkaca$^{+/-}$* mice showed an overall gain in bone formation that was derived primarily from cortical bone; trabecular bone in *Prkaca$^{+/-}$* mice tended to be decreased (Figure 3.13).

In 6 month-old *Prkar1a$^{+/-}$Prkaca$^{+/-}$* animals, bright-field and polarization transmission microscopy and RMS showed that the unaffected bones had the expected lamellar/fine-fibered bone (well-oriented osteocyte lacunae, uniform birefringence pattern, and uniform matrix mineralization) at the midline, and

woven bone (disoriented lacunae, patchy birefringence pattern, and non-uniform mineralization) at other sites (Figure 3.14A, C). In contrast, in affected bones, these normal patterns were replaced by mineralized material that had intermediate organization and mineralization heterogeneity closer to woven than to lamellar bone in all cortical regions; the normally sharp mineralization boundary between periosteum and cortical regions was now replaced by a gradual increase of mineralization from the periosteal to the endosteal surface (Figure 3.14B), indicating a lag between bone matrix formation and mineralization and abnormal coordination of these processes with bone resorption.

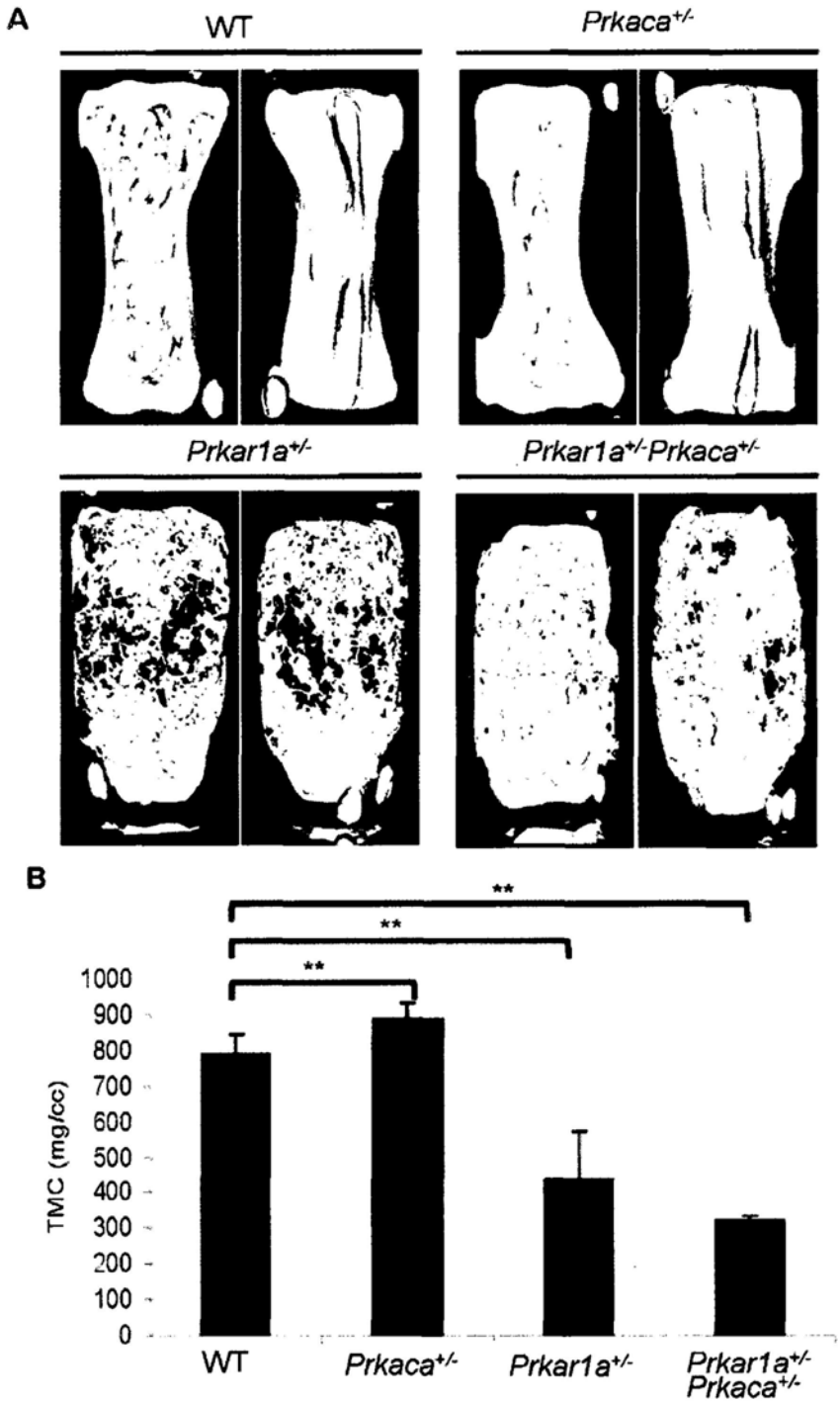

Figure 3.13 Undermineralization of caudal vertebrae in both *Prkar1a*$^{+/-}$ and *Prkar1a*$^{+/-}$*Prkaca*$^{+/-}$ mice. (**A**) μCT images of caudal vertebrae from WT, *Prkaca*$^{+/-}$, *Prkar1a*$^{+/-}$ and *Prkar1a*$^{+/-}$ *Prkaca*$^{+/-}$ mice at the age of 12 months. (**B**) Average of tissue mineral content (TMC) measurement of caudal vertebrae from WT, *Prkaca*$^{+/-}$, *Prkar1a*$^{+/-}$ and *Prkar1a*$^{+/-}$*Prkaca*$^{+/-}$ mice at 12 month-old. n=3, $^{**}P<0.01$. Error bars represent means ± SD.

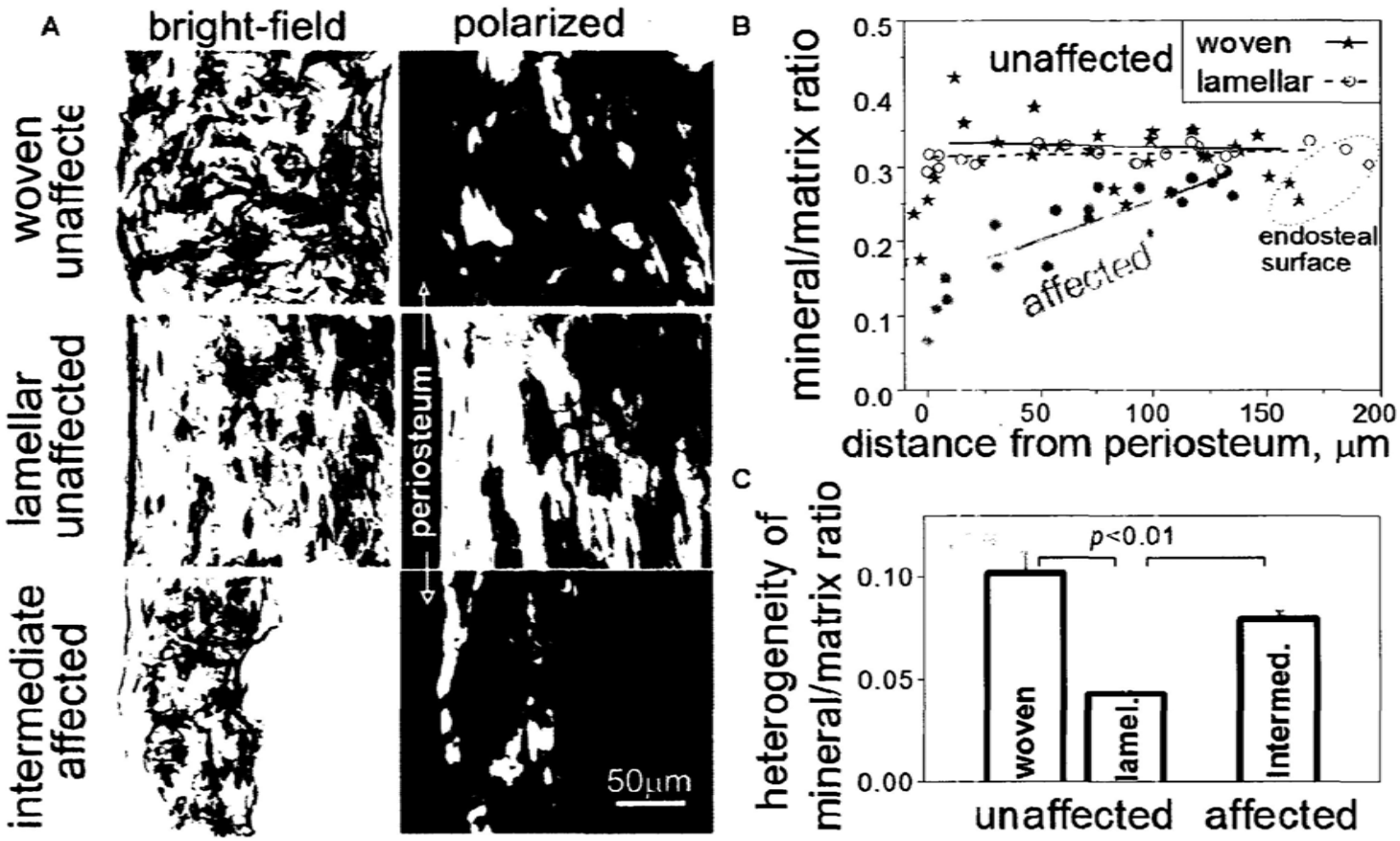

Figure 3.14 Structure and mineralization of cortical bone in adjacent affected and unaffected caudal vertebrae. (**A**) Lamellar or fine-fibered cortical bone was observed at the vertebra midline and woven bone closer to the ends of unaffected vertebrae. In contrast, thinner cortex with intermediate organization was observed through the whole length of affected vertebrae. Well-organized, lamellar/fine-fibered bone was indicated by well-oriented spindle-shaped osteocyte lacunae (arrows) and more uniform polarized images due to regular collagen fiber orientation. Woven bone was indicated by irregular-shaped, disoriented lacunae and patchy appearance of polarized images due to irregular fiber orientation. (**B**) Even (-0.1±0.2 mm-1 slope) mineral/matrix ratio across the cortical layer (the intensity ratio of mineral PO4 to organic CH Raman peaks) is characteristic of well-mineralized, mature bone in unaffected vertebrae. Gradually increasing mineral/matrix ratio from periosteal to endosteal surface (+0.8±0.2(st.d.) mm-1 slope, $p<0.003$) indicates lagging mineralization characteristic of rapidly growing, immature bone in affected vertebrae. (**C**) High mineralization heterogeneity (coefficient of variation for the mineral/matrix ratio) in all cortical regions of affected vertebrae is also consistent with rapid formation of immature bone.

Chapter Four

Biochemical Characterization of Bone Lesions from Mice Deficient in Protein Kinase A Regulatory Subunit Type 1A (*prkar1a*) and Catalytic Subunit A (*prkaca*)

4.1 Increased protein kinase A (PKA) activity and cyclic adenosine monophosphate (cAMP) level in bone lesions from *Prkar1a$^{+/-}$Prkaca$^{+/-}$* mice

Previous studies have shown that *prkar1a* haploinsufficiency leads to increased cAMP-responsive total PKA activity, which is due to dysregulation of catalytic subunits (56, 57, 135, 136, 158, 159). Accordingly, it is essential to study the PKA activity and cAMP level in bone lesions from mice with *prkar1a* and *prkaca* haploinsufficiency.

The loss of one *prkar1a* allele and one *prkaca* allele led to an increase in cAMP-stimulated kinase activity in bone tumors (*Prkar1a$^{+/-}$Prkaca$^{+/-}$* tumor vs. WT tail bone, 2724.7 ±866.8 vs. 912.4 ±283.6, p-value <0.05); *Prkar1a$^{+/-}$* tumors had a smaller increase in kinase activity when compared to WT bone (p-value =0.079) (Figure 4.1A), consistent with previously published data (57). Like in *Prkar1a$^{+/-}$* tumors (57), the bone lesions from *Prkar1a$^{+/-}$Prkaca$^{+/-}$* mice did not show any LOH of the normal *Prkar1a* or *Prkaca* allele (Figure 4.1C).

Unexpectedly, cAMP levels were increased in bone tumors from both *Prkar1a$^{+/-}$* (*Prkar1a$^{+/-}$* tumor *vs.* WT normal tail, 155.0 ±18.9 *vs.* 119.4 ±15.8, p-value =0.06) and *Prkar1a$^{+/-}$Prkaca$^{+/-}$* mice (*Prkar1a$^{+/-}$Prkaca$^{+/-}$* tumor *vs.* WT normal tail, 177.5 ±46.3 *vs.* 119.4 ±15.8, p-value=0.06) (Figure 4.1B).

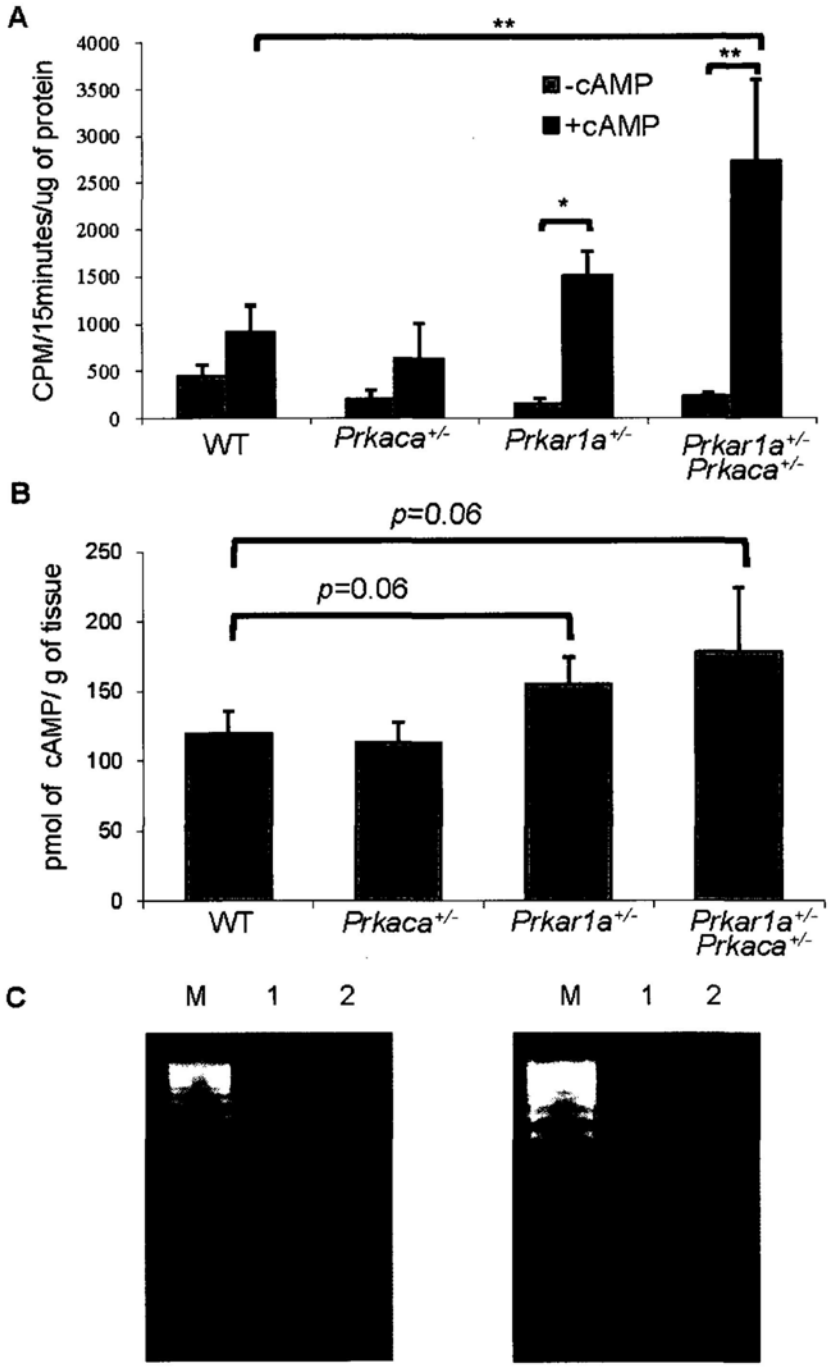

Figure 4.1 Increased cAMP level and cAMP-stimulated total PKA activity and absence of loss of heterozygosity (LOH) in bone lesions from *Prkar1a*$^{+/-}$*Prkaca*$^{+/-}$ mice. (**A**) Basal and total PKA activity (**B**) cAMP level in bone tissues from WT, *Prkaca*$^{+/-}$ and bone lesions from *Prkar1a*$^{+/-}$ and *Prkar1a*$^{+/-}$*Prkaca*$^{+/-}$ mice. n=3. ** $P < 0.05$; **$P < 0.01$. Error bars represent means ± SD. (**C**) Absence of LOH in *Prkar1a*$^{+/-}$*Prkaca*$^{+/-}$ bone tumor. PCR experiments using the primers described in Material and Methods were performed for (left panel) *Prkar1a* gene and (right panel) for *Prkaca* gene. M, 100bp ladder; 1, peripheral DNA was used as template; 2, tumor DNA was used as template.

4.2 Increased phosphodiesterase (PDE) activity and adenylate cyclases expression in bone lesions from *Prkar1a$^{+/-}$Prkaca$^{+/-}$* mice

To address whether the increase in cAMP levels was the result of a decrease in phosphodiesterase (PDE) activity, which degrades cAMP, we measured the latter. Total PDE activity in tumor protein extracts was significantly increased in both tumors from *Prkar1a$^{+/-}$* and *Prkar1a$^{+/-}$Prkaca$^{+/-}$* mice (Figure 4.2A). By Western blot analysis (Figure 4.2B) and immunohistochemistry (IHC) (Figure 4.2C), we determined that cAMP-binding Pde11a and Pde4d, but not Pde7a *[which has been suggested to be involved in cAMP signaling in BSCs (160)]*, were highly expressed in tumors. This suggested that the increase in cAMP levels did not result from a decrease in degradation by PDEs.

Instead of decreased rate in degradation, increase cAMP level may result from increased production by adenylate cyclases(AC, *Adcy*). Since there is no information on the type of AC expressed in bone, we tested all 9 trans-membrane AC enzymes and one soluble AC; *Adcy1*, *Adcy6* and *Adcy9* were found to be up-regulated at both the mRNA and protein level (Figure 4.3). With higher level of AC enzymes in the lesions, the rate of cAMP production could be enhanced when compared to normal bone tissues. Thus, the increase in cAMP levels was at least in part mediated by an increased expression of ACs.

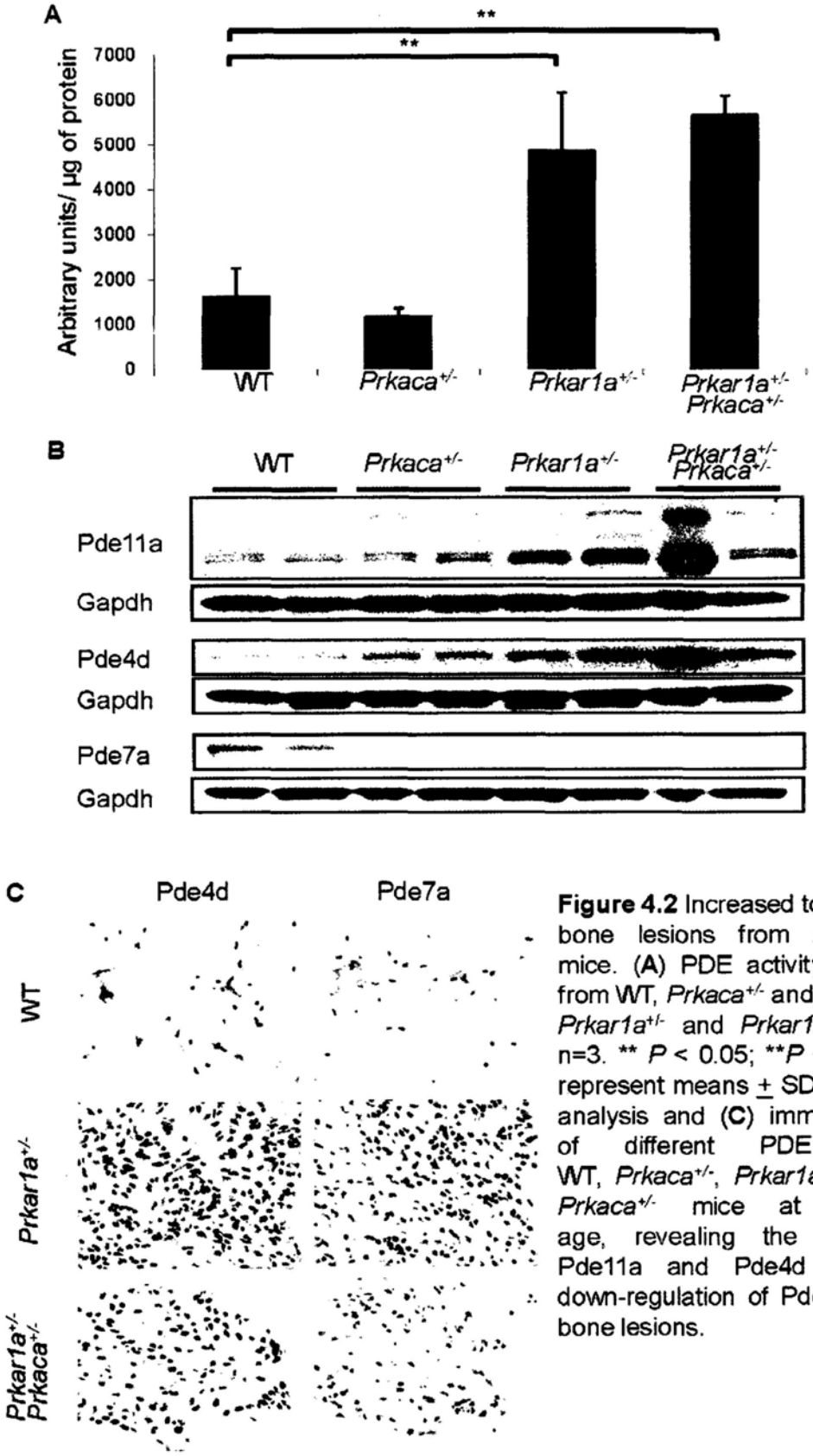

Figure 4.2 Increased total PDE activity in bone lesions from *Prkar1a$^{+/-}$Prkaca$^{+/-}$* mice. (**A**) PDE activity in bone tissues from WT, *Prkaca$^{+/-}$* and bone lesions from *Prkar1a$^{+/-}$* and *Prkar1a$^{+/-}$Prkaca$^{+/-}$* mice. n=3. ** $P < 0.05$; ** $P < 0.01$. Error bars represent means ± SD. (**B**) Western blot analysis and (**C**) immunohistochemistry of different PDE proteins on WT, *Prkaca$^{+/-}$*, *Prkar1a$^{+/-}$* and *Prkar1a$^{+/-}$ Prkaca$^{+/-}$* mice at one year of age, revealing the up-regulation of Pde11a and Pde4d expression and down-regulation of Pde7a expression in bone lesions.

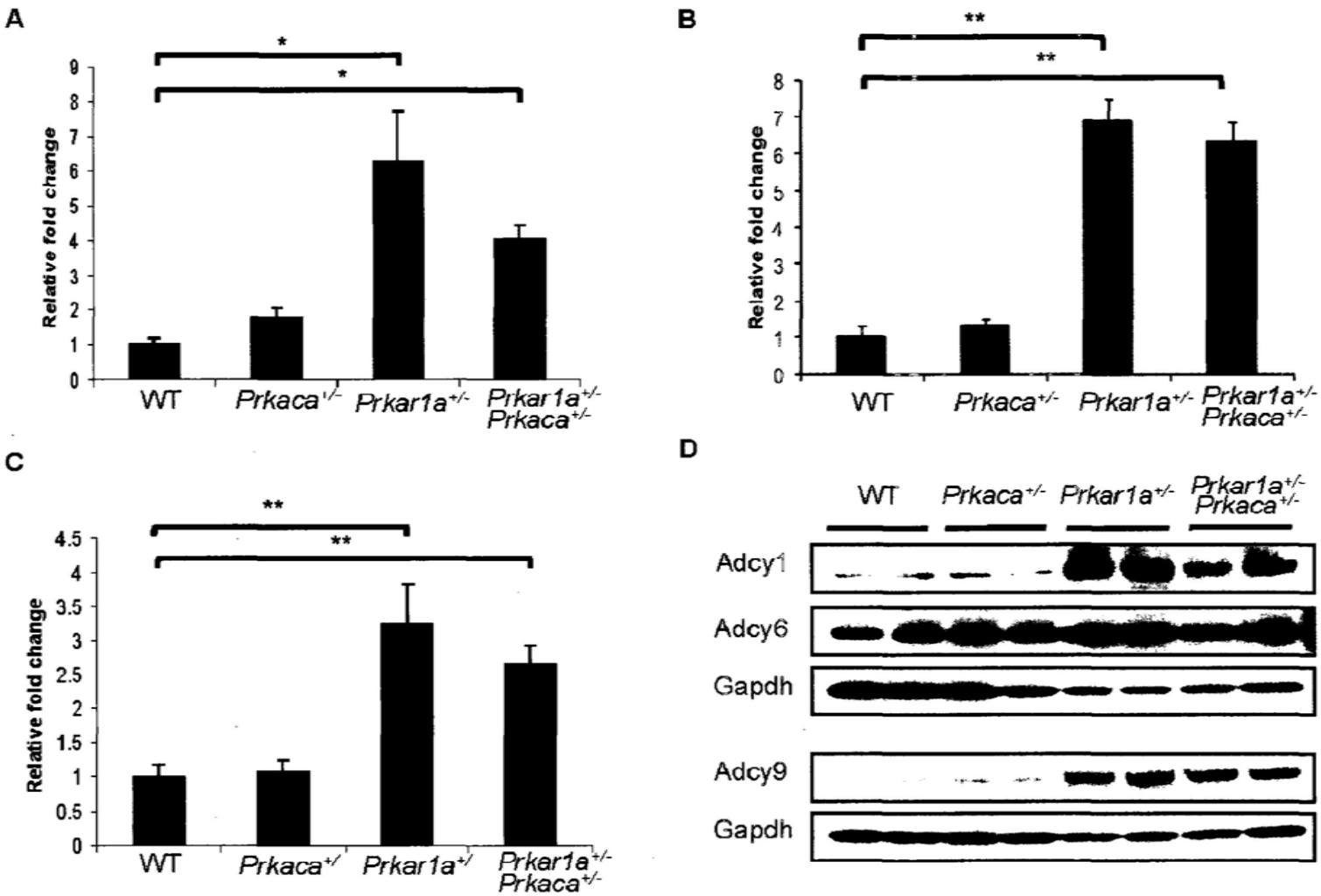

Figure 4.3 Increased expression of adenylate cyclase 1, 6 and 9 in *Prkar1a*$^{+/-}$*Prkaca*$^{+/-}$ bone lesions. Quantitative analysis of mRNA expression of (**A**) Adcy1, (**B**) Adcy6, (**C**) Adcy9 in 12 month-old tail bone tissues from WT, *Prkaca*$^{+/-}$ and bone lesions from *Prkar1a*$^{+/-}$ and *Prkar1a*$^{+/-}$*Prkaca*$^{+/-}$ mice. n=3. *$P < 0.05$; **$P < 0.01$. Error bars represent means ± SD. (**D**) Western blot analysis on protein expression level of Adcy1, Adcy6 and Adcy9 in tail bone tissues from 12 month-old WT, *Prkaca*$^{+/-}$ and bone lesions from 12 month-old *Prkar1a*$^{+/-}$ and *Prkar1a*$^{+/-}$*Prkaca*$^{+/-}$ mice.

4.3 Increase of PKA type II (PKA-II) isozyme and regulatory subunits (RIIα and RIIβ) in bone lesions from *Prkar1a$^{+/-}$Prkaca$^{+/-}$* mice

It has been reported that reduction of R1α levels, mainly due to loss of function mutation in *PRKAR1A*, leads to decrease in PKA type I (PKA-I) and an increase in PKA-II in human tissues, primary and transformed cell lines (56, 139, 161). These are also observed in mouse cells with 50% reduction of R1α protein. This change is believed to be responsible for the increase in cAMP-responsive kinase activity. In order to investigate if higher PKA-II was also seen in bone lesions and led to increased total PKA activity, we performed diethylaminoethyl cellulose (DEAE) ion-exchange column chromatography followed by elution with a linear sodium chloride gradient on total proteins extracted from the primary cells derived from bone tumors and normal bone tissues. The fractions were then measured for PKA activity: PKA-I complex was eluted between 40mM to 80mM of NaCl while PKA-II complex was eluted between 180mM to 270mM of NaCl under these conditions (Figure 8A). There were no free forms of regulatory or catalytic subunits under these ranges of NaCl concentration. PKA-II to PKA-I ratio was calculated from averaging the intensities of 10 fractions within the peaks.

In normal bone from WT mouse, PKA-II was the main PKA holoenzyme (PKA-II to PKA-I ratio = 2.46) (Figure 4.4A, top left). In bone tissue from *Prkaca$^{+/-}$* mouse, the levels of PKA-II and PKA-I were similar (Figure 4.4A, top right). Loss of one *prkar1a* allele led to a PKA-II to PKA-I ratio of 1.82 *vs* WT bone (p=0.02)

(Figure 4.4A, bottom left). In the tumors from *Prkar1a*$^{+/-}$*Prkaca*$^{+/-}$ mice, both PKA-II and PKA-I kinase activities were decreased when compared to WT. However, the tumor had significantly more PKA-II complexes (PKA-II to PKA-I ratio =3.10, p=0.057 compared to WT; p<0.001 compared to *Prkar1a*$^{+/-}$) (Figure 4.4A, bottom right). These data indicated that there was an excess of PKA-II in the lesions from *Prkar1a*$^{+/-}$*Prkaca*$^{+/-}$ mice.

Consistent with these data, Western blot analysis showed an up-regulated expression of type II regulatory subunits in bone tumors (Figure 4.4B), also confirmed by IHC (Figure 4.5). The Western blots showed doublet bands in the *Prkar1a*$^{+/-}$*Prkaca*$^{+/-}$ tumor cells (Figure 4.4B), suggesting that the presence of phosphorylated forms of type II regulatory subunits was increased. By using an antibody specific for the phosphorylated form, this was shown to be the case only for the tumors from *Prkar1a*$^{+/-}$*Prkaca*$^{+/-}$ mice (Figure 4.4B).

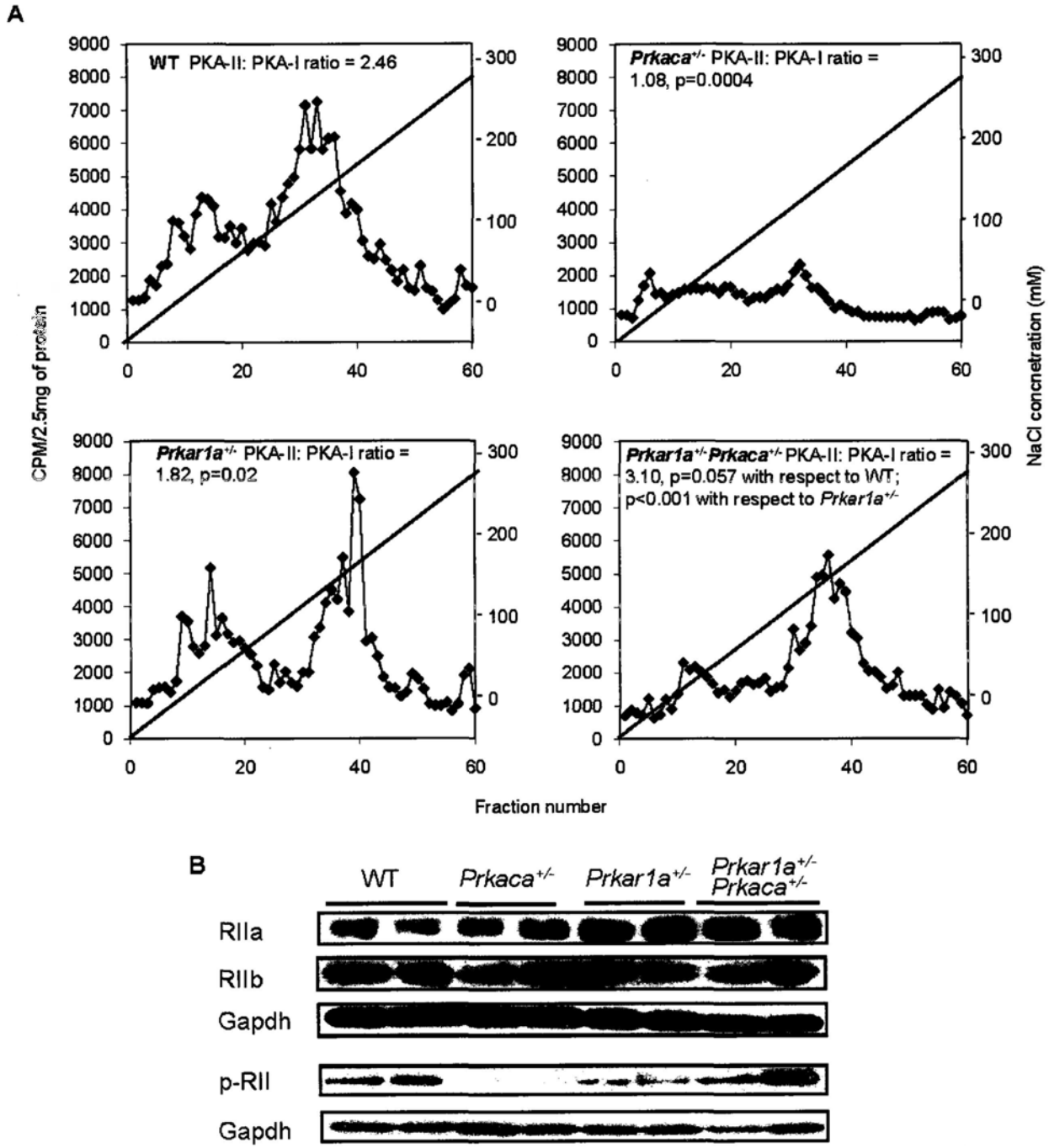

Figure 4.4 Increased PKA-II complex and type II regulatory subunit in *Prkar1a$^{+/-}$ Prkaca$^{+/-}$* mice bone tumors. (**A**) DEAE-chromatography of PKA isozymes in tail tissues of WT and *Prkaca$^{+/-}$* mice and tail lesions of *Prkar1a$^{+/-}$* and *Prkar1a$^{+/-}$Prkaca$^{+/-}$* mice. PKA-II to PKA-I ratio was calculated from averaging the intensities of 10 fractions within the peaks. Note that tail lesions of *Prkar1a$^{+/-}$Prkaca$^{+/-}$* mice had the highest PKA-II to PKA-I ratio. n=3. (**B**) Western blot analysis on RIIα, RIIβ and phosphorylated form of RII in WT, *Prkaca$^{+/-}$*, *Prkar1a$^{+/-}$* and *Prkar1a$^{+/-}$Prkaca$^{+/-}$* mice at one year of age, showing the up-regulation of RII subunits in bone lesion and increase in phosphorylated form of RII in *Prkar1a$^{+/-}$Prkaca$^{+/-}$* tumors.

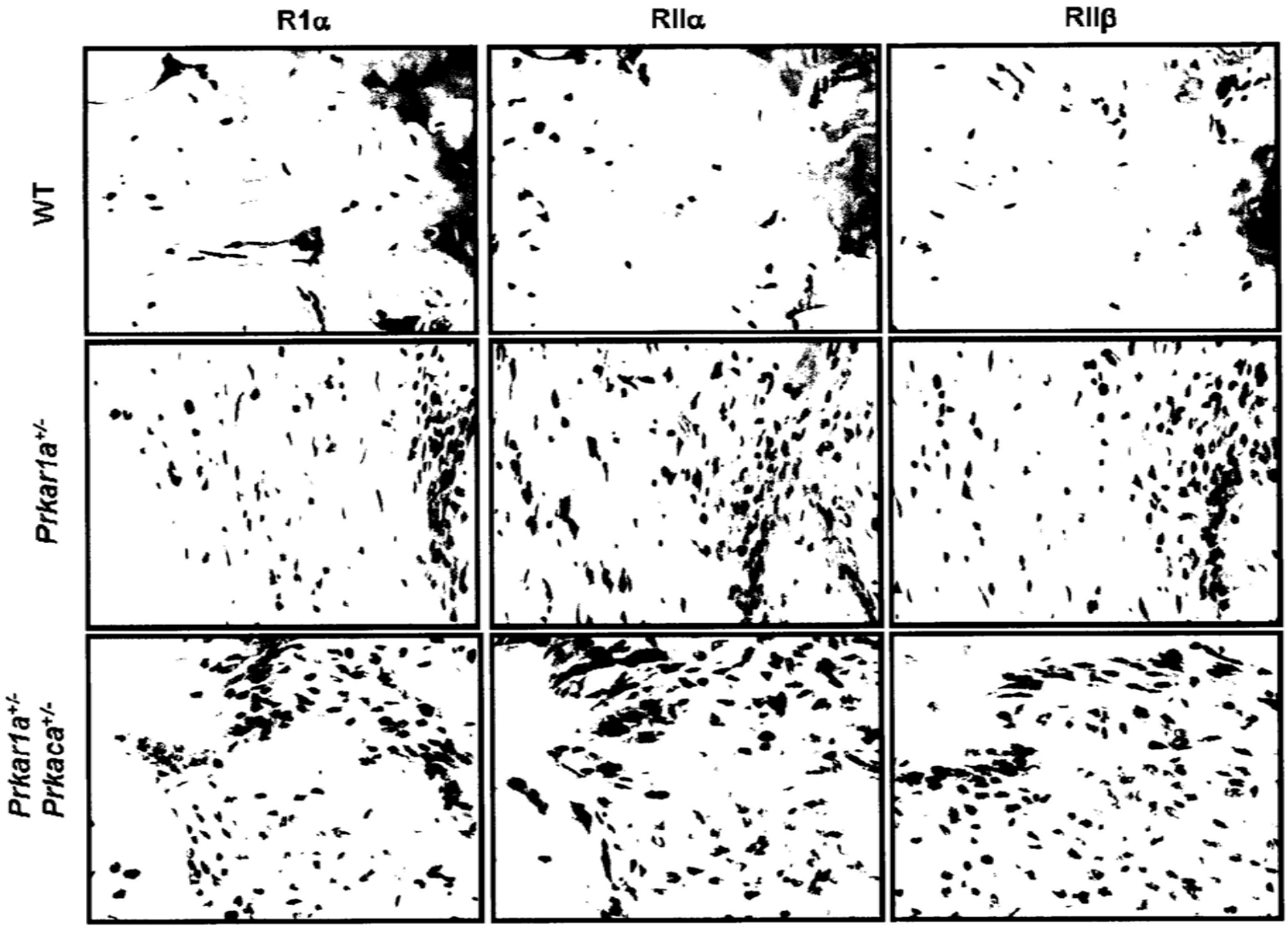

Figure 4.5 Up-regulation of type II regulatory subunits in bone tumors. Immunohistochemistry for R1α, RIIα and RIIβ on WT bones, *Prkar1a*$^{+/-}$ and *Prkar1a*$^{+/-}$*Prkaca*$^{+/-}$ bone lesions. Original magnification, 40x.

4.4 Increased expression of PKA catalytic subunits α, β1, γ and Prkx in bone lesions from *Prkar1a$^{+/-}$Prkaca$^{+/-}$* mice

Previous studies in mice and human cell lines have all suggested that coordinated inhibition of the catalytic subunit is the most important function of the PKA regulatory subunits (24, 141-143). We hypothesized that 50% reduction of *prkar1a* and *prkaca* genetically in mice would lead to altered expression of different catalytic isoforms, and result in dysregulated PKA signaling.

Both bone tumors from *Prkar1a$^{+/-}$* and *Prkar1a$^{+/-}$Prkaca$^{+/-}$* showed an induction in the expression of Prkx and Cβ1 and a reduction in Cβ2 when compared with WT bone tissue. When tumors from *Prkar1a$^{+/-}$* mice were compared to those of *Prkar1a$^{+/-}$Prkaca$^{+/-}$* animals, the latter had a higher expression of Cβ2 (Figure 4.6). Cα protein levels in *Prkar1a$^{+/-}$Prkaca$^{+/-}$* tumors were not significantly decreased from those of the WT bone and *Prkar1a$^{+/-}$* tumor cells (most likely due to compensatory upregulation of the remaining *prkaca* allele, since there was no LOH, as shown in Figure 4.1C) but like Western blotting, IHC confirmed that now Cβ, Cγ and the Prkx proteins, in addition to Cα, were upregulated in the bone lesions (Figure 4.7).

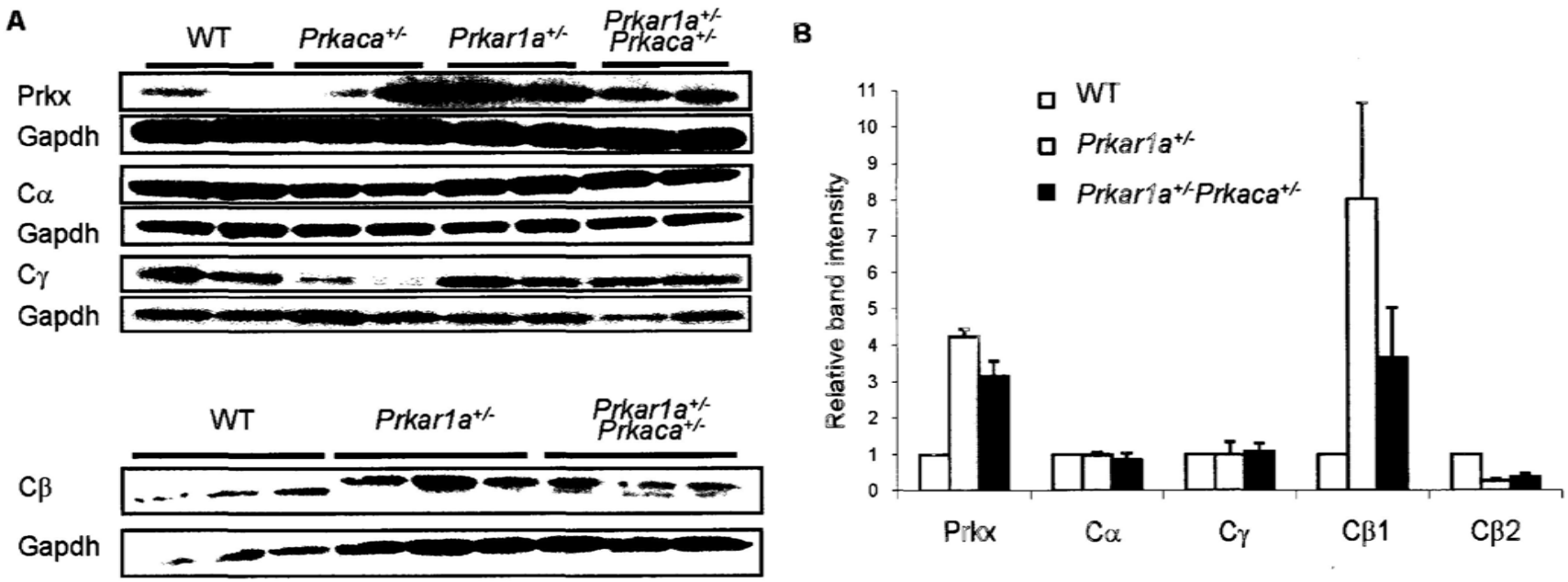

Figure 4.6 Change in the expression of catalytic subunit α, β1, β2, γ and Prkx in *Prkar1a$^{+/-}$Prkaca$^{+/-}$* bone lesions. (**A**) Western blot analysis on different PKA catalytic subunits of WT, *Prkaca$^{+/-}$*, *Prkar1a$^{+/-}$* and *Prkar1a$^{+/-}$Prkaca$^{+/-}$* mice at one year of age. (**B**) Relative quantification of Prkx, Cα, Cγ, Cβ1 and Cβ2 protein in bone lesion against WT normal bone.

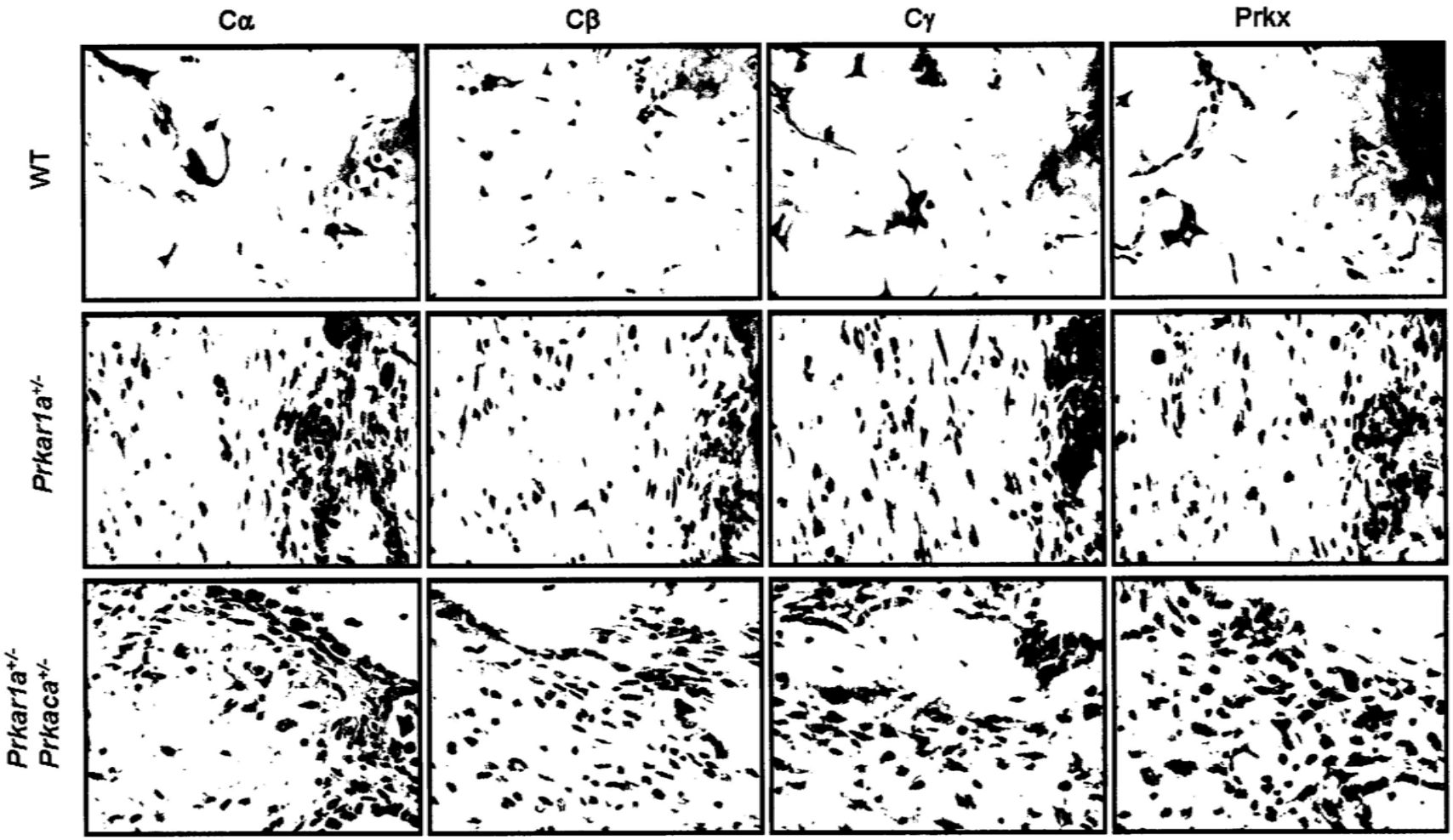

Figure 4.7 Up-regulation of PKA catalytic subunits β, γ and Prkx in bone tumors. Immunohistochemistry for Cα, Cβ, Cγ and Prkx on WT bones, *Prkar1a*$^{+/-}$ and *Prkar1a*$^{+/-}$*Prkaca*$^{+/-}$ bone lesions. Original magnification 40x.

Chapter Five

Molecular characterization of Bone Lesions from Mice Deficient in Protein Kinase A Regulatory Subunit Type 1A (*prkar1a*) and Catalytic Subunit A (*prkaca*)

5.1 Molecular characterization of cells forming the lesions in affected bones from *Prkar1a$^{+/-}$Prkaca$^{+/-}$* mice

In order to identify the cellular origin of the cells forming the lesions, we performed flow cytometry analysis, by using different cell surface markers Cd44, Cd45, Cd90 and Vcam, on primary cells derived from *Prkar1a$^{+/-}$* and *Prkar1a$^{+/-}$ Prkaca$^{+/-}$* bone lesions. MC3T3 (ATCC CRL-2593), which is a preosteoblasts cell line, was used as control cells. Tumor cells from *Prkar1a$^{+/-}$* and *Prkar1a$^{+/-}$ Prkaca$^{+/-}$* bone lesions expressed Cd44 (97% and 94%, respectively), Cd90 (94% and 80%, respectively) and Vcam (96% and 92% respectively) but stained negative for Cd45, indicating that the indentified population of cells consisted of bone stromal cells (Figure 5.1).

A previous study reported that *Prkar1a$^{+/-}$* mouse bone tumor cells were of the osteoblast lineage, arrested at a partially differentiated stage (57). Although these cells expressed alkaline phosphatase, they had relatively lower protein expression of Runx2, the master regulator of osteogenic commitment (105). We compared the expression of genes, which are involved in osteogenesis, between *Prkar1a$^{+/-}$* and *Prkar1a$^{+/-}$Prkaca$^{+/-}$* bone lesions (Table 5.1) by real time quantitative PCR (RT-qPCR) array analysis. We found that *Runx2* was significantly upregulated in lesions from *Prkar1a$^{+/-}$Prkaca$^{+/-}$* mice at both the mRNA and protein level. The actively growing fibroblasts inside the marrow cavities were strongly stained by an antibody specific for Runx2 (Figure 5.2A) and, consistently, Western blot analysis confirmed that the expression of Runx2 was induced in the bone lesions (Figure 5.2B). Real-time quantitative PCR (RT-

qPCR) analysis by gene specific primers confirmed that the tumors, too, from *Prkar1a*$^{+/-}$*Prkaca*$^{+/-}$ mice had significantly higher *Runx2* mRNA expression (Figure 5.2C).

On the other hand, the fibroblast-like cells did not show a strong signal for osteocalcin, a marker of mature osteoblasts (Figure 5.3A), and were negative for osteopontin, as in *Prkar1a*$^{+/-}$ cells (57); the only cells in the lesions that stained for osteocalcin were those that lined the trabeculae (Figure 5.3A). Taken together, these data suggested that the fibroblastoid cells within the lesions were committed osteogenic (*Runx2*-positive) (162), unlike the case in *Prkar1a*$^{+/-}$ lesions (57). Furthermore, cells lining newly formed bone were more mature, differentiated osteoblasts.

The presence of osteoclasts were also increased in the lesions: tartrate-resistant acid phosphatase 5 (Acp5) and cathepsin K were highly expressed in sections from *Prkar1a*$^{+/-}$*Prkaca*$^{+/-}$ bone lesions in the cells lined along the trabeculae bone as well as inside the pool of fibrotic cells; only the cells next to the trabecular bone expressed these markers in *Prkar1a*$^{+/-}$ lesions (Figure 5.3B).

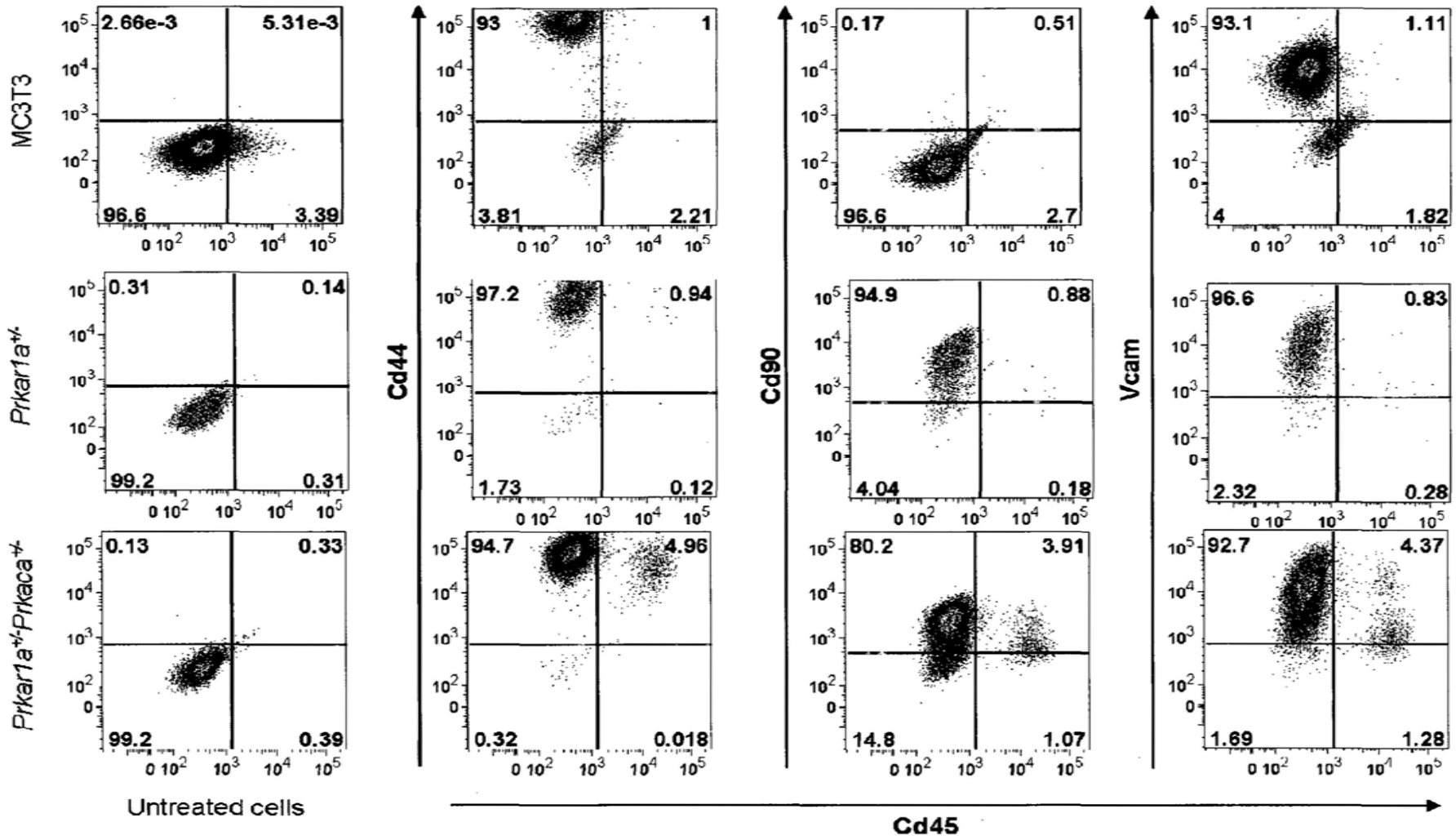

Figure 5.1 Expression of mouse bone stromal cell markers Cd44, Cd90 and Vcam in primary cells derived from *Prkar1a*$^{+/-}$ and *Prkar1a*$^{+/-}$*Prkaca*$^{+/-}$ bone tumors. Flow cytometry analysis for the expression of Cd44, Cd45, Cd90 and Vcam on primary cells from bone tumors.

	Up- or down- regulation of bone-related genes (compared to WT mice)		
	Prkar1a$^{+/-}$ **Vs WT**	***Prkar1a$^{+/-}$ Prkaca$^{+/-}$*** **vs WT**	***Prkar1a$^{+/-}$ Prkaca$^{+/-}$*** **vs *Prkar1a$^{+/-}$***
Ahsg	-1.6814	2.0716	3.493421053
Alpl	38.6438	23.4351	0.606440142
Ambn	1.5943	2.6863	1.684596577
Anxa5	2.1378	4.2024	1.965730759
Bgn	5.8775	13.1653	2.239949343
Bmp1	6.0114	10.4425	1.737123115
Bmp2	3.1697	2.5051	0.790257578
Bmp3	4.4412	7.6739	1.727934097
Bmp4	-1.0901	7.2793	7.935432016
Bmp5	4.8903	10.7532	2.198889281
Bmp6	1.0698	1.2269	1.146796657
Bmpr1a	-14.2244	-5.5354	2.569700474
Bmpr1b	-2.2318	-1.0868	2.053724816
Cd36	-2.943	-2.3411	1.257081787
Cdh11	13.5304	54.9749	4.063059326
Col10a1	2.8002	2.4938	0.8907173
Col11a1	9.1183	32.7238	3.588798139
Col12a1	11.666	27.2258	2.333776604
Col14a1	2.6761	4.3454	1.623798965
Col1a1	30.1176	32.6852	1.08525467
Col1a2	10.0533	30.4457	3.02842286
Col2a1	-1.2299	1.0976	1.351145038
Col3a1	12.1881	23.1055	1.895747308
Col4a1	3.0836	4.3858	1.422271128
Col4a2	1.2254	2.6484	2.161301666
Col5a1	11.7748	12.756	1.083326185
Col6a1	3.8242	7.4388	1.945175183
Col6a2	10.7128	10.9711	1.024106141
Col7a1	5.6825	4.8888	0.860307614
Comp	1.4757	1.4025	0.950395817
Csf2	2.1264	2.3673	1.114583333
Csf3	1.1032	2.4318	2.201413428
Ctsk	18.6745	42.7603	2.289765664
Dmp1	9.7698	42.1648	4.31580808
Egf	-3.2498	-2.973	1.09336983
Enam	-1.6814	2.0716	3.493421053
Fgf1	-3.6391	-1.2209	2.980758302
Fgf2	-1.0151	1.4167	1.438069524
Fgf3	3.2021	2.1546	0.672350792
Fgfr1	2.3509	7.0502	2.998896758
Fgfr2	2.1997	8.2129	3.733689824
Flt1	1.3707	2.2836	1.666178356

	Up- or down- regulation of bone-related genes (compared to WT mice)		
	Prkar1a$^{+/-}$ **Vs WT**	***Prkar1a$^{+/-}$ Prkaca$^{+/-}$*** **vs WT**	***Prkar1a$^{+/-}$ Prkaca$^{+/-}$*** **vs *Prkar1a$^{+/-}$***
Fn1	11.5677	10.3159	0.89178429
Gdf10	1.141	1.4018	1.228601253
Icam1	5.316	12.6752	2.384329263
Igf1	3.5536	15.366	4.324001461
Igf1r	1.2012	2.2482	1.871551763
Itga2	3.4133	5.5025	1.612232341
Itga2b	1.174	2.6708	2.274922942
Itga3	2.0688	2.3696	1.145439606
Itgam	3.042	9.6737	3.18013288
Itgav	6.6741	14.6135	2.1896045
Itgb1	1.8198	2.9077	1.597815329
Mmp10	5.8524	40.769	6.96816685
Mmp2	4.7791	15.8363	3.313677782
Mmp8	3.3214	16.9401	5.100874243
Mmp9	18.2476	35.3793	1.938848467
Msx1	1.1322	7.653	6.759294202
Nfkb1	1.4578	3.316	2.274644491
Pdgfa	1.9942	2.7274	1.367613519
Phex	5.3053	17.9047	3.374861406
Runx2	4.5857	15.732	3.430692157
Scarb1	5.3395	7.0801	1.325996914
Serpinh1	16.1751	11.6619	0.720982515
Smad1	1.5133	5.8901	3.892152403
Smad2	2.5232	4.3964	1.742408781
Smad3	2.0944	2.9064	1.387664371
Smad4	2.7654	3.0659	1.108664307
Sost	-1.096	-1.0552	1.038652517
Sox9	2.1327	2.9469	1.381853786
Tfip11	1.3685	2.6046	1.903224205
Tgfb1	8.4072	13.117	1.560233074
Tgfb2	2.6923	3.0863	1.146327628
Tgfb3	4.2863	4.9115	1.145861227
Tgfbr1	3.5797	7.6637	2.140864382
Tgfbr2	3.9359	6.2333	1.583700957
Tgfbr3	1.4141	1.7207	1.216758826
Tnf	3.1411	4.3409	1.381881533
Tuft1	1.2167	2.9977	2.463869867
Twist1	3.0543	10.5544	3.455592699
Vcam1	3.3325	13.4342	4.031261821
Vdr	2.6644	13.3697	5.017839474
Vegfa	1.8954	2.035	1.073618033
Vegfb	1.1847	1.5128	1.277016743

	Up- or down- regulation of bone-related genes (compared to WT mice)		
	Prkar1a$^{+/-}$ **Vs WT**	***Prkar1a$^{+/-}$ Prkaca$^{+/-}$*** **vs WT**	***Prkar1a$^{+/-}$ Prkaca$^{+/-}$*** **vs *Prkar1a$^{+/-}$***
Gusb	4.3152	9.3196	2.15970375
Hprt1	-1.1694	2.7253	3.187001701
Hsp90ab1	-1.8515	1.4163	2.622361837
Gapdh	1	1	1
Actb	6.085	7.6274	1.253474818

Table 5.1 Up-regulation of Runx2 mRNA level in bone lesions from *Prkar1a$^{+/-}$ Prkaca$^{+/-}$* mice. Data from RT-qPCR on osteogenesis pathway genes (N=84) was presented in a tabular format by comparing WT normal bone and the lesions from *Prkar1a$^{+/-}$* and *Prkar1a$^{+/-}$Prkaca$^{+/-}$* mice. Negative values indicate down-regulated genes. Genes highlighted in yellow indicate significant upregulation and those in red significant downregulation.

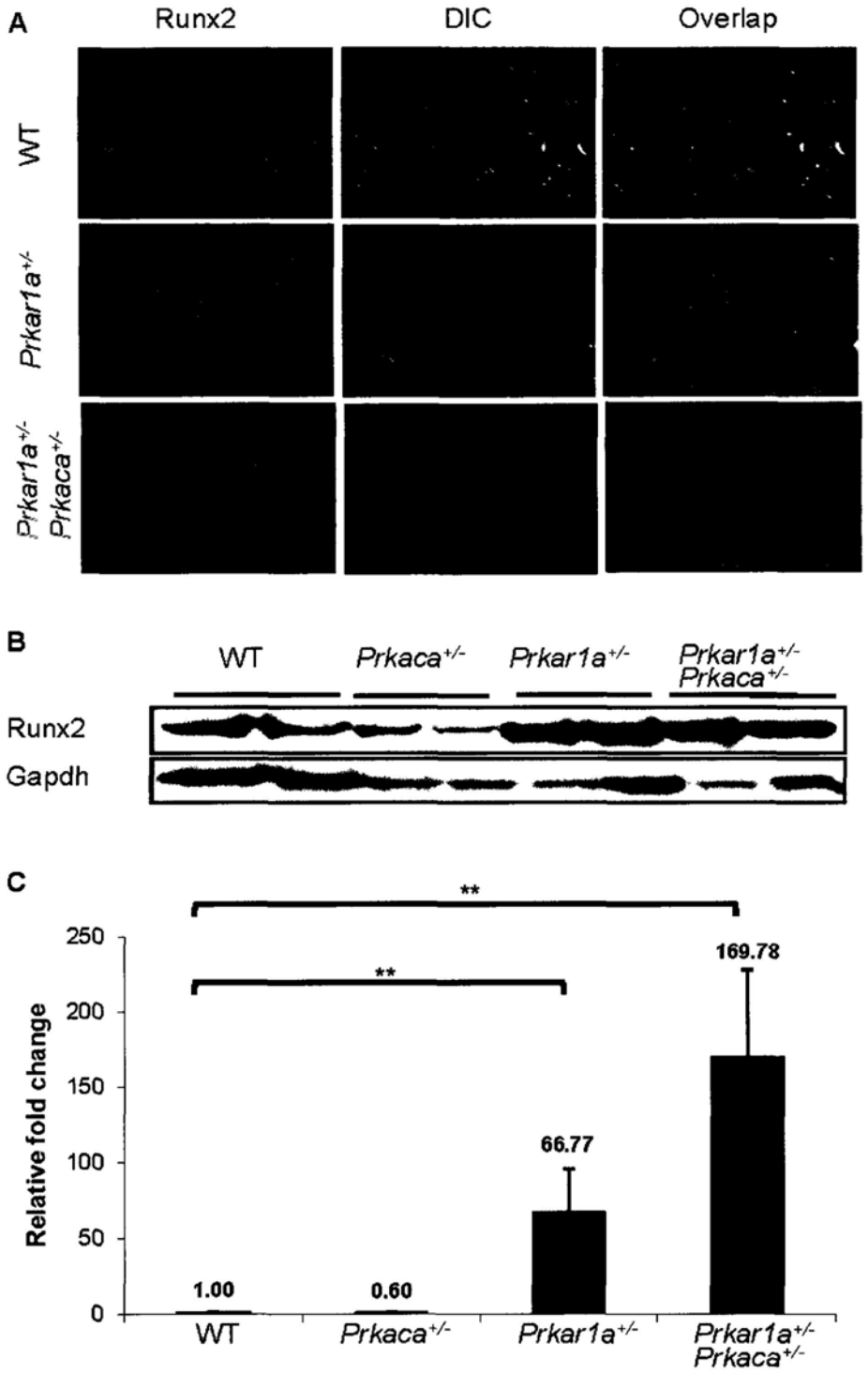

Figure 5.2 Both mRNA and protein expression level of Runx2 were increased in bone lesions from *Prkar1a$^{+/-}$Prkaca$^{+/-}$* mice. (**A**) Immunofluorescence staining, (**B**) western blot analysis and (**C**) quantitative analysis on the expression level of Runx2, pre-osteoblast markers, in bone tissues from WT, *Prkaca$^{+/-}$* and bone lesions from *Prkar1a$^{+/-}$* and *Prkar1a$^{+/-}$Prkaca$^{+/-}$* mice. n=3, **P<0.01.

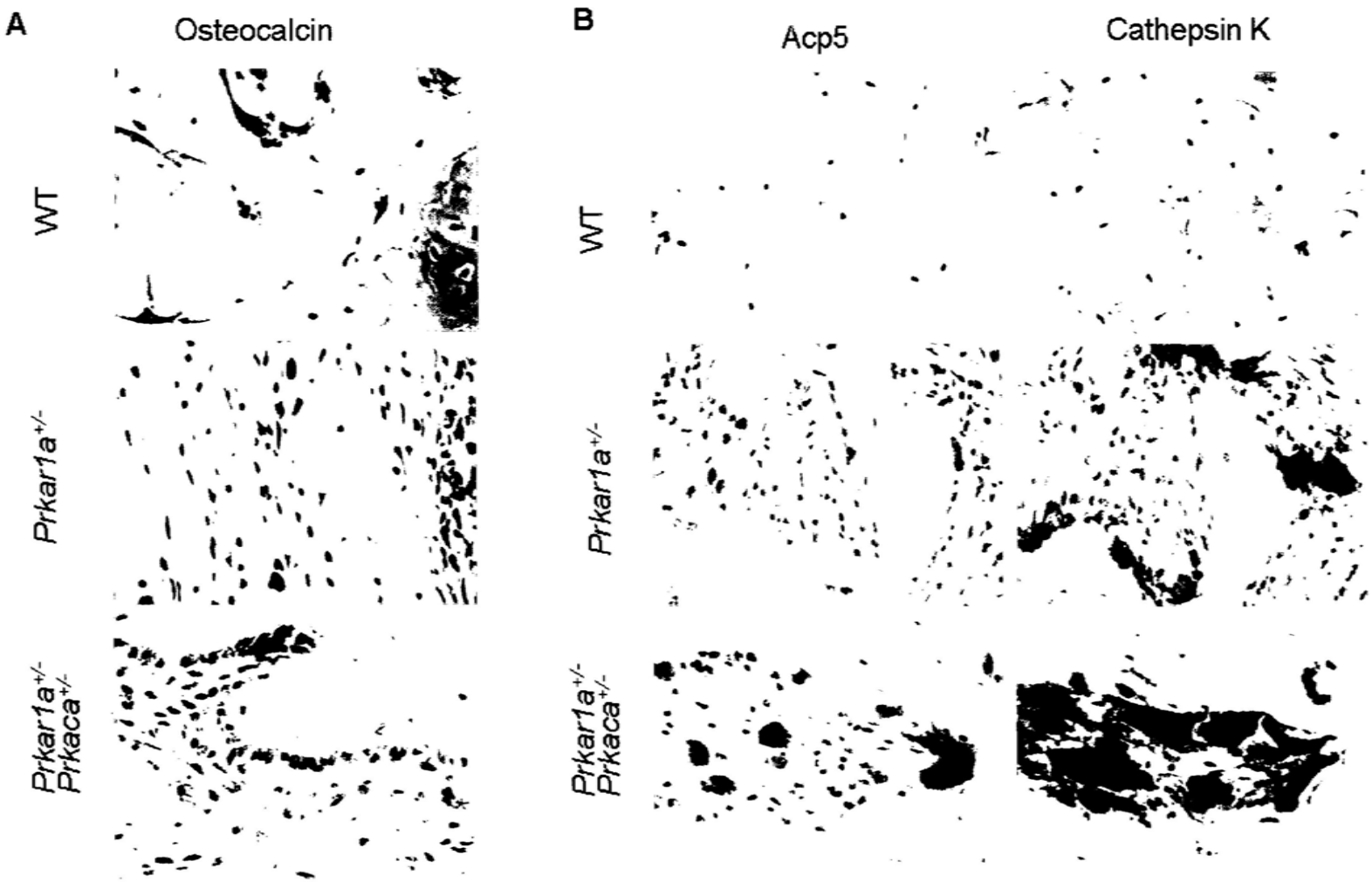

Figure 5.3 Increased osteoclastic activity in bone lesions from *Prkar1a$^{+/-}$Prkaca$^{+/-}$* mice. (**A**) Immunohistochemistry for osteocalcin, mature osteoblasts markers, on WT bones, *Prkar1a$^{+/-}$* and *Prkar1a$^{+/-}$Prkaca$^{+/-}$* bone lesions. (**B**) Immunohistochemistry for Acp5 and Cathepsin K, active osteoclast markers, on WT bones, *Prkar1a$^{+/-}$* and *Prkar1a$^{+/-}$Prkaca$^{+/-}$* bone lesions.

To better understand the molecular mechanisms and differences leading to the formation of more aggressive bone tumors in *Prkar1a*$^{+/-}$*Prkaca*$^{+/-}$ mice, we performed whole genome cDNA microarray study. The raw and normalized array data have been deposited in National Center for Biotechnology Information's Gene Expression Omnibus (GEO) (163) and are accessible through GEO Series accession number GSE20984. Tumor tissues from *Prkar1a*$^{+/-}$ and *Prkar1a*$^{+/-}$ *Prkaca*$^{+/-}$ mice had similar whole genome gene expression signatures when compared against WT tail bone (Figure 5.4A). Both expressed high levels of mesenchymal markers, like *n-cadherin*, *vimentin*, *snail1*, *twist*, *mmp2*, *mmp9*, *tgfb1* and *col1a1* (Table 5.2A, see also Table 5.1); confirmed by IHC studies, mesenchymal proteins n-cadherin and vimentin were highly expressed by abnormally proliferating fibroblasts in bone lesions (Figure 5.5A). Western blot analysis also confirmed the induction of mmp2 and mmp9 protein expression in bone tumors (Figure 5.5B). Mmp9 serum levels were not significantly different between WT, *Prkar1a*$^{+/-}$ and *Prkar1a*$^{+/-}$*Prkaca*$^{+/-}$ mice (Figure 5.5C). We also performed flow cytometry study on the primary cultures of bone tumors. Again, this confirmed the mesenchymal nature of the cells since they expressed high level of vimentin, c-kit and foxo1 (Figure 5.6).

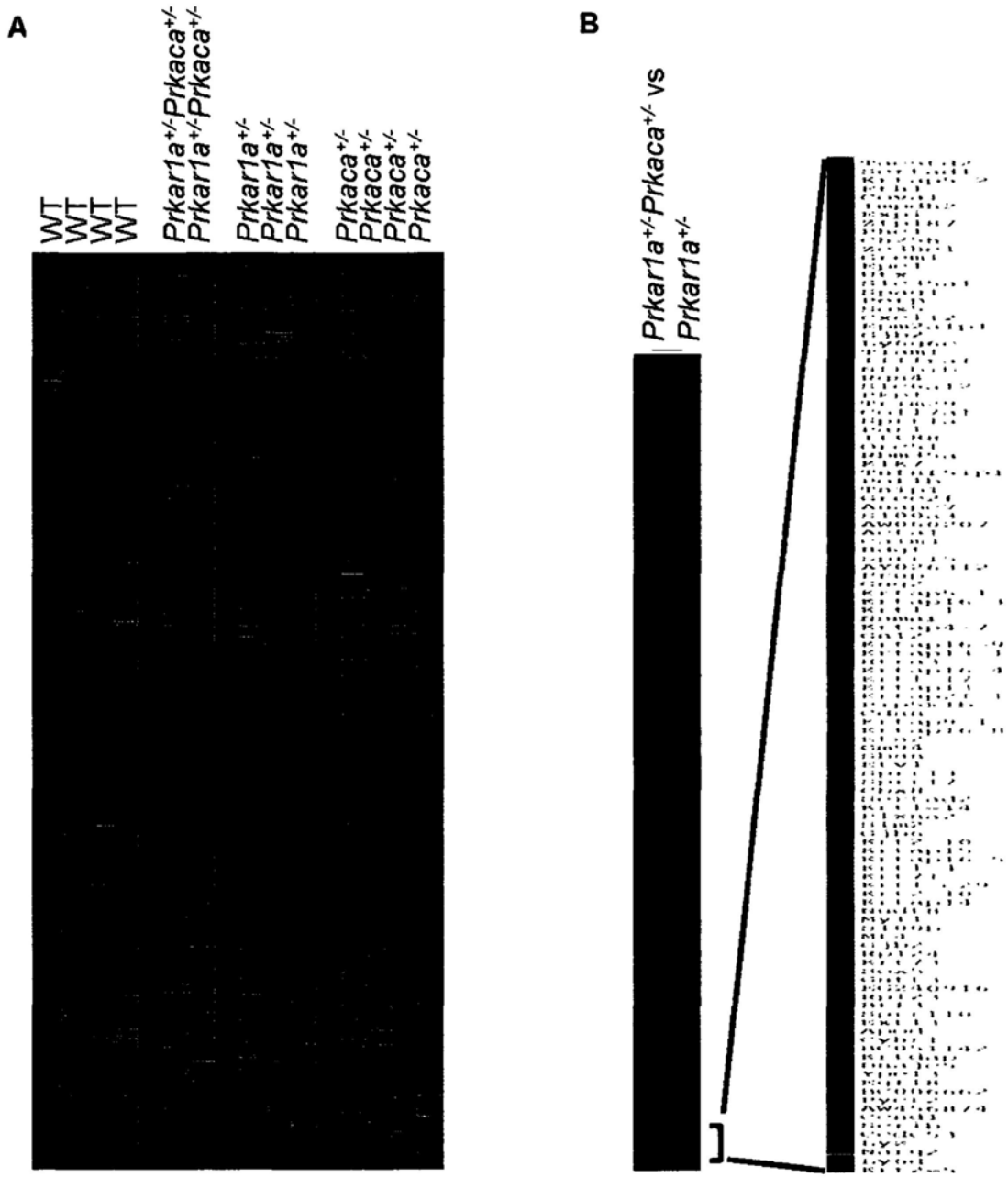

Figure 5.4 Bone lesions from *Prkar1a*$^{+/-}$ and *Prkar1a*$^{+/-}$*Prkaca*$^{+/-}$ mice had a very different gene expression pattern when compared to normal bone. (**A**) Heat map visualization of gene expression data from the bone tissues of WT, *Prkaca*$^{+/-}$ and bone lesions of *Prkar1a*$^{+/-}$ and *Prkar1a*$^{+/-}$*Prkaca*$^{+/-}$ mice. (**B**) Left, heat map visualization of gene expression data comparing *Prkar1a*$^{+/-}$*Prkaca*$^{+/-}$ and *Prakr1a*$^{+/-}$ bone tumors. Right, enlargement of image showing the up-regulation of a group of keratin and keratin-related genes.

A

Genes	Fold change (up-regulated) *Prkar1a*$^{+/-}$ vs WT	*Prkar1a*$^{+/-}$ *Prkaca*$^{+/-}$ vs WT	Remarks
N-cadherin (*Cdh2*)	2.8	2.0	Mesenchymal protein
Vimentin (*Vim*)	1.4	1.3	Mesenchymal protein
Snail1 (*Snail1*)	4.2	3.8	E-cadherin repressor
Twist1	2.1	1.9	Up-regulated by loss of E-cadherin
Foxc2	2.0	1.9	Up-reguates mesenchymal gene transcription
Mmp-2	2.9	5.2	Degradation of basement membrane
Mmp-9	11.0	11.5	Degradation of basement membrane

B

	Genes	Fold change (*Prkar1a*$^{+/-}$ *Prkaca*$^{+/-}$ vs *Prkar1a*$^{+/-}$)
Hair shaft precursor-associated	*S100A3*	3.5
	Bmp4	4.3
	Msx1	3.6
	Foxq1	2.5
	Foxn1	2.1
Hair shaft keratins	*Krt31*	2.1
	Krt34	8.2
	Krt86	6.3
Hair shaft keratin-associated protein	*Krtap16-3*	11.0
	Krtap16-4	2.6
	Krtap16-5	5.2
	Krtap16-8	4.2
	Krtap16-9	3.5
Hair follicle	*Krt71*	4.1
Keratin specific for IRS cuticle	*Krt73*	2.1
Keratin expressed in IRS cuticle and other IRS layers	*Krt27*	4.0
	Krt71	3.4
Fillform tongue papilla	*Krt84*	11.5
Epidermal stratification	*Krt14*	14.0
	Krt10	4.8

Table 5.2 *Prkar1a* and *Prkaca* haploinsufficiency led to the induction of mesenchymal-to-epithelial transition. (**A**) Calculated fold changes from microarray study of different mesechymal genes in *Prkar1a*$^{+/-}$ and *Prkar1a*$^{+/-}$ *Prkaca*$^{+/-}$ tumors when compared to WT. (**B**) Differentially expressed genes shown in microarray study, which are involved in hair follicle and epithelial differentiation, in lesions from *Prkar1a*$^{+/-}$*Prkaca*$^{+/-}$ mice when compared to those of *Prkar1a*$^{+/-}$ animal.

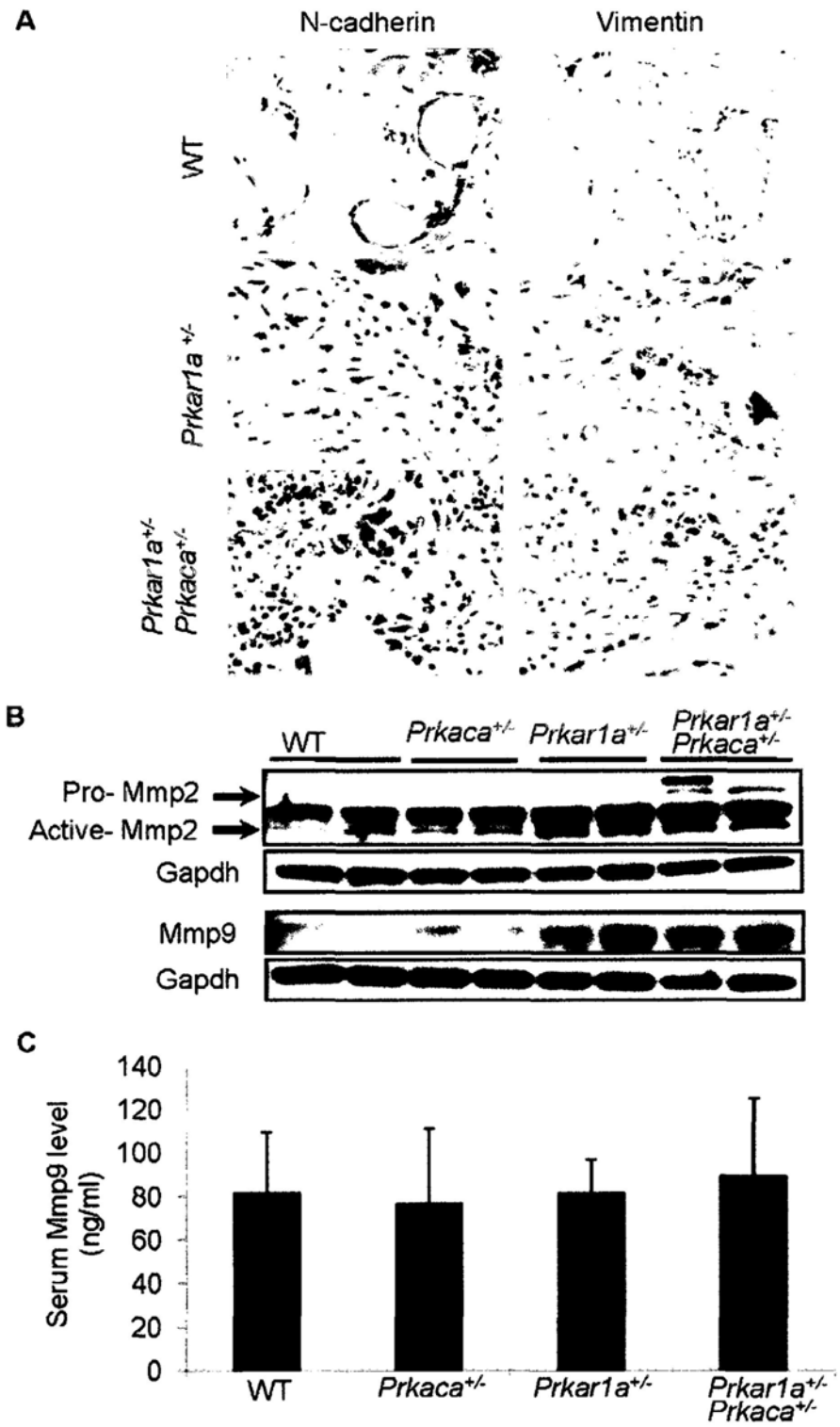

Figure 5.5 Expression of mesenchymal proteins in bone lesions from *Prkar1a*$^{+/-}$ and *Prkar1a*$^{+/-}$*Prkaca*$^{+/-}$ mice. (**A**) Immunohistochemistry for n-cadherin and vimentin, mesenchymal proteins. (**B**) Western blot analysis on Mmp2 and Mmp9. (**C**) No difference in serum Mmp9 level among WT, *Prkaca*$^{+/-}$, *Prkar1a*$^{+/-}$ and *Prkar1a*$^{+/-}$*Prkaca*$^{+/-}$ mice.

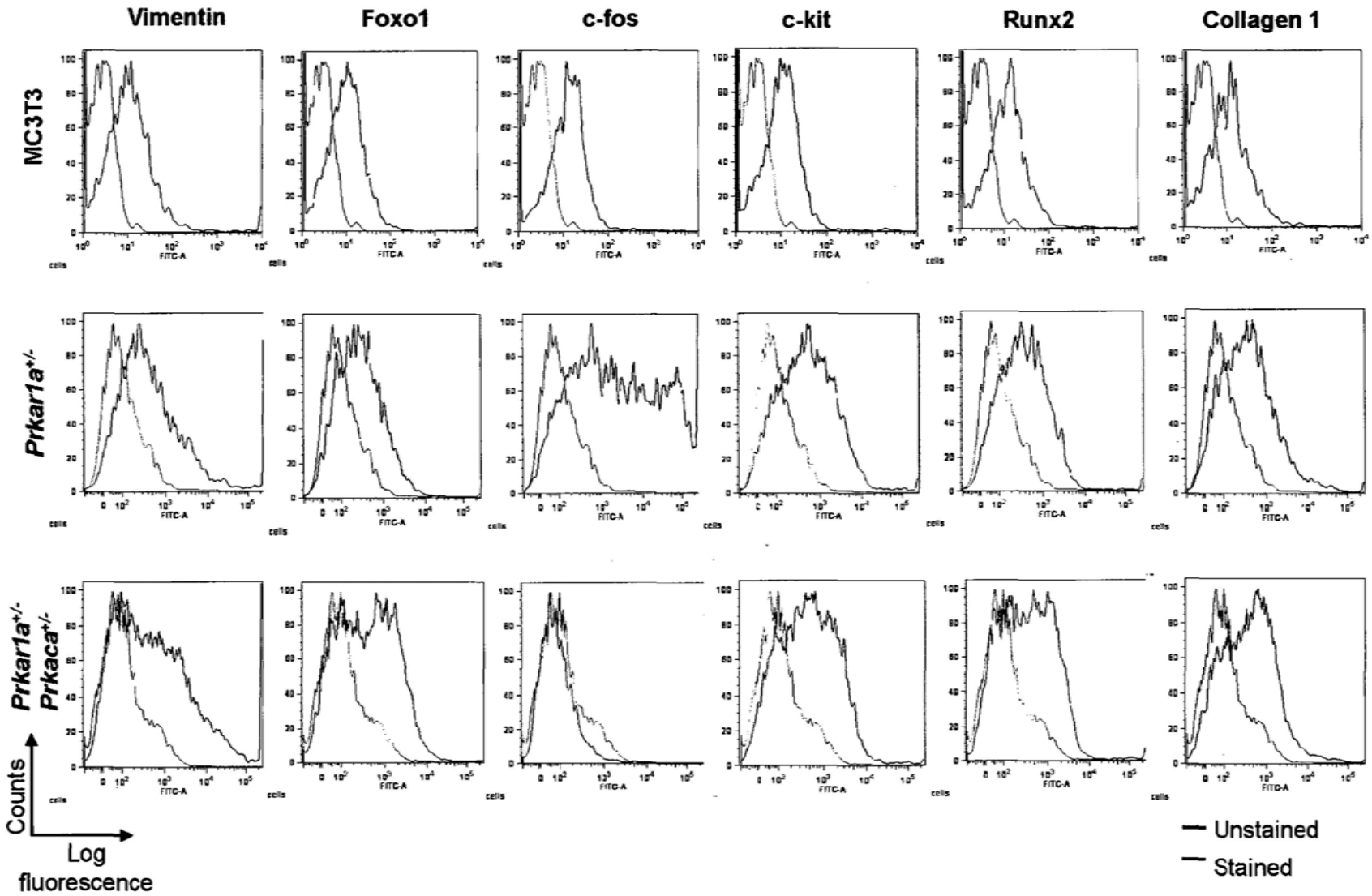

Figure 5.6 Expression of mesenchymal markers and osteoblastic markers in primary cells derived from *Prkar1a*$^{+/-}$ and *Prkar1a*$^{+/-}$ *Prkaca*$^{+/-}$ bone tumors. Flow cytometry analysis for the expression of mesenchymal markers vimentin, foxo1, c-fos, c-kit and osteogenic markers runx2 and collagen 1 in bone tumor cells from mice studied in the present investigation.

We then compared *Prkar1a*$^{+/-}$ and *Prkar1a*$^{+/-}$*Prkaca*$^{+/-}$ bone tumors using a hierarchical clustering algorithm (164) (Suppl. Figure 11B). We identified 258 significantly up-regulated genes in bone tumors from *Prkar1a*$^{+/-}$*Prkaca*$^{+/-}$ mice; they included 20 genes associated with hair and epithelial differentiation, such as keratin and keratin-related genes, *S100A3*, *Bmp4*, *Msx1*, *Foxq1*, and *Foxn1* (Table 5.2B, Figure 5.4B). IHC staining for epithelial markers, E-cadherin and cytokeratin 18 (Figure 5.7A), also revealed that, whereas most of the fibroblast-like cells were mesenchymal, islands of cells within the *Prkar1a*$^{+/-}$*Prkaca*$^{+/-}$ lesions expressed epithelial markers. Several other genes were increased in the *Prkar1a*$^{+/-}$*Prkaca*$^{+/-}$ tumors including *cFos* and *Foxo1*; IHC confirmed these data (Figure 5.7B). *c-fos* upregulation were not shown in flow cytometry analysis that may result from the cellular changes under *in vitro* conditions during primary tumor cells development. It may also due to the suitability of the antibody for flow cytometry analysis. However what appeared to be the most upregulated molecular pathway in these lesions was that of the *Wnt* signaling. We then performed RT-qPCR array analysis of *Wnt* signaling pathway genes (N=84) that showed that the lesions from *Prkar1a*$^{+/-}$*Prkaca*$^{+/-}$ mice had increased expression of *brachyury* (the *T* gene), *Wnt3*, *Wnt3a*, *Wnt7a*, *Wnt8a*, and *Wnt8b* (Table 5.3). In accordance, the lesions also showed down-regulation of *Wnt* signaling pathway inhibitors, such as the *Dkk1*. *Brachyury* was also confirmed, by IHC, to be increased in lesions from *Prkar1a*$^{+/-}$*Prkaca*$^{+/-}$ mice (Figure 5.7B). These data suggested that *prkar1a* haploinsufficiency was able to induce the active proliferation of bone stromal cells, which are of osteogenic lineage, within the

marrow cavity; while *prkar1a* haploinsufficiency under *prkaca*$^{+/-}$ background was able to induce islands of mesenchymal-to-epithelial transition (MET) within the abnormal stromal cells population.

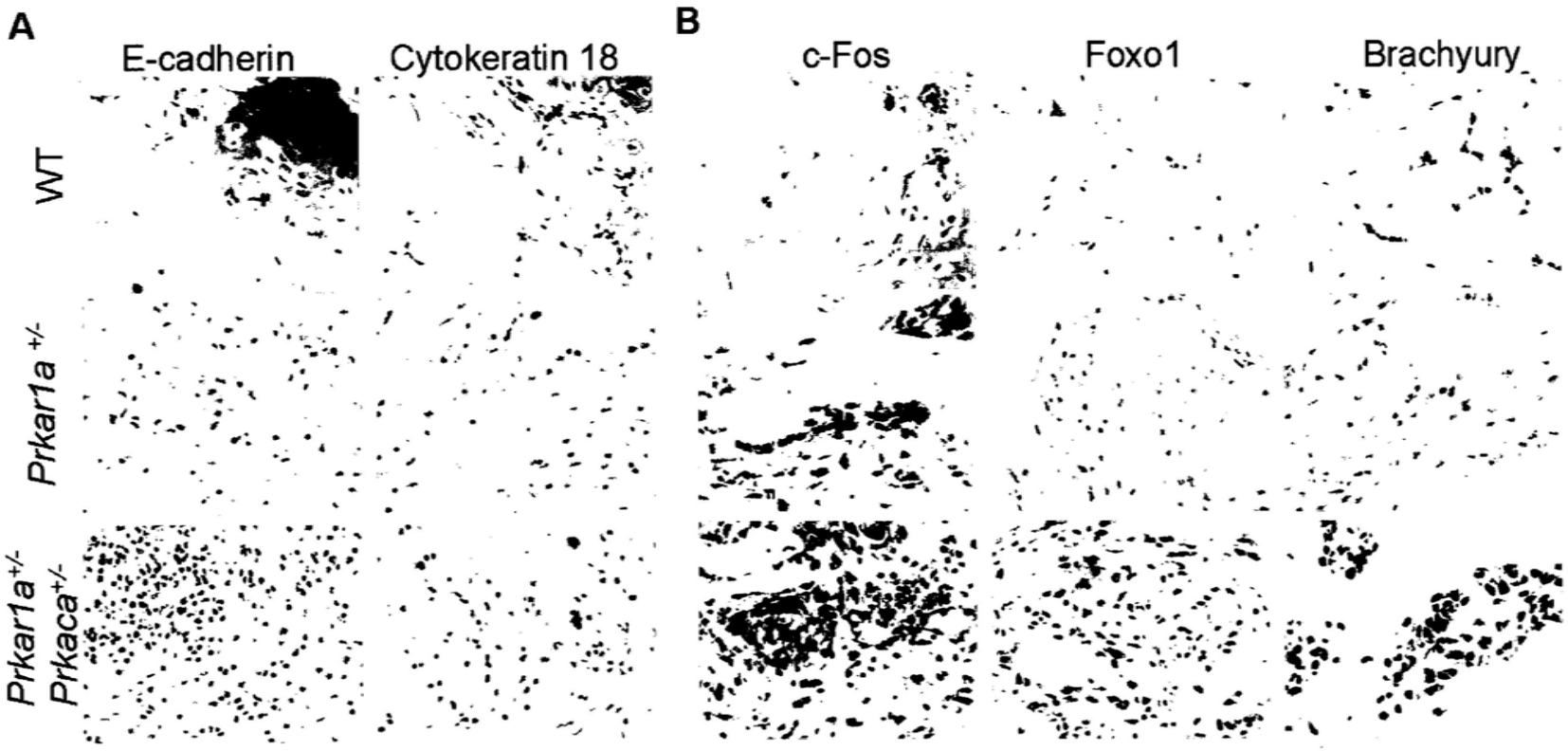

Figure 5.7 Increased expression of epithelial markers, Foxo1 and Brachyury protein in *Prkar1a$^{+/-}$Prkaca$^{+/-}$* bone tumors. (**A**) Immunohistochemistry for e-cadherin and cytokeratin 18, epithelial proteins, confirming the mesenchymal-to-epithelial gene signature in lesions from *Prkar1a$^{+/-}$Prkaca$^{+/-}$* mice. (**B**) Immunohistochemistry for c-fos, foxo1 and brachyury on WT bones, *Prkar1a$^{+/-}$* and *Prkar1a$^{+/-}$Prkaca$^{+/-}$* bone lesions.

Gene symbol	Gene	Up/Down Regulation *Prkar1a*$^{+/-}$*Prkaca*$^{+/-}$ vs *Prkar1a*$^{+/-}$
Aes	Amino-terminal enhancer of split	1.3503
Apc	Adenomatosis polyposis coli	1.5175
Axin1	Axin 1	-1.0293
Bcl9	B-cell CLL/lymphoma 9	1.2016
Btrc	Beta-transducin repeat containing protein	1.1381
Ctnnbip1	Catenin beta interacting protein 1	1.3395
Ccnd1	Cyclin D1	1.4158
Ccnd2	Cyclin D2	1.7231
Ccnd3	Cyclin D3	-1.0461
Csnk1a1	Casein kinase 1, alpha 1	1.3883
Csnk1d	Casein kinase 1, delta	1.4241
Csnk2a1	Casein kinase 2, alpha 1 polypeptide	1.3629
Ctbp1	C-terminal binding protein 1	1.2128
Ctbp2	C-terminal binding protein 2	1.4373
Ctnnb1	Catenin (cadherin associated protein), beta 1	1.2585
Daam1	Dishevelled associated activator of morphogenesis 1	1.3964
Dixdc1	DIX domain containing 1	1.0485
Dkk1	Dickkopf homolog 1 (Xenopus laevis)	-1.7033
Dvl1	Dishevelled, dsh homolog 1 (Drosophila)	2.783
Dvl2	Dishevelled 2, dsh homolog (Drosophila)	1.1019
Ep300	E1A binding protein p300	1.2368
Fbxw11	F-box and WD-40 domain protein 11	1.4306
Fbxw2	F-box and WD-40 domain protein 2	1.3119
Fbxw4	F-box and WD-40 domain protein 4	1.7112
Fgf4	Fibroblast growth factor 4	1.9207
Fosl1	Fos-like antigen 1	-1.3119
Foxn1	Forkhead box N1	2.0825
Frat1	Frequently rearranged in advanced T-cell lymphomas	-1.2283
Frzb	Frizzled-related protein	1.1083
Fshb	Follicle stimulating hormone beta	1.9656
Fzd1	Frizzled homolog 1 (Drosophila)	1.5476
Fzd2	Frizzled homolog 2 (Drosophila)	1.7532
Fzd3	Frizzled homolog 3 (Drosophila)	1.3149
Fzd4	Frizzled homolog 4 (Drosophila)	-1.0994
Fzd5	Frizzled homolog 5 (Drosophila)	1.514
Fzd6	Frizzled homolog 6 (Drosophila)	1.1329
Fzd7	Frizzled homolog 7 (Drosophila)	-1.2716
Fzd8	Frizzled homolog 8 (Drosophila)	-1.7371
Gsk3b	Glycogen synthase kinase 3 beta	1.3851
Jun	Jun oncogene	1.1225
Kremen1	Kringle containing transmembrane protein 1	1.2834
Lef1	Lymphoid enhancer binding factor 1	1.0305
Lrp5	Low density lipoprotein receptor-related protein 5	1.3441
Lrp6	Low density lipoprotein receptor-related protein 6	1.3272
Myc	Myelocytomatosis oncogene	-1.1474
Nkd1	Naked cuticle 1 homolog (Drosophila)	-1.0163
Nlk	Nemo like kinase	1.1989

Pitx2	Paired-like homeodomain transcription factor 2	-1.0867
Porcn	Porcupine homolog (Drosophila)	1.021
Ppp2ca	Protein phosphatase 2 (formerly 2A), catalytic subunit, alpha isoform	1.3195
Ppp2r1a	Protein phosphatase 2 (formerly 2A), regulatory subunit A (PR 65), alpha isoform	1.0994
Ppp2r5d	Protein phosphatase 2, regulatory subunit B (B56), delta isoform	-1.3104
Pygo1	Pygopus 1	1.4557
Rhou	Ras homolog gene family, member U	1.0755
Senp2	SUMO/sentrin specific peptidase 2	1.4658
Sfrp1	Secreted frizzled-related protein 1	1.7271
Sfrp2	Secreted frizzled-related protein 2	1.5674
Sfrp4	Secreted frizzled-related protein 4	1.2938
Slc9a3r1	Solute carrier family 9 (sodium/hydrogen exchanger), member 3 regulator 1	-1.1019
Sox17	SRY-box containing gene 17	3.2378
T	Brachyury	3.1638
Tcf3	Transcription factor 3	1.0437
Tcf7	Transcription factor 7, T-cell specific	1.6358
Tle1	Transducin-like enhancer of split 1, homolog of Drosophila E(spl)	1.0046
Tle2	Transducin-like enhancer of split 2, homolog of Drosophila E(spl)	1.2894
Wif1	Wnt inhibitory factor 1	1.4241
Wisp1	WNT1 inducible signaling pathway protein 1	1.834
Wnt1	Wingless-related MMTV integration site 1	1.1594
Wnt10a	Wingless related MMTV integration site 10a	2.4852
Wnt11	Wingless-related MMTV integration site 11	1.3195
Wnt16	Wingless-related MMTV integration site 16	1.4931
Wnt2	Wingless-related MMTV integration site 2	-1.374
Wnt2b	Wingless related MMTV integration site 2b	1.8553
Wnt3	Wingless-related MMTV integration site 3	1.7391
Wnt3a	Wingless-related MMTV integration site 3A	1.6208
Wnt4	Wingless-related MMTV integration site 4	1.1199
Wnt5a	Wingless-related MMTV integration site 5A	-1.3272
Wnt5b	Wingless-related MMTV integration site 5B	1.8383
Wnt6	Wingless-related MMTV integration site 6	1.2411
Wnt7a	Wingless-related MMTV integration site 7A	1.7391
Wnt7b	Wingless-related MMTV integration site 7B	1.5801
Wnt8a	Wingless-related MMTV integration site 8A	1.7391
Wnt8b	Wingless related MMTV integration site 8b	2.6057
Wnt9a	Wingless-type MMTV integration site 9A	-1.0705

Table 5.3 *Prkar1a*$^{+/-}$*Prkaca*$^{+/-}$ mice bone tumors had activated Wnt-signaling pathway. The table presents the data on 84 molecules involved in Wnt-signaling pathway in *Prkar1a*$^{+/-}$*Prkaca*$^{+/-}$ mice tumors in comparison to those of *Prkar1a*$^{+/-}$ mice. Negative values indicate down-regulated genes. Gene highlighted in yellow indicates significant upregulation.

Chapter Six

Further Characterization of Mice Deficient in Protein Kinase A Signaling

6.1 Generation of mice deficiency in protein kinase A regulatory subunit type 1A (*prkar1a*) and type 2B (*prkar2b*) (*Prkar1a*$^{+/-}$*Prkar2b*$^{+/-}$)

Consistent with previous studies, the present study demonstrated that loss of *prkar1a* led to upregulation of type II regulatory subunits. It is believed that increased PKA-II and/or type II regulatory subunits are responsible for increased cAMP-responsive total PKA activity. In accordance, we hypothesized that introduction of *prkar1a* haploinsufficiency in the background of *prkar2b*$^{+/-}$ would abrogate some of the tumor formation, probably through the reduction in formation of PKA-II holoenzyme. Again, double heterozygous mice were generated by breeding *Prkar1a*$^{+/-}$ mice with *Prkar2b*$^{+/-}$ mice and bred into a mixed C57BL/6x129Sv/B6 hybrid background. Genomic DNAs from tail tips were used to confirm the genotypes, using the conditions described in Materials and Methods (Figure 6.1)

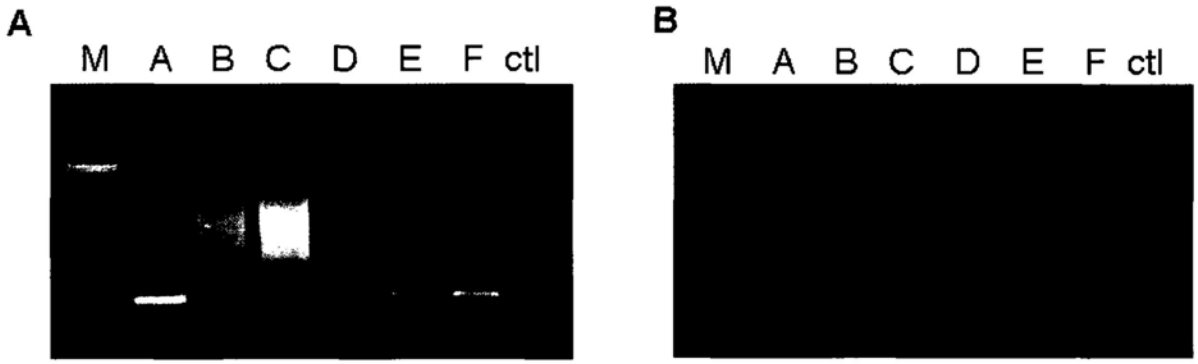

Figure 6.1 Genomic PCR experiments were used for the genotyping of *prkar2b* gene in mice. (**A**) Genotyping of *prkar2b* WT allele and (**B**) genotyping of *prkar2b* KO allele in animal A-F using the primers described in Materials and Methods. Taken together, Animal A had the genotype *Prkar2b*$^{+/+}$; Animal B had the genotype *Prkar2b*$^{+/-}$; Animal C had the genotype *Prkar2b*$^{+/+}$; Animal D had the genotype *Prkar2b*$^{+/-}$; Animal E had the genotype *Prkar2b*$^{+/+}$; Animal F had the genotype *Prkar2b*$^{+/-}$. M, 100bp ladder; ctl, negative control.

6.2 Phenotypic characterization of *Prkar1a*$^{+/-}$*Prkar2b*$^{+/-}$ double heterozygous mice

Since the *Prkar1a*$^{+/-}$*Prkar2b*$^{+/-}$ mice were bred from the same cohort of mice as *Prkar1a*$^{+/-}$*Prkaca*$^{+/-}$ mice and the breeding were preformed in parallel, we used the same 24 WT and 34 *Prkar1a*$^{+/-}$ mice to compare against 23 *Prkar2b*$^{+/-}$ and 39 *Prkar1a*$^{+/-}$*Prkar2b*$^{+/-}$ mice.

Several phenotypes were observed in both *Prkar1a*$^{+/-}$ and *Prkar1a*$^{+/-}$ *Prkar2b*$^{+/-}$ mice. First, *Prkar1a*$^{+/-}$*Prkar2b*$^{+/-}$ mice also developed thyroid tumors; these varied from 4 cases (10.3% *vs* 14.7% in *Prkar1a*$^{+/-}$ mice) of follicular adenoma and 5 cases (12.8% *vs* 2.9% in *Prkar1a*$^{+/-}$ mice) of follicular papillary adenoma to 3 cases (7.7% *vs* 5.9% in *Prkar1a*$^{+/-}$ mice) of follicular papillary cystadenoma (Figure 6.2); Second, 17 out of 39 *Prkar1a*$^{+/-}$*Prkar2b*$^{+/-}$ mice (43.6% *vs* 32.4% in *Prkar1a*$^{+/-}$ mice) also had eosinophilic cellular alteration in the liver; Third, 14 of them (35.9% *vs* 44.1% in *Prkar1a*$^{+/-}$ mice) developed adrenal subcapsular hyperplasia.

Although we observed only one case of a pituitary cyst in *Prkar1a*$^{+/-}$ *Prkar2b*$^{+/-}$ mice (2.6% *vs* 8.8% in *Prkar1a*$^{+/-}$ mice), one 18 months old *Prkar2b*$^{+/-}$ and one 18 months old *Prkar1a*$^{+/-}$*Prkar2b*$^{+/-}$ mouse developed adenoma in pars intermedia of pituitary (Figure 6.3) that were not found in *Prkar1a*$^{+/-}$ mice.

Seven out of 39 *Prkar1a*$^{+/-}$*Prkar2b*$^{+/-}$ mice (17.9%) developed osteomyxoma (Figure 6.4A, B) in caudal vertebrae that was less frequent than in *Prkar1a*$^{+/-}$ and *Prkar1a*$^{+/-}$*Prkaca*$^{+/-}$ mice. However, 50% of *Prkar1a*$^{+/-}$*Prkar2b*$^{+/-}$ mice developed fibro-osseous lesions (Figure 6.4C, D), which were considered

being an early stage of osteomyxoma; and 10% of them had active osteoblastic activity in trabecular, endosteal and periosteum of the caudal vertebrae. Moreover, one 14 month-old and one 18 month-old *Prkar1a*$^{+/-}$*Prkar2b*$^{+/-}$ mice developed osteochondromyxoma (Figure 6.4E, F). In contrast to *Prkar1a*$^{+/-}$ and *Prkar1a*$^{+/-}$*Prkaca*$^{+/-}$ mice, we did not observed any cartilaginous hyperplasia and osteochondrodysplasia in marrow cavities of the long bones (femur, tibia), instead only fibro-osseous to osteomyxoma lesions were observed in long bone of *Prkar1a*$^{+/-}$*Prkar2b*$^{+/-}$ mice. We also saw four cases of chondroma in spinal column and fibro-osseous lesions in phalanx, tarsal bone and metacarpal bone as well as one osteomyxoma in phalanx.

Haploinsufficiency of *prkar1a* under *prkar2b*$^{+/-}$ background also lead to development of tumors in the craniofacial and skull bones. The lesions varied from osteoblastic proliferation of median median nasal septal bone and maxilla bone (Figure 6.5A, B, C, D) to chondroma in palatine bone (Figure 6.5E). One *Prkar1a*$^{+/-}$*Prkar2b*$^{+/-}$ mouse developed myxosarcoma of skull (Figure 6.5F).

Another significant observation was that 17 out of 39 *Prkar1a*$^{+/-}$*Prkar2b*$^{+/-}$ mice (43.6% *vs* 11.8% in *Prkar1a*$^{+/-}$ mice) developed peliotic lesions in spleen (Figure 6.6); while none of the *Prkar1a*$^{+/-}$*Prkaca*$^{+/-}$ mice showed this type of lesion.

Similarly, we did not observe any gender differences in the incidence of bone lesions. Blood cell counts and biochemical values (i.e. total and ionized calcium, phosphate, and others) were within normal range, although elevated

alkaline phosphatase level and decreased glucose, cholesterol and triglyceride level were observed in *Prkar1a*$^{+/-}$*Prkar2b*$^{+/-}$ mice (Table 6.1 and Figure 6.7).

These data suggested that the reduction of *prkar1a* under p*rkar2b* haploinsufficiency background can not obrogate the development of tumors from thyroid follicles, pituitary and bone cells. *Prkar1a*$^{+/-}$*Prkar2b*$^{+/-}$ mice developed the same spectrum of tumors as in *Prkar1a*$^{+/-}$ mice in similar frequency and time of onset, indicating that RIIβ may not be the primary subunit leading to tumorigenesis under *Prkar1a* haploinsuffciency background.

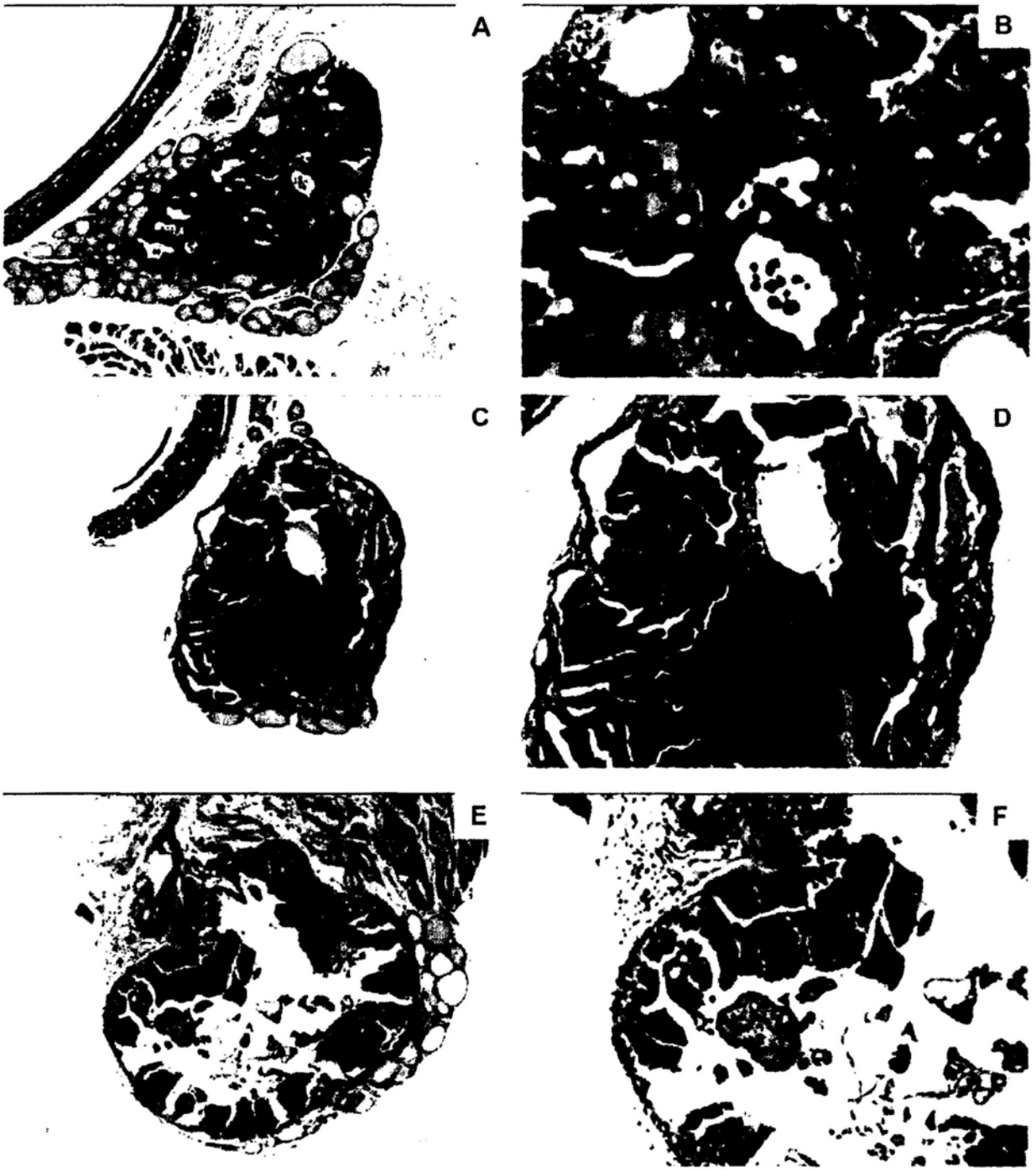

Figure 6.2 Representative views of thyroid neoplasms in *Prkar1a*$^{+/-}$ *Prkar2b*$^{+/-}$ mice. (**A-F**) Haematoxylin and eosin (H&E) staining of section of thyroid from *Prkar1a*$^{+/-}$ *Prkar2b*$^{+/-}$ mice. (A, B) Thyroid follicular adenoma from a 15 month-old *Prkar1a*$^{+/-}$ *Prkar2b*$^{+/-}$ mouse. (A) Original magnification, 10x. (B) Original magnification, 40x. (C, D) Thyroid follicular papillary adenoma from a 12 month-old *Prkar1a*$^{+/-}$ *Prkar2b*$^{+/-}$ mouse. (C) Original magnification, 10x. (D) Original magnification, 20x. (E, F) Thyroid follicular papillary cystadenoma from a 14 month-old *Prkar1a*$^{+/-}$ *Prkar2b*$^{+/-}$ mouse. (E) Original magnification, 10x. (F) Original magnification, 20x.

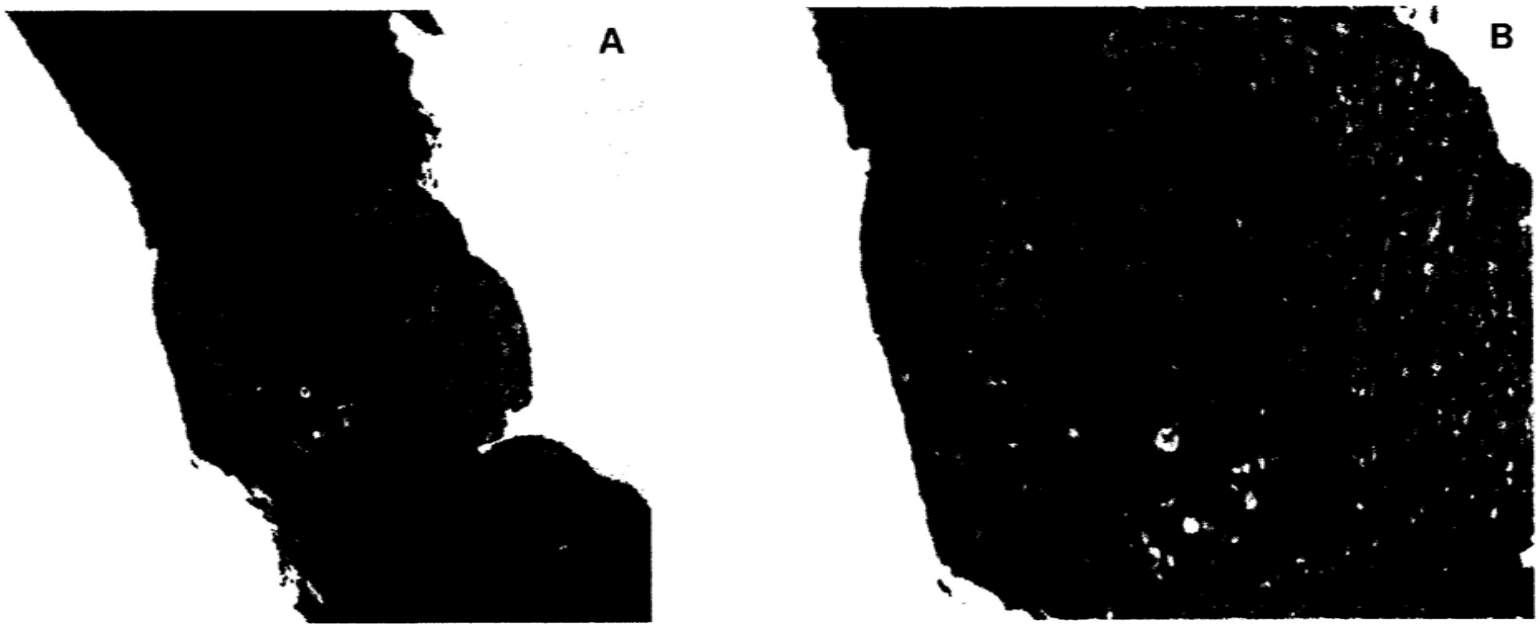

Figure 6.3 Representative views of pituitary adenoma in *Prkar1a*$^{+/-}$ *Prkar2b*$^{+/-}$ mice. (**A,B**) Haematoxylin and eosin (H&E) staining of section of pituitary from a 17 month-old *Prkar1a*$^{+/-}$ *Prkar2b*$^{+/-}$ mouse. (A) Original magnification, 10x. (B) Original magnification, 20x.

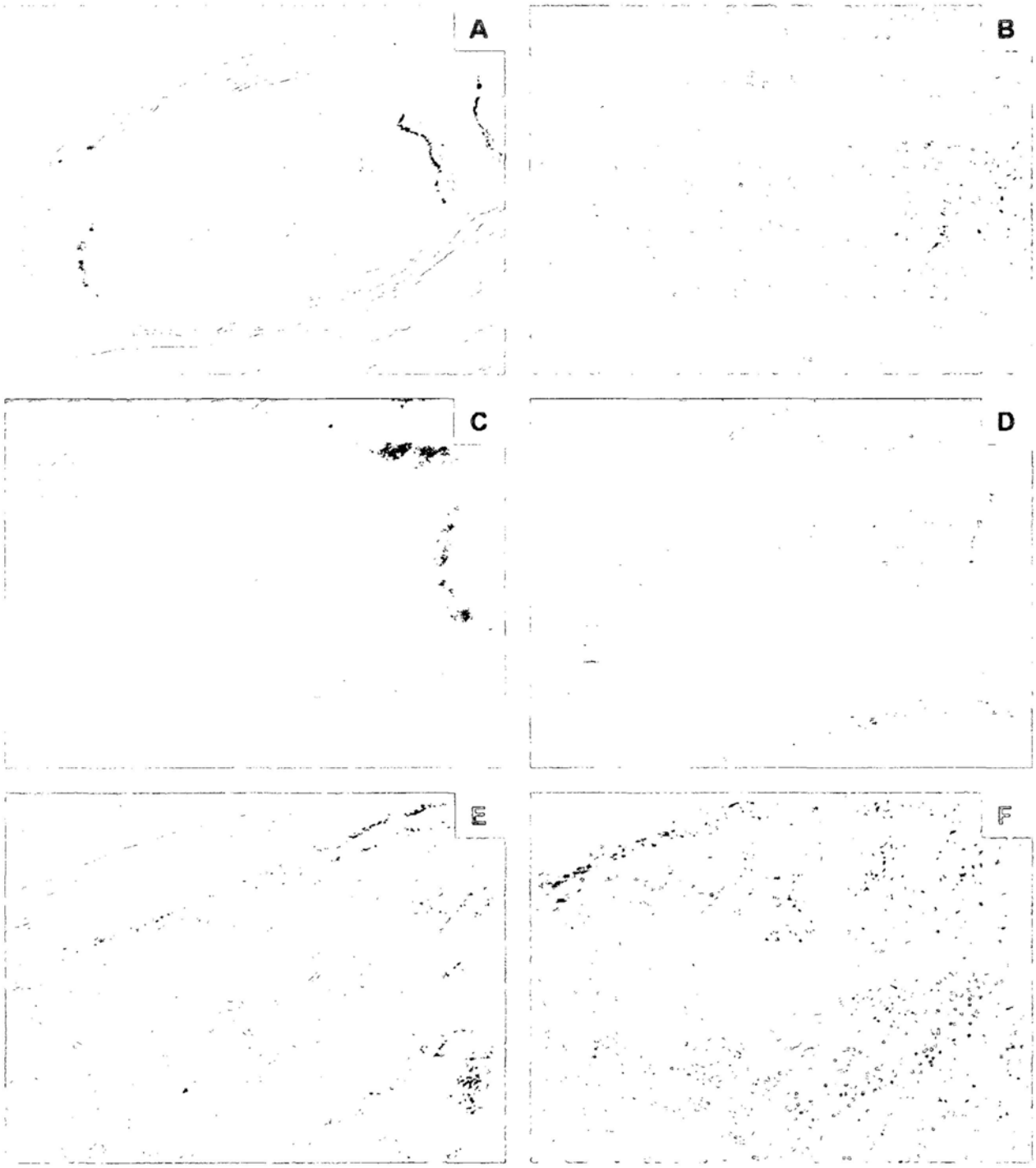

Figure 6.4 Representative views of bone lesions in *Prkar1a*$^{+/-}$ *Prkar2b*$^{+/-}$ mice. (**A-F**) Haematoxylin and eosin (H&E) staining of longitudinal sections of caudal bones from a 14 month-old *Prkar1a*$^{+/-}$ *Prkar2b*$^{+/-}$ mouse. (A, B) Osteomyxoma. (A) Original magnification, 2x. (B) Original magnification, 20x. (C, D) Fibro-osseous lesion. (C) Original magnification, 10x. (D) Original magnification, 20x. (E, F) Osteochondromyxoma . (E) Original magnification, 10x. (F) Original magnification, 20x.

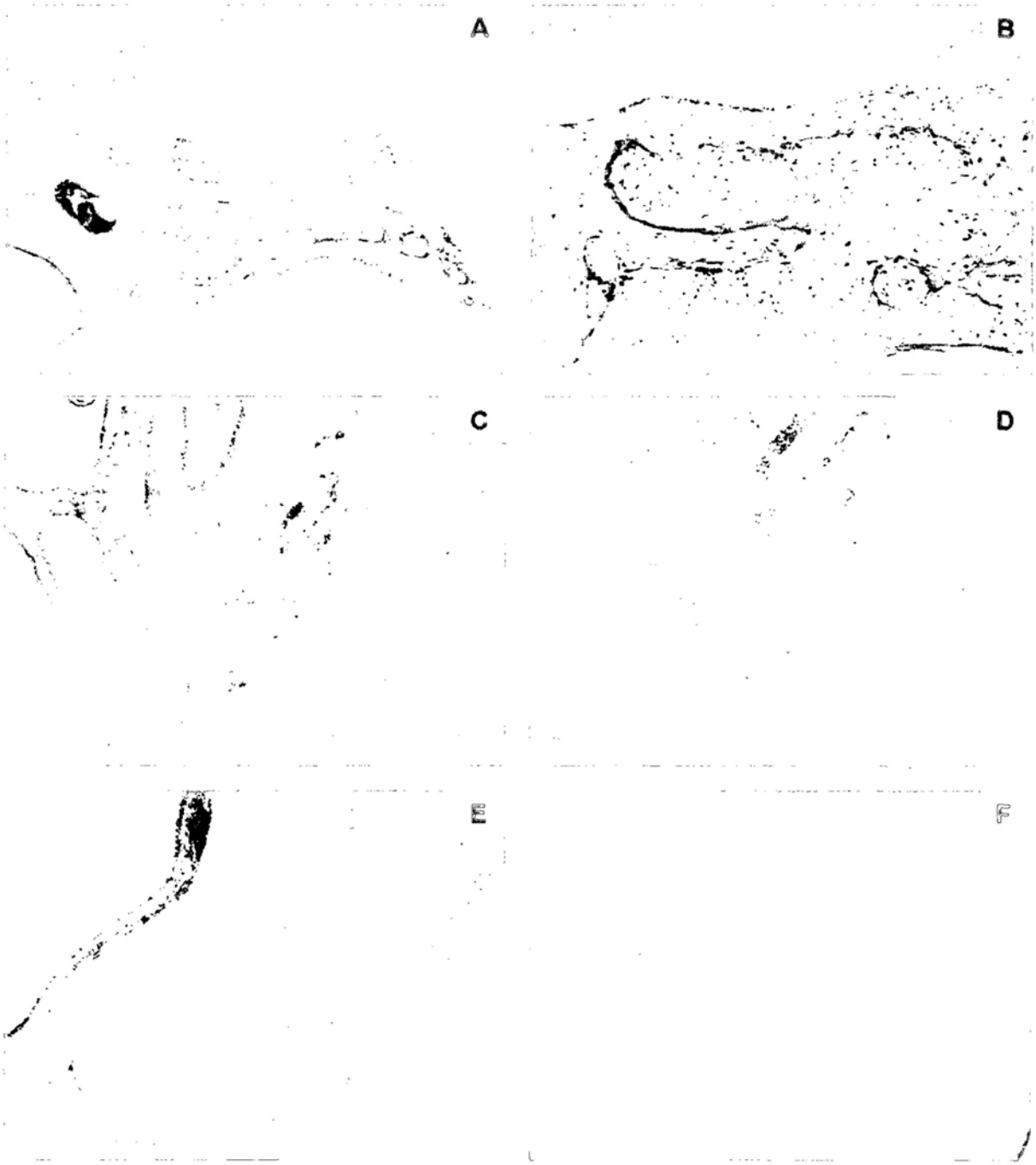

Figure 6.5 Representative views of flat bone lesions in *Prkar1a*$^{+/-}$ *Prkar2b*$^{+/-}$ mice. (**A-F**) Haematoxylin and eosin (H&E) staining of sections of skull bones from *Prkar1a*$^{+/-}$ *Prkar2b*$^{+/-}$ mice. (A, B) Fibro-osseous to osteomyxoma lesions in petrosal bone of a 17 month-old *Prkar1a*$^{+/-}$ *Prkar2b*$^{+/-}$ mouse. (A) Original magnification, 10x. (B) Original magnification, 40x. (C, D) Osteoblastic proliferation in maxilla bone of a 18 month-old *Prkar1a*$^{+/-}$ *Prkar2b*$^{+/-}$ mouse. (C) Original magnification, 10x. (D) Original magnification, 20x. (E) Chondroma in the palatine bone of a 12 month-old *Prkar1a*$^{+/-}$ *Prkar2b*$^{+/-}$ mouse (original magnification, 2x). (F) Myxosarcoma in skull of a 18 month-old *Prkar1a*$^{+/-}$ *Prkar2b*$^{+/-}$ mouse (original magnification, 2x.)

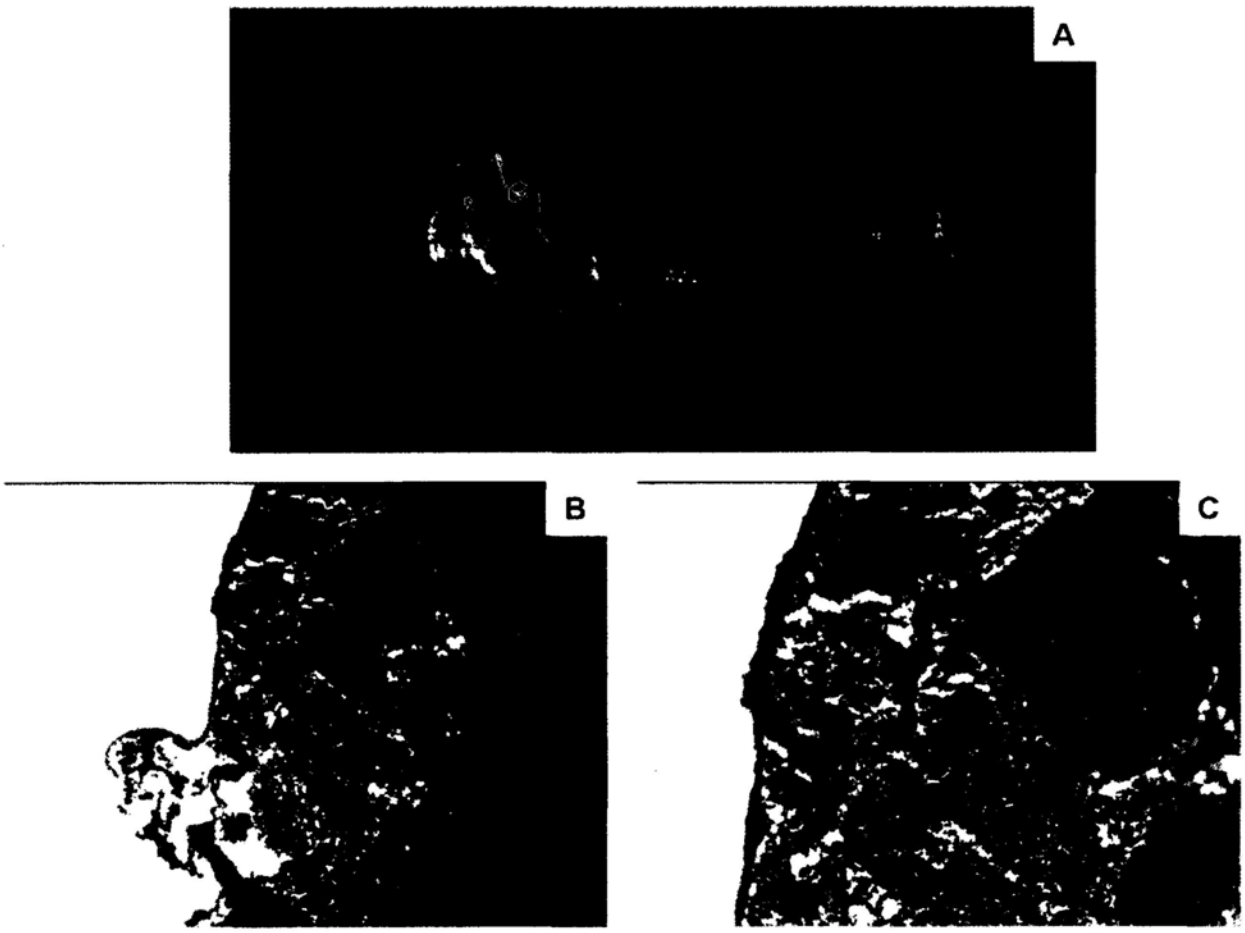

Figure 6.6 Representative views of spleen peliosis in *Prkar1a*$^{+/-}$ *Prkar2b*$^{+/-}$ mice. (**A**) Gross picture of the spleen from a 12 month-old *Prkar1a*$^{+/-}$ *Prkar2b*$^{+/-}$ mouse. (**B, C**) Haematoxylin and eosin (H&E) staining of section spleen from a 12 month-old *Prkar1a*$^{+/-}$ *Prkar2b*$^{+/-}$ mouse. (B) Original magnification, 10x. (C) Original magnification, 20x.

Genotype	Sex	GLU*	CHOL*	TRIG*	ALB*	Ca*	PHOS*	ALP*	ALT*	AST*	LDH*	CK*	Creatinine
		mg/dL	mg/dL	mg/dL	g/dL	mg/dL	mg/dL	U/L	U/L	U/L	U/L	U/L	mg/dL
WT	M	229	99	74	3	10.2	7	58	32	113	260	-	-
WT	M	269	91	65	2.8	9.2	7.3	72	81	290	752	-	-
WT	M	240	89	57	2.6	10.1	7.3	72	42	74	353	219	0.2
WT	M	190	41	69	2.8	8.8	0.6	10	11	56	16	21	0.2
WT	F	229	64	46	2.8	9.5	7.2	90	29	52	124	51	0.2
WT	F	219	80	59	2.9	10.6	5.4	115	28	157	229	-	-
WT	F	236	93	132	3	13.5	5.7	82	51	76	346	226	0.3
***Prkar2b*$^{+/-}$**	M	207	90	52	2.9	9.4	5.7	61	40	77	229	192	0.2
***Prkar2b*$^{+/-}$**	M	184	97	60	2.8	10.2	6.6	59	30	46	176	47	0.3
***Prkar2b*$^{+/-}$**	M	181	90	59	2.6	9.5	6.8	62	47	68	272	120	0.3
***Prkar2b*$^{+/-}$**	M	194	97	62	2.9	9.4	8.2	81	77	77	257	176	0.3
***Prkar2b*$^{+/-}$**	M	243	86	54	2.9	9.7	7.2	70	37	137	298	579	0.3
***Prkar2b*$^{+/-}$**	F	216	84	57	3.1	9.7	6.8	123	34	57	215	80	0.2
***Prkar2b*$^{+/-}$**	F	188	75	57	2.7	7.1	3.1	90	56	81	822	621	0
***Prkar2b*$^{+/-}$**	F	182	64	62	2.9	10.6	6.4	95	31	154	467	1096	0.3
***Prkar1a*$^{+/-}$**	M	217	94	67	3	10.4	0.1	93	69	93	254	-	-
***Prkar1a*$^{+/-}$**	M	173	68	56	2.4	9.2	6.5	41	30	142	291	762	0.3
***Prkar1a*$^{+/-}$**	F	243	89	61	1.7	-	6.4	77	-	-	-	77	0.2
***Prkar1a*$^{+/-}$**	F	263	57	52	2.7	11.1	6.6	111	35	145	365	673	0.4
***Prkar1a*$^{+/-}$**	F	200	85	73	3	10.5	6	68	49	69	305	142	0.3
***Prkar1a*$^{+/-}$**	F	222	87	68	3	10	0	120	30	79	228	-	-
***Prkar1a*$^{+/-}$**	F	221	66	67	2.6	10.8	6.4	71	24	93	498	283	0.3
***Prkar1a*$^{+/-}$ *Prkar2b*$^{+/-}$**	M	171	67	38	2.8	9.4	9.3	82	25	63	304	329	0.3
***Prkar1a*$^{+/-}$ *Prkar2b*$^{+/-}$**	M	183	78	51	2.9	10.7	6.2	87	20	55	390	212	0.3
***Prkar1a*$^{+/-}$ *Prkar2b*$^{+/-}$**	M	122	49	40	2.3	11.4	10.6	96	52	92	364	92	0.3
***Prkar1a*$^{+/-}$ *Prkar2b*$^{+/-}$**	M	174	95	50	3.1	10.2	7.1	95	33	53	258	87	0.2

Genotype	Sex	GLU*	CHOL*	TRIG*	ALB*	Ca*	PHOS*	ALP*	ALT*	AST*	LDH*	CK*	Creatinine
		mg/dL	mg/dL	mg/dL	g/dL	mg/dL	mg/dL	U/L	U/L	U/L	U/L	U/L	mg/dL
Prkar1a$^{+/-}$ ***Prkar2b***$^{+/-}$	M	198	62	58	3	10.9	5.1	81	29	58	309	124	0.3
Prkar1a$^{+/-}$ ***Prkar2b***$^{+/-}$	M	160	39	30	2.3	9.6	8	124	62	127	501	327	0.3
Prkar1a$^{+/-}$ ***Prkar2b***$^{+/-}$	M	102	37	33	2.7	9.5	7.1	164	40	220	210	87	0.3
Prkar1a$^{+/-}$ ***Prkar2b***$^{+/-}$	F	178	70	61	2.8	10.7	6.7	93	38	81	499	180	0.3
Prkar1a$^{+/-}$ ***Prkar2b***$^{+/-}$	F	223	74	50	3	10.2	6.1	70	28	78	390	495	0.3
Prkar1a$^{+/-}$ ***Prkar2b***$^{+/-}$	F	209	79	78	3.1	9.8	4.6	131	32	63	174	104	0.1
Prkar1a$^{+/-}$ ***Prkar2b***$^{+/-}$	F	179	66	59	3	8.9	8	116	88	102	416	69	0.3
Prkar1a$^{+/-}$ ***Prkar2b***$^{+/-}$	F	155	56	65	3	9	6.5	234	28	66	226	121	0.2
Prkar1a$^{+/-}$ ***Prkar2b***$^{+/-}$	F	202	62	58	3.3	9.4	7.4	192	24	49	123	59	0.3
Prkar1a$^{+/-}$ ***Prkar2b***$^{+/-}$	F	141	52	57	2.5	10.9	7.9	80	47	152	433	495	0.3
Prkar1a$^{+/-}$ ***Prkar2b***$^{+/-}$	F	232	65	53	3	9.9	5.9	167	27	118	271	457	0.3
Prkar1a$^{+/-}$ ***Prkar2b***$^{+/-}$	F	179	47	51	2.8	10	5.5	82	27	52	201	54	0.4
Prkar1a$^{+/-}$ ***Prkar2b***$^{+/-}$	F	212	76	60	2.9	10.8	6.3	71	31	71	299	194	0.3
Prkar1a$^{+/-}$ ***Prkar2b***$^{+/-}$	F	177	54	49	3.2	10	6.9	173	30	56	235	65	0.2
Prkar1a$^{+/-}$ ***Prkar2b***$^{+/-}$	F	153	64	55	2.6	8.8	6.2	78	29	104	378	392	0.1

Genotype	Sex	GLU*	CHOL *	TRIG*	ALB*	Ca*	PHOS *	ALP*	ALT*	AST*	LDH*	CK*	Creatinine
		mg/dL	mg/dL	mg/dL	g/dL	mg/dL	mg/dL	U/L	U/L	U/L	U/L	U/L	mg/dL
***Prkar1a*$^{+/-}$ *Prkar2b*$^{+/-}$**	F	224	74	60	2.9	10.4	7.9	99	27	76	736	220	0.4
#*p*-value		**0.001**	**0.03**	**0.017**	0.87	0.578	0.128	**0.03**	0.675	0.228	0.6	0.34	0.239

*GLU, glucose; CHOL, cholesterol; TRIG, triglyceride; ALB, albumin; Ca, calcium; PHOS, inorganic phosphorus; ALP, alkaline phosphatase; ALT, alanine aminotransferase; AST, aspartate aminotransferase; LDH, lactate dehydrogenase; CK, creatine kinase. # *p*-value was calculated with Student T-test. *p*-value was comparing WT and *Prkar1a*$^{+/-}$*Prkar2b*$^{+/-}$ mice and less than 0.05 were considered significant which are shown in Figure 6.7.

Table 6.1 Serum chemistries of 1-year old WT, *Prkar2b*$^{+/-}$, *Prkar1a*$^{+/-}$ and *Prkar1a*$^{+/-}$*Prkar2b*$^{+/-}$ mice.

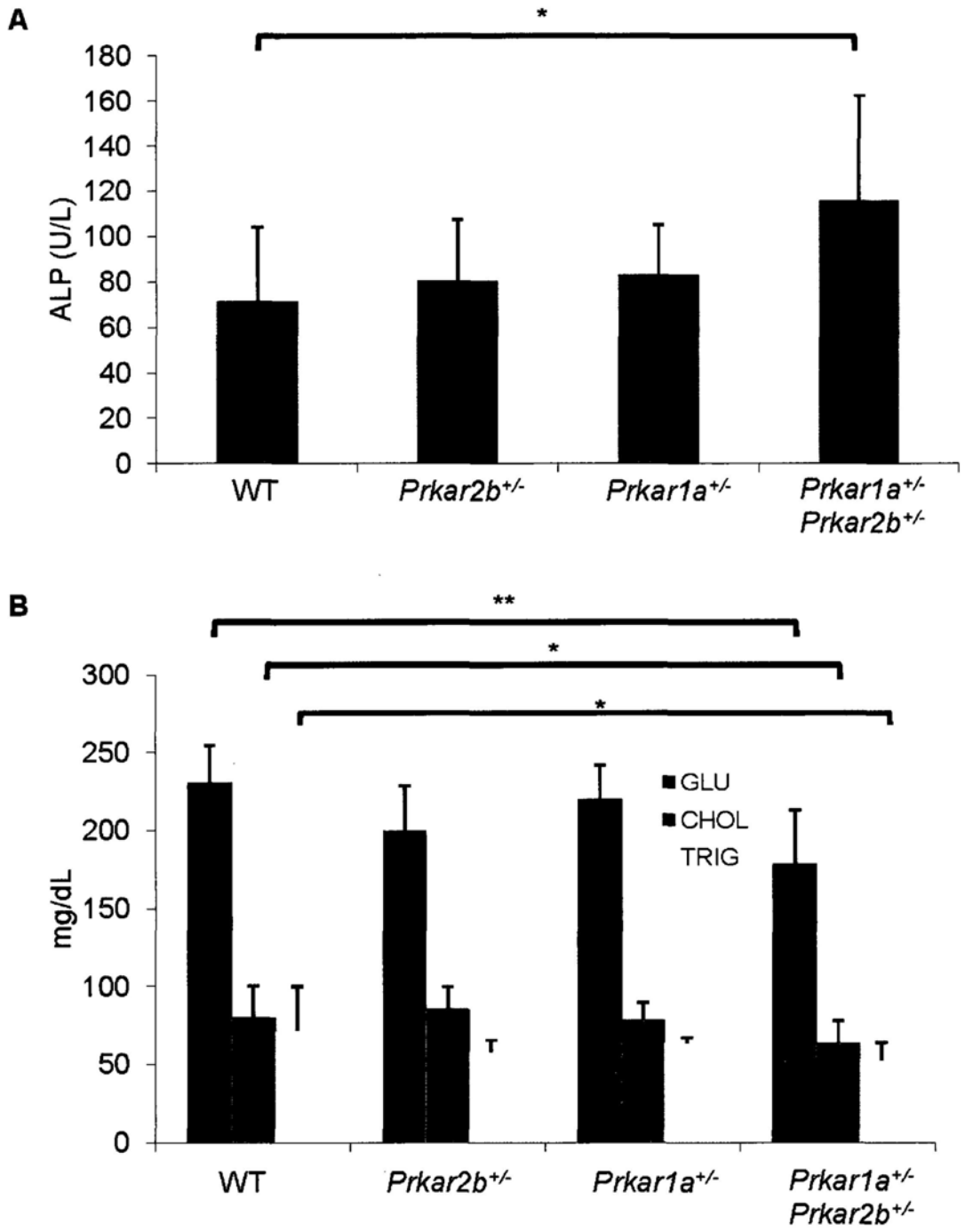

Figure 6.7 Increased serum alkaline phosphatase and decreased serum glucose, cholesterol and triglyceride in *Prkar1a*$^{+/-}$*Prkar2b*$^{+/-}$ mice. (**A**) Average of serum ALP level in WT, *Prkar2b*$^{+/-}$, *Prkar1a*$^{+/-}$ and *Prkar1a*$^{+/-}$*Prkar2b*$^{+/-}$ mice. (**B**) Average of serum glucose, cholesterol and triglyceride levels in WT, *Prkar2b*$^{+/-}$, *Prkar1a*$^{+/-}$ and *Prkar1a*$^{+/-}$*Prkar2b*$^{+/-}$ mice. *P<0.05; **P<0.01. Error bars represent means ± SD.

Chapter Seven

Discussion

The present studies showed that *Prkar1a*$^{+/-}$*Prkaca*$^{+/-}$ mice developed extensive bone lesions, although they did not form any thyroid tumors or schwannomas that developed in *Prkar1a*$^{+/-}$ mice (57), pointing to the significance of Cα for the development of certain tumors in cAMP-responsive tissues. This finding was associated with an overall increase in PKA-II activity that was mediated by increased RIIα and RIIβ and their phosphorylation (Figure 4.4), and Cβ, Cγ and Prkx catalytic subunits (Figure 4.6). However, *Prkar1a*$^{+/-}$*Prkar2b*$^{+/-}$ mice developed not only bone lesions, but also pituitary and thyroid adenoma as well as spleen peliosis that developed in *Prkar1a*$^{+/-}$ littermates, suggesting that 50% reduction of RIIβ, predicted by haploinsufficiency, do not exhibit protective effects against *Prkar1a* haploinsufficiency-induced tumor development. The present study on these two double heterozygous mouse models demonstrates that tissues are sensitive to changes in the type of PKA signaling, which is due to unbalanced type I and type II regulatory subunits.

7.1 R1α and Cα haploinsufficiency leads to the increased formation of PKA-II isozyme

Previous studies have demonstrated that R1α competes less effectively than RIIα and RIIβ in the formation of the holoenzyme (62, 63) and an increase in type-II regulatory subunits in mouse cells displaces R1α from the holoenzyme (165), suggesting that PKA-I is most sensitive to changes in different PKA subunits, in particular Cα protein. Thus, even a modest decrease in PKA-I leads

to an "amplification" effect on the type of PKA holoenzyme. These data explain why in tissues of both the *Prkar1a*$^{+/-}$ mice and the *Prkar1a*$^{+/-}$*Prkaca*$^{+/-}$ mice, which have 50% reduction of R1α predicted by *Prkar1a* haploinsufficiency, there is an increase in PKA-II. In the *Prkar1a*$^{+/-}$*Prkaca*$^{+/-}$ mice, with Cα haploinsufficiency in addition to R1α haploinsufficiency, there is an even further decrease of PKA-I (Figure 4.4), because (i) R1α haploinsufficiency leads to compensatory increases in protein levels of both RIIα and RIIβ, as we and others have demonstrated elsewhere (57, 58, 135, 166); and (ii) less Cα leads to less R1α protein which is rapidly degraded when free (167, 168), unlike free RIIα and RIIβ that are more stable (169). Studies from both *Prkaca*$^{-/-}$ mice (62) and fruit flies with dominant negative mutations of the catalytic subunit (170) have also demonstrated that absence of Cα results in elevated levels of type-II regulatory subunits. Indeed, the total amount of free Cα subunit determines the type of PKA-holoenzyme in normal cells: it leads first to the formation of PKA-II and then, when Cα levels exceed RII subunits levels, PKA-I forms (165, 171). Thus, in cells with lower R1α and Cα levels, PKA-II formation would be favored.

7.2 Alternate use of PKA catalytic subunits β, γ and Prkx contribute to dysregulated cAMP-dependant PKA signaling in *Prkar1a*$^{+/-}$*Prkaca*$^{+/-}$ mice

Besides the change in the type of PKA, Cα haploinsufficiency in *Prkar1a*$^{+/-}$ *Prkaca*$^{+/-}$ (compared to *Prkar1a*$^{+/-}$) mice led to an increase in the relative ratio of

other catalytic subunits. Since these catalytic subunits have different properties towards substrate and regulatory subunits binding as well as protein kinase inhibitor (PKI), alternate expression and use of a particular catalytic subunit would lead to an uncontrolled cAMP-dependent PKA signaling.

The Cα gene encodes two splice variants, Cα1 which expresses in all tissues and Cα2 which is limited to male germ cells (172, 173), in mouse (173), human (174) and sheep (175); the *Prkaca*$^{-/-}$ allele affects both (62).

The gene coding for the Cβ catalytic subunit encodes for three splice variants, Cβ1, Cβ2 and Cβ3; Cβ1 is ubiquitously expressed, whereas the Cβ2 and Cβ3 variants are specific for neural tissues (62, 63). In most tissues and under normal circumstances, Cβ1 contributes less that 27% of the total PKA activity (176). However, in *Prkaca*$^{-/-}$ mice Cβ1 can be upregulated by as much as 4-fold (62). Despite the fact that Cα and Cβ1 isoforms are 91% identical at the protein sequence (177), Cβ1 has a 3.5 fold higher K_m for specific substrates and 3 fold higher IC_{50} for inhibition by protein kinase inhibitor (PKI) and for binding to RIIα than does Cα (53, 54). These data point to the preferential formation of PKA-II holoenzyme with Cβ1, but not Cα, as the catalytic subunit which is more sensitive to cAMP, less inhibited by PKI and an overall more potent cAMP-signaling mediator (64, 178). Accordingly, *Prkacb*$^{-/-}$ mice showed a generally lower basal kinase activity than WT mice, despite the compensatory upregulation of Cα (64). Therefore, in *Prkar1a*$^{+/-}$*Prkaca*$^{+/-}$ mice, having high expression of Cβ1

and RII subunits favors the formation of PKA-II with the use of Cβ1 catalytic subunits over the others, and leads to increased PKA signaling.

The Cα and Cγ isoforms share 83% of their protein sequence (179) but, they have quite different properties: although generally Cα is a more potent cAMP mediator than Cγ (in terms of target promoter activity) (180), Cγ is not inhibited by the endogenous PKI, has lower affinity for the regulatory subunits than Cα, and phosphorylates histone better than kemptide (179, 181), pointing to the regulation of a different set of cAMP-responsive genes (180).

Finally, Prkx, the X-linked PKA catalytic subunit encoded by the mouse *Pkare* gene, has 50.2% homology with Cα and even less with Cβ and Cγ (182), but is expressed in most tissues and is a significant regulator of PKA-I (183). Prkx binds *only* to PKA-I, since *in vitro* experiments showed that 25-fold excess of RIIα is needed to inhibit Prkx activity by 40% (184). It is 20-fold weaker than Cα in phosphorylating kemptide (182, 184) but it phosphorylates the type-II regulatory subunits in a cAMP-independent manner (184). Phosphorylation of PKA regulatory subunits is an important regulator of overall PKA activity (185). Although both R1α and the RII subunits are phosphorylated, the phosphorylation of R1α has no clear biological effects (186). Phosphorylation of RIIα, however, reduces its affinity for the Cα and increases its association with A-kinase anchoring proteins (AKAPs) (185, 187), and has other effects on PKA-II localization and role in the cell cycle (188). Thus, in *Prkar1a*$^{+/-}$*Prkaca*$^{+/-}$ mice, with

reduction in R1α subunits, Prkx activity is not inhibited leading to an increases in phosphorylation of RII subunits and, finally, PKA-II activity.

In summary, haploinsufficiency of R1α and Cα favors i) the formation of PKA-II that has a higher affinity to specific A-kinase anchoring proteins (AKAPs) than PKA-I to achieve subcellular compartmentalization (189, 190) and dissociate completely upon cAMP binding (191); ii) the alternate use of other catalytic subunits, Cβ1, Cγ and Prkx, leading to increased and dysregulated cAMP-dependent PKA-II signaling in specific cAMP-responsive cell type and tissues., i.e. in this case, a specific population of bone cells in *Prkar1a*$^{+/-}$*Prkaca*$^{+/-}$ mice.

7.3 Involvement of RIIα subunit in the development of tumors in cAMP-responsive tissues under R1α and RIIβ haploinsufficiency

Our study on *Prkar1a*$^{+/-}$*Prkaca*$^{+/-}$ mice support the hypothesis that deficiency of *prkar1a* leads to dysregulated PKA activity, which is associated with PKA-II up-regulation. Studies in mouse model with *prkar1a* haploinsufficiency (57, 136, 138) and in human *PRKAR1A*-haploinsufficient cell lines showed that this PKA-II up-regulation was associated with increased RIIβ expression, resulting in increased growth and cell cycle abnormalities (139, 158, 192). Accordingly, one would predict that *Prkar1a*$^{+/-}$*Prkar2b*$^{+/-}$ mice, with RIIβ haploinsufficiency in addition to R1α haploinsufficiency, would have less or

delayed tumor formation (compared to *Prkar1a*$^{+/-}$ mice) due to both decreased PKA-I and PKA-II. However, this is not the case. *Prkar1a*$^{+/-}$*Prkar2b*$^{+/-}$ mice developed almost the same type of tumors as in *Prkar1a*$^{+/-}$ mice and at similar frequency and time of onset. Here, several previous findings are worthy of discussion. Studies on *Prkar2b*$^{-/-}$ mice showed a dramatic compensation by R1α via protein stabilization in a holoenzyme complex with catalytic subunits, protecting the cells from dysregulated PKA activity (61, 135). Its significance lies in the idea that R1α acts as a universal buffer against unregulated PKA activity (166). In *Prkar1a*$^{+/-}$*Prkar2b*$^{+/-}$ mice, however, due to R1α haploinsufficiency, less R1α proteins were present to inhibit the action of free catalytic subunits even there was no competition with RIIβ, leading to uncontrolled PKA activity by free catalytic subunits and thereby, tumor formation. Furthermore, loss of R1α in *Prkar1a*$^{-/-}$ embryo showed an up-regulation of RIIα, which was responsible for the increased PKA-II activity (58); And compensation by RIIα has been oberseved in the brain of *Prkar2b*$^{-/-}$ mice (193), suggesting the possible role of RIIα in unregulated PKA activity under RIIβ and R1α haploinsufficiency. However, the mechanism of tumorgenesis in *Prkar1a*$^{+/-}$*Prkar2b*$^{+/-}$ mice requires further investigation.

Furthermore, preliminary data showed that 9-month old *Prkar1a*$^{+/-}$ *Prkar2b*$^{+/-}$*Prkaca*$^{+/-}$, a triple heterozygous mouse model, developed fibro-osseous lesions, sacrum osteomyxoma and spinal chondrosarcoma (Fig. 7.1), indicating that lack of *Prkar1a*, *Prkar2b* and *Prkaca* did not abrogate the bone tumor

formation. Again, this data further supports the possible role of RIIα or alternate use of catalytic subunits in unregulated PKA activity and tumorigenesis.

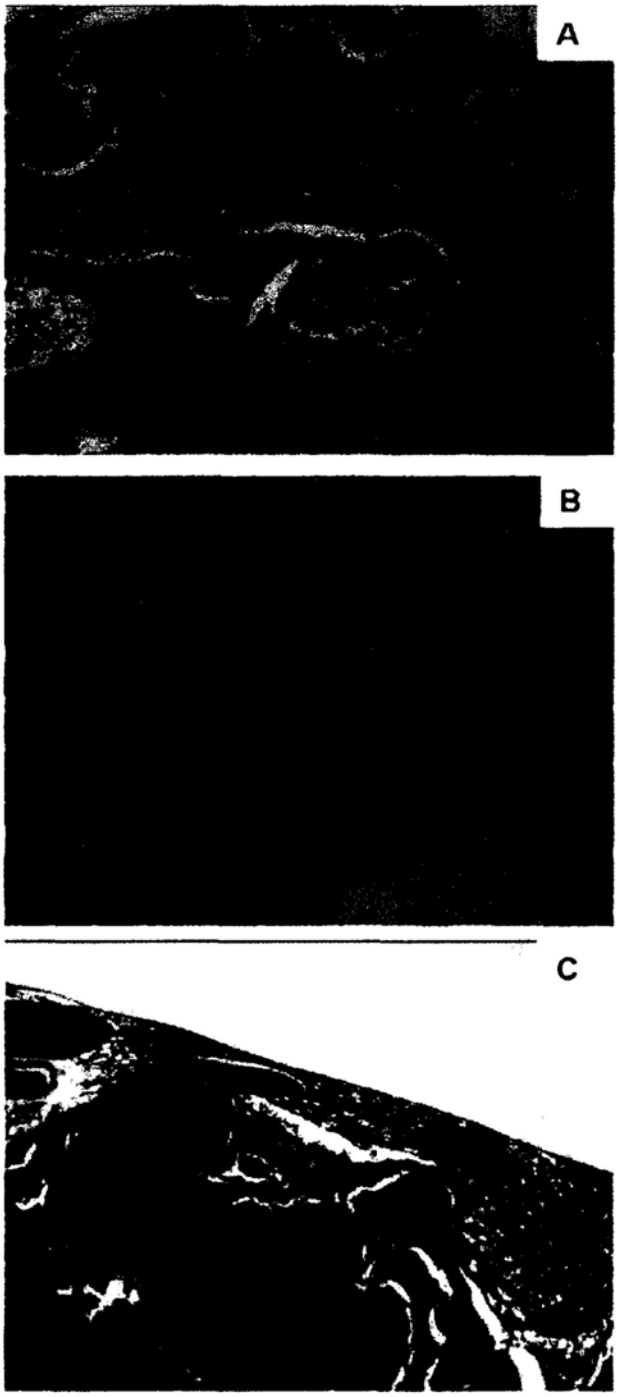

Figure 7.1 Bone lesions in *Prkar1a*$^{+/-}$*Prkar2b*$^{+/-}$*Prkaca*$^{+/-}$ mouse. (**A**) H&E staining of the longitudinal section of caudal vertebrae from 9 month-old *Prkar1a*$^{+/-}$*Prkar2b*$^{+/-}$*Prkaca*$^{+/-}$ mouse, showing fibroosseous lesion. (original magnification 10x). (**B**) H&E staining of section of sarcum from 9 month-old *Prkar1a*$^{+/-}$*Prkar2b*$^{+/-}$*Prkaca*$^{+/-}$ mouse, showing osteomyxoma. (original magnification 20x). (**C**) H&E staining of section of vertebral body from 9 month-old *Prkar1a*$^{+/-}$*Prkar2b*$^{+/-}$*Prkaca*$^{+/-}$ mouse, showing chondrosarcoma. (original magnification 20x).

7.4 Increased PKA-II activity under moderate rise of cAMP levels leads to unabated recruitment of bone stromal cells (BSCs) in *Prkar1a*$^{+/-}$*Prkaca*$^{+/-}$ mice

cAMP is an important second messenger for intracellular signal transduction. It has been known for years that cAMP, generated by activating adenylate cyclases (ACs) through the action of stimulatory G-alpha protein (Gs_{α}) in response to parathyroid hormone (PTH) or PTP-related protein (PTHrP), have different effects on bone development and physiology (77, 194, 195). Both PTH and PTHrP act through their G-protein coupled receptor (GPCR), the PTH/PTHRP receptor (PTHR1 coded by the *Pthr1* gene) which are expressed primarily on osteoblasts (195-198) and pre-hypertrophic chondrocytes (80). As described in the introduction, PTHrP activates and maintains the proliferating properties of chondrocytes. It also involves in PTHrP-IHH negative feedback loop to determine the precise site at which the proliferation of chondrocytes stop. In *Pthrp*$^{-/-}$ and *Pthr1*$^{-/-}$ mice, chondrocytes exhibited accelerated differentiation, resulting in shortened columns of proliferating chondrocytes (199, 200). PTH is secreted from the parathyroid glands in response to changes in serum calcium levels (201, 202), indirectly activating osteoclasts that results in bone resorption (195, 203).

Gs_{α} is the primary mediator of the actions of PTHR1 on chondrocytes (204, 205). Activation of Gs_{α} leads to fibrous dysplasia (FD) in human (146) and mice (145), a disease affecting bone stromal cells (BSCs) (147, 162). FD is

characterized by an expansion of osteoprogenitor cells, i.e. BSCs committing osteogenic linage, within the marrow cavity in response to overproduction of cAMP, resulting in the development of fibrotic areas (146). The local enrichment of these osteoprogenitor cells is shown to be associated with increased expression of c-fos (206). High levels of cAMP, generated by overstimulation of ACs by the mutated Gs_{α}, results in Sharpey fiber bone and osteoblast retraction (207). It has also been suggested that formation of abnormal bone in FD is associated with the late response of mature osteoblasts to increased cAMP, resulting in abnormal patterns of osteoblast-matrix interaction (207).

These studies demonstrated that any abnormalities upstream of cAMP production results in bone abnormalities, pointing to the important role of cAMP level in bone development, in particular, the proliferation and differentiation of specific bone cells, i.e. proliferating chondrocytes in *Pthrp*$^{-/-}$ and *Pthr1*$^{-/-}$ mice and BSCs in FD.

The present study showed that the abnormalities of PKA subunits, a downstream effector of cAMP signaling, could also lead to bone abnormalities characterized by uncontrolled proliferation of BSCs which commits to osteogenic lineage (identities of the cells was confirmed by FASC study, Figure 5.1 and 5.6). These PKA abnormalities were enhanced in the bone of *Prkar1a*$^{+/-}$*Prkaca*$^{+/-}$ mice by modest rise of cAMP levels which were due to increased expression of ACs Adcy1, Adcy6 and Adcy9 (Figure 4.3), despite the concurrent increased expression of PDEs, such as Pde11a and Pde4d (Figure 4.2). Indeed, *in vitro* studies have shown that cAMP-specific Pdes (Pde4 in particular) can be

phosphorylated and activated by PKA in rat thyroid follicular cells (208), mouse Leydig tumor cells (209), and cardiac myocytes (210). A recent study showed expression of PDE7A in human BSCs (160), but we could not document high levels of Pde7a expression in *Prkar1a*$^{+/-}$*Prkaca*$^{+/-}$ mouse bone cells (Figure 4.2). The expression of ACs and PDEs are important because they determine cAMP levels, which in turn play an important role in determining PKA responses. High cAMP levels, in *Prkar1a*$^{+/-}$*Prkaca*$^{+/-}$ mice, not only led to increased PKA activity, but also increase significantly the transcription of all regulatory and catalytic subunits. However, R1α and Cα mRNA induction does not exceed 2- to 4-fold over baseline, whereas, in response to cAMP, RIIβ levels rise by 40-fold (211, 212). In short, haploinsufficency of R1α and Cα leads to increased AC activity and by which increased cAMP level, resulting in, again, the up-regulation and preferential formation of PKA-II and its activity.

These data converge in the following hypothesis supported by our present findings and previous reports on R1α-haploinsufficiency-related bone abnormalities in mice and humans with CNC (48, 57, 144): In bone, PKA activation, through increasing cAMP production either by PTHRP, PTHR1, Gs$_\alpha$ (62, 77, 80, 145, 147, 204, 205, 213-215), or deficient inhibitory control of the catalytic subunit Cα, leads to excess PKA-II and in turn, unabated recruitment of BSCs from the pool of bone marrow stem cells. These cells are unable to follow the regular process of maturation to hypetrophic chondrocytes or mature osteoblasts and develop a matrix that is irregular and undermineralized (Figure 3.13).

7.5 Increased osteoclastic activity in bone lesions from *Prkar1a*$^{+/-}$*Prkaca*$^{+/-}$ mice

Besides activation of osteoprogenitor cells, osteoclastic function is also increased in FD which results from overexpression of IL-6 under excess stimulation by cAMP (216). It has been shown that overexpression of Runx2 and treatment with biologically active form of vitamin D_3 in cells of osteoblastic lineage has positive effect on osteoclast differentiation through the expression of receptor activator of NF-κB ligand (RANKL) (217, 218), an important factor for osteoclast differentiation (203). Other studies have also suggested a linkage between cAMP/PKA signaling and RANKL expression in osteoblasts (219) and human mesenchymal stem cells (MSCs) (220). Our studies supported the role of increased PKA signaling, mainly by PKA-II, in inducing osteoclast activity via regulating osteoblast-dependent Runx2 expression and IL-6 expression, since both genes were up-regulated in bone lesions from *Prkar1a*$^{+/-}$*Prkaca*$^{+/-}$ mice. cAMP and PKA also have osteoblast-independent effects on osteoclasts (220, 221), also mainly due to PKA-II (220, 222). Although some morphologically abnormal osteocytes were observed in *Prkar1a*$^{+/-}$*Prkaca*$^{+/-}$ mice, there was no abnormality in phosphate homeostasis and Fgf23 expression, a molecule that is secreted mainly by osteocytes in bone (223, 224) and dysregulated in FD (225).

7.6 Differences between bone lesions from *Prkar1a*$^{+/-}$*Prkaca*$^{+/-}$ and FD

Despite the similarities noted above, there are some important differences between bone lesions from *Prkar1a*$^{+/-}$*Prkaca*$^{+/-}$ and FD. First, the defects that we saw in *Prkar1a*$^{+/-}$*Prkaca*$^{+/-}$ mice developed postnatally, starting well after 3 months and peaking between 6 and 9 months of age. In human FD, lesions are present in toddlerhood and peak in late childhood and young adulthood (145, 146). In fact, in older patients with FD, normal bone histology can be seen, apparently due to apoptosis of the mutant Gs_{α}-bearing BSCs (226). Second, in both humans (146) and mice (145) with FD, the disease is caused by a post-zygotic defect; all bones are chimeras of normal and abnormal Gs_{α}, which creates a totally different tissue microenvironment. In *Prkar1a*$^{+/-}$ and *Prkar1a*$^{+/-}$ *Prkaca*$^{+/-}$ mice, as well as humans with CNC, the defect is in the germline and the mutant allele is present in all cells (48, 57, 144).

7.7 Identity of BSCs in *Prkar1a*$^{+/-}$*Prkaca*$^{+/-}$ mice

PKA defects appear to affect specific areas that are characterized by high amount of metabolically active trabecular bone and residual cartilage (such as adult mouse vertebrae) or have a high natural population of pre-chondrocytes (i.e. tibia). It is of note that the earliest lesion in *Prkar1a*$^{+/-}$*Prkaca*$^{+/-}$ mice was a tibial chondroma (Figure 3.6); in humans with CNC, humerus and tibia are the most frequently affected long bones, too (48). The particular susceptibility of the

mouse tibia to cAMP signaling defects is also further supported by the development of ectopic cartilage in tibia of chondrocyte-specific knockout mouse model of *Gnas* (205).

Thus, PKA defects reveal a particular population of adult stromal cells, aBSCs that reside in specific regions of the skeleton. These are probably the same stromal cells that i) respond to intermittent PTH in mouse vertebrae, ii) found in abundance among the trabeculae of transgenic mice with constitutively active PTHR1 expression in osteoblastic cells (a model of Jansen metaphyseal chondrodysplasia) (227), and iii) accumulated in the tibiae of a similar mouse model with PTHR1 overexpression (228). These are also most likely the same cells that were recently identified in adult mice after tamoxifen-induced deletion of *Smoothened* (Smo) (229), the indispensable factor for *Ihh* and *Sonic hedgehog* (*Shh*) signaling (230). In that study, too, these osteogenic cells were located between trabecular bone and proximal to the growth plate (229).

7.8 Molecular signature of aBSCs with PKA defects

The identified stromal cells expressed alkaline phosphatase (*Alp1*) (Table 5.1), osteocalcin (Figure 5.3), *cFos* (Figure 5.7), as in FD (206), collagen I, matrix metalloproteinases (MMP), MMP9 and MMP10 in particular, and other known markers of bone development. However, there were some significant differences between *Prkar1a*$^{+/-}$ and *Prkar1a*$^{+/-}$*Prkaca*$^{+/-}$ cells (Table 5.1). *Prkar1a*$^{+/-}$*Prkaca*$^{+/-}$ cells were closer to chondrocytes than osteocytes in their gene signature. They

expressed less alkaline phosphatase (*Alp1*) and bone morphogenetic protein-2 (*Bmp2*), but expressed more i) Collagen 11 (*Col11a1*), the gene mutated in the chondrodysplastic (*cho*) mouse (231) and in Stickler and Marshall syndromes (232), ii) enamel, iii) fibroblast growth factor receptor 2 (*Fgfr2*), iv) *Bmp4*, and v) Smad 1. The latter molecules pointed to a gene signature of *Prkar1a*$^{+/-}$*Prkaca*$^{+/-}$ cells that is closer to that of cells involved in ectopic ossification in fibrodysplasia ossificans progressiva (FOP) (233): overexpression of BMP4 (234) and SMAD1 (235) is seen in human cells from this condition. Furthermore, proximal chondromas in the tibia [the long bone most affected in *Prkar1a*$^{+/-}$*Prkaca*$^{+/-}$ mice, in humans with CNC (48), and in a chondrocyte-specific knockout mouse model of *Gnas* (205)] occur in more than 90% of patients with FOP (236). It is thus conceivable that the aBSCs identified in the bone of *Prkar1a*$^{+/-}$*Prkaca*$^{+/-}$ mice are as pluripotential as those progenitor cells that contribute to ectopic bone formation after activation of inflammation in FOP (237).

7.9 Induction of Wnt signaling by PKA-II leads to MET

Prkar1a$^{+/-}$*Prkaca*$^{+/-}$ cells also showed, as in other settings of R1α defects (238, 239) in humans and mice, induction of *Wnt*-signaling genes (Table 5.3), including β-catenin and *brachyury*, and had a molecular signature consistent with mesenchymal-to-epithelial transition (MET) (Table 5.2), that has also been seen in complete R1α loss (240). The increased expression of *brachyury* (Figure 5.7) in *Prkar1a*$^{+/-}$*Prkaca*$^{+/-}$ vs. *P*rkar1a$^{+/-}$ cells (Table 5.3) is of particular importance.

Brachyury (the product of the *T* gene) regulates *Wnt*-signaling in posterior mesoderm formation in all vertebrates by inducing *wnt8* and *wnt3a* (they also increased in *Prkar1a*$^{+/-}$*Prkaca*$^{+/-}$ cells, Table 5.3) (241). Increased expression of *brachyury* is seen in familial chondroma (242) , and it is a marker along with cytokeratin for skull base, extra-axial skeletal and soft tissue chordomas, distinguishing them from mixed tumors and chondrosarcomas (243, 244). Increased expression of brachyury in *Prkar1a*$^{+/-}$*Prkaca*$^{+/-}$ cells may be due to the overall increased Wnt-signaling or it could also be a marker of the particular subpopulation of aBSCs that was identified in this study, since it can stain chondroblastomas in the metaphyseal cortex of the tibia (245).

Chapter Eight

Conclusion and Future prospects

8.1 Conclusion

In conclusion, genetic manipulation of the PKA pathway in mice revealed a particular population of aBSCs that are responsive to cAMP signaling mediated mainly by PKA-II and alternate PKA catalytic subunits. It has only been recently recognized that stromal or mesenchymal cells respond to cAMP *in vitro* (147, 162, 246); it was also shown that BSCs need proximity to cartilage for growth, proliferation and differentiation (247), and for settlement when they repopulate bone marrow (248). Our study extends these observations *in vivo*, showing where exactly aBSCs reside in the adult mouse skeleton and what makes them proliferate. The discovery of an alternate PKA activity as a factor that develops aBSCs had not been recognized earlier. These data may help in growing these cells *ex vivo* and explain some of the inconsistencies noted by investigators on cAMP signaling and growth of mesenchymal cells (221, 246, 248-250). The present data are also helpful in understanding better the process of malignant transformation that BSCs and other pluripotential cells are at risk for (251). Finally, our study provides the first mouse model of an FD-like condition caused by a germline defect.

8.2 Future prospects

Prkar1a$^{+/-}$*Prkaca*$^{+/-}$ mouse provides an excellent mouse model on studying the role of dysregulated PKA activity and cAMP signaling in aBSCs. However, the responsible type II regulatory (RIIα or RIIβ) subunits and catalytic subunits in increased PKA acivity as well as the stimulants in cAMP production are still unknown. Preliminary data showed that *Prkar1a*$^{+/-}$*Prkar2b*$^{+/-}$ and *Prkar1a*$^{+/-}$ *Prkar2b*$^{+/-}$*Prkaca*$^{+/-}$ mice also developed bone lesions. By comparing these lesions with those from *Prkar1a*$^{+/-}$*Prkaca*$^{+/-}$ mice would provide a more comprehensive explanation on tumorigenesis, i.e. uncontrolled proliferation of aBSCs, led by dysregulated PKA signaling.

Moreover, the bone lesions from *Prkar1a*$^{+/-}$*Prkaca*$^{+/-}$ mouse resembled FD, which is caused by Gsα acitivation, in human and mouse. It would be interesting to study the *Prkar1a*$^{+/-}$ and *Prkar1a*$^{+/-}$*Prkaca*$^{+/-}$ animal in the background of *gnas* haploinsufficiency (*Gnas*$^{+/-}$). Combining the data from the present study and previous studies on FD, we would predict reduction of *gnas* would lead to decreased cAMP production and thus, abrogate most if not all of the bone lesions that developed in *Prkar1a*$^{+/-}$ and *Prkar1a*$^{+/-}$*Prkaca*$^{+/-}$ animals.

The present study demonstrated that activation of ACs led to the increased production of cAMP, which in turn led to increased PKA-II activity under *prkar1a* and *prkaca* haploinsufficiency. However, the mechanism remains to be investigated. We speculated that increased signaling via prostaglandin E2 receptor (EP_2) and/or leucine-rich repeat-containing G protein-coupled receptor

(Lgr5), which are G protein-coupled receptors, may activate Gsα, driving excess cAMP production. It would be necessary to measure the expression level of prostaglandin E2 (Pge2), EP_2 and Lgr5 in the bone lesions from *Prkar1a*$^{+/-}$ and *Prkar1a*$^{+/-}$*Prkaca*$^{+/-}$ animals. Moreover, both *Pge2* and *Lgr5* are linked to Wnt-signaling pathway, which was upregulated under *prakr1a* haploinsufficiency. Based on these stuies, one would predict that activation of Wnt signaling in *Prkar1a*$^{+/-}$ and *Prkar1a*$^{+/-}$*Prkaca*$^{+/-}$ animals would lead to increased expression of *Pge2* and *Lgr5*, finally generating excess cAMP and leading to increased PKA activity. In order to proof this hypothesis, we should study the effects of activation of Wnt signaling, for instance by overexpressing β-catenin, in bone stromal cell line on the expression levels of *Pge2*, EP_2 and *Lgr5* as well as basal cAMP production. In long run, it would be interesting to study the *Prkar1a*$^{+/-}$ and *Prkar1a*$^{+/-}$*Prkaca*$^{+/-}$ animals in the background of *lgr5* haploinsufficiency (*lgr5*$^{+/-}$).

This study also showed that PKA-II was activated in bone from *Prkar1a*$^{+/-}$ *Prkaca*$^{+/-}$ animals. To validate the effects of PKA-II on aBSCs proliferation and differentiation, *prkar2a* and *prkar2b* stable transfected bone stromal cell lines should be used for further study. Expression of different bone markers, PKA activity, cAMP level and proliferation rate should be investigated in these cell lines.

References

1. Falchetti A, Marini F, Luzi E, Tonelli F, & Brandi ML (2008) Multiple endocrine neoplasms. *Best Pract Res Clin Rheumatol* 22:149-163.
2. Marx SJ & Stratakis CA (2005) Multiple endocrine neoplasia--introduction. *J Intern Med* 257:2-5.
3. Callender GG, Rich TA, & Perrier ND (2008) Multiple endocrine neoplasia syndromes. *Surg Clin North Am* 88:863-895, viii.
4. Lakhani VT, You YN, & Wells SA (2007) The multiple endocrine neoplasia syndromes. *Annu Rev Med* 58:253-265.
5. Lemos MC & Thakker RV (2008) Multiple endocrine neoplasia type 1 (MEN1): analysis of 1336 mutations reported in the first decade following identification of the gene. *Hum Mutat* 29:22-32.
6. Vandeva S, Tichomirowa MA, Zacharieva S, Daly AF, & Beckers A (2010) Genetic Factors in the Development of Pituitary Adenomas. *Endocr Dev* 17:121-133.
7. Marx SJ (2005) Molecular genetics of multiple endocrine neoplasia types 1 and 2. *Nat Rev Cancer* 5:367-375.
8. Hai N, Aoki N, Shimatsu A, Mori T, & Kosugi S (2000) Clinical features of multiple endocrine neoplasia type 1 (MEN1) phenocopy without germline MEN1 gene mutations: analysis of 20 Japanese sporadic cases with MEN1. *Clin Endocrinol (Oxf)* 52:509-518.

9. Cebrian A, Ruiz-Llorente S, Cascon A, Pollan M, Diez JJ, Pico A, Telleria D, Benitez J, & Robledo M (2003) Mutational and gross deletion study of the MEN1 gene and correlation with clinical features in Spanish patients. *J Med Genet* 40:e72.

10. Pellegata NS, Quintanilla-Martinez L, Siggelkow H, Samson E, Bink K, Hofler H, Fend F, Graw J, & Atkinson MJ (2006) Germ-line mutations in p27Kip1 cause a multiple endocrine neoplasia syndrome in rats and humans. *Proc Natl Acad Sci U S A* 103:15558-15563.

11. Georgitsi M, Raitila A, Karhu A, van der Luijt RB, Aalfs CM, Sane T, Vierimaa O, Makinen MJ, Tuppurainen K, Paschke R, Gimm O, Koch CA, Gundogdu S, Lucassen A, Tischkowitz M, Izatt L, Aylwin S, Bano G, Hodgson S, De Menis E, Launonen V, Vahteristo P, & Aaltonen LA (2007) Germline CDKN1B/p27Kip1 mutation in multiple endocrine neoplasia. *J Clin Endocrinol Metab* 92:3321-3325.

12. Carling T (2005) Multiple endocrine neoplasia syndrome: genetic basis for clinical management. *Curr Opin Oncol* 17:7-12.

13. Marini F, Falchetti A, Del Monte F, Carbonell Sala S, Tognarini I, Luzi E, & Brandi ML (2006) Multiple endocrine neoplasia type 2. *Orphanet J Rare Dis* 1:45.

14. Donis-Keller H, Dou S, Chi D, Carlson KM, Toshima K, Lairmore TC, Howe JR, Moley JF, Goodfellow P, & Wells SA, Jr. (1993) Mutations in the RET proto-oncogene are associated with MEN 2A and FMTC. *Hum Mol Genet* 2:851-856.

15. Mulligan LM, Kwok JB, Healey CS, Elsdon MJ, Eng C, Gardner E, Love DR, Mole SE, Moore JK, Papi L, & et al. (1993) Germ-line mutations of the RET proto-oncogene in multiple endocrine neoplasia type 2A. *Nature* 363:458-460.

16. Santoro M, Carlomagno F, Melillo RM, & Fusco A (2004) Dysfunction of the RET receptor in human cancer. *Cell Mol Life Sci* 61:2954-2964.

17. Neumann HP & Wiestler OD (1991) Clustering of features and genetics of von Hippel-Lindau syndrome. *Lancet* 338:258.

18. Nordstrom-O'Brien M, van der Luijt RB, van Rooijen E, van den Ouweland AM, Majoor-Krakauer DF, Lolkema MP, van Brussel A, Voest EE, & Giles RH (2010) Genetic analysis of von Hippel-Lindau disease. *Hum Mutat.*

19. Lu-Emerson C & Plotkin SR (2009) The Neurofibromatoses. Part 1: NF1. *Rev Neurol Dis* 6:E47-53.

20. Wallace MR, Marchuk DA, Andersen LB, Letcher R, Odeh HM, Saulino AM, Fountain JW, Brereton A, Nicholson J, Mitchell AL, & et al. (1990) Type 1 neurofibromatosis gene: identification of a large transcript disrupted in three NF1 patients. *Science* 249:181-186.

21. DeClue JE, Papageorge AG, Fletcher JA, Diehl SR, Ratner N, Vass WC, & Lowy DR (1992) Abnormal regulation of mammalian p21ras contributes to malignant tumor growth in von Recklinghausen (type 1) neurofibromatosis. *Cell* 69:265-273.

22. Carney JA, Gordon H, Carpenter PC, Shenoy BV, & Go VL (1985) The complex of myxomas, spotty pigmentation, and endocrine overactivity. *Medicine (Baltimore)* 64:270-283.

23. Groussin L, Kirschner LS, Vincent-Dejean C, Perlemoine K, Jullian E, Delemer B, Zacharieva S, Pignatelli D, Carney JA, Luton JP, Bertagna X, Stratakis CA, & Bertherat J (2002) Molecular analysis of the cyclic AMP-dependent protein kinase A (PKA) regulatory subunit 1A (PRKAR1A) gene in patients with Carney complex and primary pigmented nodular adrenocortical disease (PPNAD) reveals novel mutations and clues for pathophysiology: augmented PKA signaling is associated with adrenal tumorigenesis in PPNAD. *Am J Hum Genet* 71:1433-1442.

24. Kirschner LS, Sandrini F, Monbo J, Lin JP, Carney JA, & Stratakis CA (2000) Genetic heterogeneity and spectrum of mutations of the PRKAR1A gene in patients with the carney complex. *Hum Mol Genet* 9:3037-3046.

25. Stergiopoulos SG & Stratakis CA (2003) Human tumors associated with Carney complex and germline PRKAR1A mutations: a protein kinase A disease! *FEBS Lett* 546:59-64.

26. Stratakis CA (2002) Mutations of the gene encoding the protein kinase A type I-alpha regulatory subunit (PRKAR1A) in patients with the "complex of spotty skin pigmentation, myxomas, endocrine overactivity, and schwannomas" (Carney complex). *Ann N Y Acad Sci* 968:3-21.

27. Stratakis CA (2000) Genetics of Carney complex and related familial lentiginoses, and other multiple tumor syndromes. *Front Biosci* 5:D353-366.

28. Sandrini F & Stratakis C (2003) Clinical and molecular genetics of Carney complex. *Mol Genet Metab* 78:83-92.

29. Bertherat J (2006) Carney complex (CNC). *Orphanet J Rare Dis* 1:21.

30. Stratakis CA, Kirschner LS, & Carney JA (2001) Clinical and molecular features of the Carney complex: diagnostic criteria and recommendations for patient evaluation. *J Clin Endocrinol Metab* 86:4041-4046.

31. Veugelers M, Wilkes D, Burton K, McDermott DA, Song Y, Goldstein MM, La Perle K, Vaughan CJ, O'Hagan A, Bennett KR, Meyer BJ, Legius E, Karttunen M, Norio R, Kaariainen H, Lavyne M, Neau JP, Richter G, Kirali K, Farnsworth A, Stapleton K, Morelli P, Takanashi Y, Bamforth JS, Eitelberger F, Noszian I, Manfroi W, Powers J, Mochizuki Y, Imai T, Ko GT, Driscoll DA, Goldmuntz E, Edelberg JM, Collins A, Eccles D, Irvine AD, McKnight GS, & Basson CT (2004) Comparative PRKAR1A genotype-phenotype analyses in humans with Carney complex and prkar1a haploinsufficient mice. *Proc Natl Acad Sci U S A* 101:14222-14227.

32. Carney JA & Ferreiro JA (1996) The epithelioid blue nevus. A multicentric familial tumor with important associations, including cardiac myxoma and psammomatous melanotic schwannoma. *Am J Surg Pathol* 20:259-272.

33. Bossis I, Voutetakis A, Bei T, Sandrini F, Griffin KJ, & Stratakis CA (2004) Protein kinase A and its role in human neoplasia: the Carney complex paradigm. *Endocr Relat Cancer* 11:265-280.

34. Atherton DJ, Pitcher DW, Wells RS, & MacDonald DM (1980) A syndrome of various cutaneous pigmented lesions, myxoid neurofibromata and atrial myxoma: the NAME syndrome. *Br J Dermatol* 103:421-429.

35. Rhodes AR, Silverman RA, Harrist TJ, & Perez-Atayde AR (1984) Mucocutaneous lentigines, cardiomucocutaneous myxomas, and multiple blue nevi: the "LAMB" syndrome. *J Am Acad Dermatol* 10:72-82.

36. Radin R & Kempf RA (1995) Carney complex: report of three cases. *Radiology* 196:383-386.

37. Carney JA (1995) Carney complex: the complex of myxomas, spotty pigmentation, endocrine overactivity, and schwannomas. *Semin Dermatol* 14:90-98.

38. Allen PW (2000) Myxoma is not a single entity: a review of the concept of myxoma. *Ann Diagn Pathol* 4:99-123.

39. Sarlis NJ, Chrousos GP, Doppman JL, Carney JA, & Stratakis CA (1997) Primary pigmented nodular adrenocortical disease: reevaluation of a patient with carney complex 27 years after unilateral adrenalectomy. *J Clin Endocrinol Metab* 82:1274-1278.

40. Travis WD, Tsokos M, Doppman JL, Nieman L, Chrousos GP, Cutler GB, Jr., Loriaux DL, & Norton JA (1989) Primary pigmented nodular

adrenocortical disease. A light and electron microscopic study of eight cases. *Am J Surg Pathol* 13:921-930.

41. Pack SD, Kirschner LS, Pak E, Zhuang Z, Carney JA, & Stratakis CA (2000) Genetic and histologic studies of somatomammotropic pituitary tumors in patients with the "complex of spotty skin pigmentation, myxomas, endocrine overactivity and schwannomas" (Carney complex). *J Clin Endocrinol Metab* 85:3860-3865.

42. Premkumar A, Stratakis CA, Shawker TH, Papanicolaou DA, & Chrousos GP (1997) Testicular ultrasound in Carney complex: report of three cases. *J Clin Ultrasound* 25:211-214.

43. Stratakis CA, Courcoutsakis NA, Abati A, Filie A, Doppman JL, Carney JA, & Shawker T (1997) Thyroid gland abnormalities in patients with the syndrome of spotty skin pigmentation, myxomas, endocrine overactivity, and schwannomas (Carney complex). *J Clin Endocrinol Metab* 82:2037-2043.

44. Carney JA (1990) Psammomatous melanotic schwannoma. A distinctive, heritable tumor with special associations, including cardiac myxoma and the Cushing syndrome. *Am J Surg Pathol* 14:206-222.

45. Carney JA & Stratakis CA (1998) Epithelioid blue nevus and psammomatous melanotic schwannoma: the unusual pigmented skin tumors of the Carney complex. *Semin Diagn Pathol* 15:216-224.

46. Carney JA & Toorkey BC (1991) Ductal adenoma of the breast with tubular features. A probable component of the complex of myxomas,

spotty pigmentation, endocrine overactivity, and schwannomas. *Am J Surg Pathol* 15:722-731.

47. Carney JA & Stratakis CA (1996) Ductal adenoma of the breast and the Carney complex. *Am J Surg Pathol* 20:1154-1155.

48. Carney JA, Boccon-Gibod L, Jarka DE, Tanaka Y, Swee RG, Unni KK, & Stratakis CA (2001) Osteochondromyxoma of bone: a congenital tumor associated with lentigines and other unusual disorders. *Am J Surg Pathol* 25:164-176.

49. Boikos SA & Stratakis CA (2006) Carney complex: pathology and molecular genetics. *Neuroendocrinology* 83:189-199.

50. Mabuchi T, Shimizu M, Ino H, Yamguchi M, Terai H, Fujino N, Nagata M, Sakata K, Inoue M, Yoneda T, & Mabuchi H (2005) PRKAR1A gene mutation in patients with cardiac myxoma. *Int J Cardiol* 102:273-277.

51. Perdigao PF, Stergiopoulos SG, De Marco L, Matyakhina L, Boikos SA, Gomez RS, Pimenta FJ, & Stratakis CA (2005) Molecular and immunohistochemical investigation of protein kinase a regulatory subunit type 1A (PRKAR1A) in odontogenic myxomas. *Genes Chromosomes Cancer* 44:204-211.

52. Urban C, Weinhausel A, Fritsch P, Sovinz P, Weinhandl G, Lackner H, Moritz A, & Haas OA (2007) Primary pigmented nodular adrenocortical disease (PPNAD) and pituitary adenoma in a boy with sporadic Carney complex due to a novel, de novo paternal PRKAR1A mutation (R96X). *J Pediatr Endocrinol Metab* 20:247-252.

53. Skalhegg BS & Tasken K (2000) Specificity in the cAMP/PKA signaling pathway. Differential expression,regulation, and subcellular localization of subunits of PKA. *Front Biosci* 5:D678-693.

54. Gamm DM, Baude EJ, & Uhler MD (1996) The major catalytic subunit isoforms of cAMP-dependent protein kinase have distinct biochemical properties in vitro and in vivo. *J Biol Chem* 271:15736-15742.

55. McKnight GS, Clegg CH, Uhler MD, Chrivia JC, Cadd GG, Correll LA, & Otten AD (1988) Analysis of the cAMP-dependent protein kinase system using molecular genetic approaches. *Recent Prog Horm Res* 44:307-335.

56. Bossis I & Stratakis CA (2004) Minireview: PRKAR1A: normal and abnormal functions. *Endocrinology* 145:5452-5458.

57. Kirschner LS, Kusewitt DF, Matyakhina L, Towns WH, 2nd, Carney JA, Westphal H, & Stratakis CA (2005) A mouse model for the Carney complex tumor syndrome develops neoplasia in cyclic AMP-responsive tissues. *Cancer Res* 65:4506-4514.

58. Amieux PS, Howe DG, Knickerbocker H, Lee DC, Su T, Laszlo GS, Idzerda RL, & McKnight GS (2002) Increased basal cAMP-dependent protein kinase activity inhibits the formation of mesoderm-derived structures in the developing mouse embryo. *J Biol Chem* 277:27294-27304.

59. Burton KA, McDermott DA, Wilkes D, Poulsen MN, Nolan MA, Goldstein M, Basson CT, & McKnight GS (2006) Haploinsufficiency at the protein

kinase A RI alpha gene locus leads to fertility defects in male mice and men. *Mol Endocrinol* 20:2504-2513.

60. Burton KA, Johnson BD, Hausken ZE, Westenbroek RE, Idzerda RL, Scheuer T, Scott JD, Catterall WA, & McKnight GS (1997) Type II regulatory subunits are not required for the anchoring-dependent modulation of Ca2+ channel activity by cAMP-dependent protein kinase. *Proc Natl Acad Sci U S A* 94:11067-11072.

61. Cummings DE, Brandon EP, Planas JV, Motamed K, Idzerda RL, & McKnight GS (1996) Genetically lean mice result from targeted disruption of the RII beta subunit of protein kinase A. *Nature* 382:622-626.

62. Skalhegg BS, Huang Y, Su T, Idzerda RL, McKnight GS, & Burton KA (2002) Mutation of the Calpha subunit of PKA leads to growth retardation and sperm dysfunction. *Mol Endocrinol* 16:630-639.

63. Guthrie CR, Skalhegg BS, & McKnight GS (1997) Two novel brain-specific splice variants of the murine Cbeta gene of cAMP-dependent protein kinase. *J Biol Chem* 272:29560-29565.

64. Howe DG, Wiley JC, & McKnight GS (2002) Molecular and behavioral effects of a null mutation in all PKA C beta isoforms. *Mol Cell Neurosci* 20:515-524.

65. Clarke B (2008) Normal bone anatomy and physiology. *Clin J Am Soc Nephrol* 3 Suppl 3:S131-139.

66. Yang Y (2009) Skeletal morphogenesis during embryonic development. *Crit Rev Eukaryot Gene Expr* 19:197-218.

67. Aubin JE & Liu F (1996) The osteoblast lineage. *Principles of bone biology*, eds Bilezikian JP, Raisz LG, & Rodan GA (Academic Press, San Diego), pp 51-67.

68. Langille RM (1994) Differentiation of craniofacial mesenchyme. *Bone*, ed Hall BK (CRC Press, Boca Raton), pp 1-63.

69. Opperman LA (2000) Cranial sutures as intramembranous bone growth sites. *Dev Dyn* 219:472-485.

70. Day TF, Guo X, Garrett-Beal L, & Yang Y (2005) Wnt/beta-catenin signaling in mesenchymal progenitors controls osteoblast and chondrocyte differentiation during vertebrate skeletogenesis. *Dev Cell* 8:739-750.

71. Nie X, Luukko K, & Kettunen P (2006) BMP signalling in craniofacial development. *Int J Dev Biol* 50:511-521.

72. Muenke M, Schell U, Hehr A, Robin NH, Losken HW, Schinzel A, Pulleyn LJ, Rutland P, Reardon W, Malcolm S, & et al. (1994) A common mutation in the fibroblast growth factor receptor 1 gene in Pfeiffer syndrome. *Nat Genet* 8:269-274.

73. Wilkie AO & Morriss-Kay GM (2001) Genetics of craniofacial development and malformation. *Nat Rev Genet* 2:458-468.

74. Seto ML, Hing AV, Chang J, Hu M, Kapp-Simon KA, Patel PK, Burton BK, Kane AA, Smyth MD, Hopper R, Ellenbogen RG, Stevenson K, Speltz ML, & Cunningham ML (2007) Isolated sagittal and coronal craniosynostosis associated with TWIST box mutations. *Am J Med Genet A* 143:678-686.

75. Jabs EW, Muller U, Li X, Ma L, Luo W, Haworth IS, Klisak I, Sparkes R, Warman ML, Mulliken JB, & et al. (1993) A mutation in the homeodomain of the human MSX2 gene in a family affected with autosomal dominant craniosynostosis. *Cell* 75:443-450.

76. Kronenberg HM (2007) The role of the perichondrium in fetal bone development. *Ann N Y Acad Sci* 1116:59-64.

77. Kronenberg HM (2006) PTHrP and skeletal development. *Ann N Y Acad Sci* 1068:1-13.

78. Vortkamp A, Lee K, Lanske B, Segre GV, Kronenberg HM, & Tabin CJ (1996) Regulation of rate of cartilage differentiation by Indian hedgehog and PTH-related protein. *Science* 273:613-622.

79. Kobayashi T, Soegiarto DW, Yang Y, Lanske B, Schipani E, McMahon AP, & Kronenberg HM (2005) Indian hedgehog stimulates periarticular chondrocyte differentiation to regulate growth plate length independently of PTHrP. *J Clin Invest* 115:1734-1742.

80. Kronenberg HM (2003) Developmental regulation of the growth plate. *Nature* 423:332-336.

81. Ornitz DM (2005) FGF signaling in the developing endochondral skeleton. *Cytokine Growth Factor Rev* 16:205-213.

82. Rousseau F, Bonaventure J, Legeai-Mallet L, Pelet A, Rozet JM, Maroteaux P, Le Merrer M, & Munnich A (1994) Mutations in the gene encoding fibroblast growth factor receptor-3 in achondroplasia. *Nature* 371:252-254.

83. Naski MC, Wang Q, Xu J, & Ornitz DM (1996) Graded activation of fibroblast growth factor receptor 3 by mutations causing achondroplasia and thanatophoric dysplasia. *Nat Genet* 13:233-237.

84. Shiang R, Thompson LM, Zhu YZ, Church DM, Fielder TJ, Bocian M, Winokur ST, & Wasmuth JJ (1994) Mutations in the transmembrane domain of FGFR3 cause the most common genetic form of dwarfism, achondroplasia. *Cell* 78:335-342.

85. Rousseau F, Saugier P, Le Merrer M, Munnich A, Delezoide AL, Maroteaux P, Bonaventure J, Narcy F, & Sanak M (1995) Stop codon FGFR3 mutations in thanatophoric dwarfism type 1. *Nat Genet* 10:11-12.

86. Tavormina PL, Shiang R, Thompson LM, Zhu YZ, Wilkin DJ, Lachman RS, Wilcox WR, Rimoin DL, Cohn DH, & Wasmuth JJ (1995) Thanatophoric dysplasia (types I and II) caused by distinct mutations in fibroblast growth factor receptor 3. *Nat Genet* 9:321-328.

87. Colvin JS, Bohne BA, Harding GW, McEwen DG, & Ornitz DM (1996) Skeletal overgrowth and deafness in mice lacking fibroblast growth factor receptor 3. *Nat Genet* 12:390-397.

88. Deng C, Wynshaw-Boris A, Zhou F, Kuo A, & Leder P (1996) Fibroblast growth factor receptor 3 is a negative regulator of bone growth. *Cell* 84:911-921.

89. Murakami S, Balmes G, McKinney S, Zhang Z, Givol D, & de Crombrugghe B (2004) Constitutive activation of MEK1 in chondrocytes

causes Stat1-independent achondroplasia-like dwarfism and rescues the Fgfr3-deficient mouse phenotype. *Genes Dev* 18:290-305.

90. Liu Z, Xu J, Colvin JS, & Ornitz DM (2002) Coordination of chondrogenesis and osteogenesis by fibroblast growth factor 18. *Genes Dev* 16:859-869.

91. Ohbayashi N, Shibayama M, Kurotaki Y, Imanishi M, Fujimori T, Itoh N, & Takada S (2002) FGF18 is required for normal cell proliferation and differentiation during osteogenesis and chondrogenesis. *Genes Dev* 16:870-879.

92. Pizette S & Niswander L (2000) BMPs are required at two steps of limb chondrogenesis: formation of prechondrogenic condensations and their differentiation into chondrocytes. *Dev Biol* 219:237-249.

93. Minina E, Kreschel C, Naski MC, Ornitz DM, & Vortkamp A (2002) Interaction of FGF, Ihh/Pthlh, and BMP signaling integrates chondrocyte proliferation and hypertrophic differentiation. *Dev Cell* 3:439-449.

94. Minina E, Wenzel HM, Kreschel C, Karp S, Gaffield W, McMahon AP, & Vortkamp A (2001) BMP and Ihh/PTHrP signaling interact to coordinate chondrocyte proliferation and differentiation. *Development* 128:4523-4534.

95. Yoon BS, Pogue R, Ovchinnikov DA, Yoshii I, Mishina Y, Behringer RR, & Lyons KM (2006) BMPs regulate multiple aspects of growth-plate chondrogenesis through opposing actions on FGF pathways. *Development* 133:4667-4678.

96. Akiyama H, Chaboissier MC, Martin JF, Schedl A, & de Crombrugghe B (2002) The transcription factor Sox9 has essential roles in successive steps of the chondrocyte differentiation pathway and is required for expression of Sox5 and Sox6. *Genes Dev* 16:2813-2828.

97. Bi W, Deng JM, Zhang Z, Behringer RR, & de Crombrugghe B (1999) Sox9 is required for cartilage formation. *Nat Genet* 22:85-89.

98. Lefebvre V, Huang W, Harley VR, Goodfellow PN, & de Crombrugghe B (1997) SOX9 is a potent activator of the chondrocyte-specific enhancer of the pro alpha1(II) collagen gene. *Mol Cell Biol* 17:2336-2346.

99. Bi W, Huang W, Whitworth DJ, Deng JM, Zhang Z, Behringer RR, & de Crombrugghe B (2001) Haploinsufficiency of Sox9 results in defective cartilage primordia and premature skeletal mineralization. *Proc Natl Acad Sci U S A* 98:6698-6703.

100. Provot S & Schipani E (2005) Molecular mechanisms of endochondral bone development. *Biochem Biophys Res Commun* 328:658-665.

101. Akiyama H (2008) Control of chondrogenesis by the transcription factor Sox9. *Mod Rheumatol* 18:213-219.

102. Han Y & Lefebvre V (2008) L-Sox5 and Sox6 drive expression of the aggrecan gene in cartilage by securing binding of Sox9 to a far-upstream enhancer. *Mol Cell Biol* 28:4999-5013.

103. Hartmann C (2009) Transcriptional networks controlling skeletal development. *Curr Opin Genet Dev* 19:437-443.

104. Mundlos S, Otto F, Mundlos C, Mulliken JB, Aylsworth AS, Albright S, Lindhout D, Cole WG, Henn W, Knoll JH, Owen MJ, Mertelsmann R, Zabel BU, & Olsen BR (1997) Mutations involving the transcription factor CBFA1 cause cleidocranial dysplasia. *Cell* 89:773-779.

105. Ducy P, Zhang R, Geoffroy V, Ridall AL, & Karsenty G (1997) Osf2/Cbfa1: a transcriptional activator of osteoblast differentiation. *Cell* 89:747-754.

106. Komori T, Yagi H, Nomura S, Yamaguchi A, Sasaki K, Deguchi K, Shimizu Y, Bronson RT, Gao YH, Inada M, Sato M, Okamoto R, Kitamura Y, Yoshiki S, & Kishimoto T (1997) Targeted disruption of Cbfa1 results in a complete lack of bone formation owing to maturational arrest of osteoblasts. *Cell* 89:755-764.

107. Otto F, Thornell AP, Crompton T, Denzel A, Gilmour KC, Rosewell IR, Stamp GW, Beddington RS, Mundlos S, Olsen BR, Selby PB, & Owen MJ (1997) Cbfa1, a candidate gene for cleidocranial dysplasia syndrome, is essential for osteoblast differentiation and bone development. *Cell* 89:765-771.

108. Inada M, Yasui T, Nomura S, Miyake S, Deguchi K, Himeno M, Sato M, Yamagiwa H, Kimura T, Yasui N, Ochi T, Endo N, Kitamura Y, Kishimoto T, & Komori T (1999) Maturational disturbance of chondrocytes in Cbfa1-deficient mice. *Dev Dyn* 214:279-290.

109. Kim IS, Otto F, Zabel B, & Mundlos S (1999) Regulation of chondrocyte differentiation by Cbfa1. *Mech Dev* 80:159-170.

110. Hinoi E, Bialek P, Chen YT, Rached MT, Groner Y, Behringer RR, Ornitz DM, & Karsenty G (2006) Runx2 inhibits chondrocyte proliferation and hypertrophy through its expression in the perichondrium. *Genes Dev* 20:2937-2942.

111. Yoshida CA, Yamamoto H, Fujita T, Furuichi T, Ito K, Inoue K, Yamana K, Zanma A, Takada K, Ito Y, & Komori T (2004) Runx2 and Runx3 are essential for chondrocyte maturation, and Runx2 regulates limb growth through induction of Indian hedgehog. *Genes Dev* 18:952-963.

112. Ueta C, Iwamoto M, Kanatani N, Yoshida C, Liu Y, Enomoto-Iwamoto M, Ohmori T, Enomoto H, Nakata K, Takada K, Kurisu K, & Komori T (2001) Skeletal malformations caused by overexpression of Cbfa1 or its dominant negative form in chondrocytes. *J Cell Biol* 153:87-100.

113. Karsenty G, Kronenberg HM, & Settembre C (2009) Genetic control of bone formation. *Annu Rev Cell Dev Biol* 25:629-648.

114. Satokata I, Ma L, Ohshima H, Bei M, Woo I, Nishizawa K, Maeda T, Takano Y, Uchiyama M, Heaney S, Peters H, Tang Z, Maxson R, & Maas R (2000) Msx2 deficiency in mice causes pleiotropic defects in bone growth and ectodermal organ formation. *Nat Genet* 24:391-395.

115. Tribioli C & Lufkin T (1999) The murine Bapx1 homeobox gene plays a critical role in embryonic development of the axial skeleton and spleen. *Development* 126:5699-5711.

116. Schmidt K, Schinke T, Haberland M, Priemel M, Schilling AF, Mueldner C, Rueger JM, Sock E, Wegner M, & Amling M (2005) The high mobility

group transcription factor Sox8 is a negative regulator of osteoblast differentiation. *J Cell Biol* 168:899-910.

117. Holleville N, Mateos S, Bontoux M, Bollerot K, & Monsoro-Burq AH (2007) Dlx5 drives Runx2 expression and osteogenic differentiation in developing cranial suture mesenchyme. *Dev Biol* 304:860-874.

118. Lee MH, Kim YJ, Yoon WJ, Kim JI, Kim BG, Hwang YS, Wozney JM, Chi XZ, Bae SC, Choi KY, Cho JY, Choi JY, & Ryoo HM (2005) Dlx5 specifically regulates Runx2 type II expression by binding to homeodomain-response elements in the Runx2 distal promoter. *J Biol Chem* 280:35579-35587.

119. Nakashima K, Zhou X, Kunkel G, Zhang Z, Deng JM, Behringer RR, & de Crombrugghe B (2002) The novel zinc finger-containing transcription factor osterix is required for osteoblast differentiation and bone formation. *Cell* 108:17-29.

120. Yang X & Karsenty G (2004) ATF4, the osteoblast accumulation of which is determined post-translationally, can induce osteoblast-specific gene expression in non-osteoblastic cells. *J Biol Chem* 279:47109-47114.

121. Yang X, Matsuda K, Bialek P, Jacquot S, Masuoka HC, Schinke T, Li L, Brancorsini S, Sassone-Corsi P, Townes TM, Hanauer A, & Karsenty G (2004) ATF4 is a substrate of RSK2 and an essential regulator of osteoblast biology; implication for Coffin-Lowry Syndrome. *Cell* 117:387-398.

122. Yu VW, Akhouayri O, & St-Arnaud R (2009) FIAT is co-expressed with its dimerization target ATF4 in early osteoblasts, but not in osteocytes. *Gene Expr Patterns* 9:335-340.

123. Dobreva G, Chahrour M, Dautzenberg M, Chirivella L, Kanzler B, Farinas I, Karsenty G, & Grosschedl R (2006) SATB2 is a multifunctional determinant of craniofacial patterning and osteoblast differentiation. *Cell* 125:971-986.

124. Boyle WJ, Simonet WS, & Lacey DL (2003) Osteoclast differentiation and activation. *Nature* 423:337-342.

125. Karim FD, Urness LD, Thummel CS, Klemsz MJ, McKercher SR, Celada A, Van Beveren C, Maki RA, Gunther CV, Nye JA, & et al. (1990) The ETS-domain: a new DNA-binding motif that recognizes a purine-rich core DNA sequence. *Genes Dev* 4:1451-1453.

126. Klemsz MJ, McKercher SR, Celada A, Van Beveren C, & Maki RA (1990) The macrophage and B cell-specific transcription factor PU.1 is related to the ets oncogene. *Cell* 61:113-124.

127. Teitelbaum SL & Ross FP (2003) Genetic regulation of osteoclast development and function. *Nat Rev Genet* 4:638-649.

128. Yao GQ, Sun BH, Weir EC, & Insogna KL (2002) A role for cell-surface CSF-1 in osteoblast-mediated osteoclastogenesis. *Calcif Tissue Int* 70:339-346.

129. Ross FP (2000) RANKing the importance of measles virus in Paget's disease. *J Clin Invest* 105:555-558.

130. Grigoriadis AE, Schellander K, Wang ZQ, & Wagner EF (1993) Osteoblasts are target cells for transformation in c-fos transgenic mice. *J Cell Biol* 122:685-701.

131. Grigoriadis AE, Wang ZQ, Cecchini MG, Hofstetter W, Felix R, Fleisch HA, & Wagner EF (1994) c-Fos: a key regulator of osteoclast-macrophage lineage determination and bone remodeling. *Science* 266:443-448.

132. Kong YY, Yoshida H, Sarosi I, Tan HL, Timms E, Capparelli C, Morony S, Oliveira-dos-Santos AJ, Van G, Itie A, Khoo W, Wakeham A, Dunstan CR, Lacey DL, Mak TW, Boyle WJ, & Penninger JM (1999) OPGL is a key regulator of osteoclastogenesis, lymphocyte development and lymph-node organogenesis. *Nature* 397:315-323.

133. Simonet WS, Lacey DL, Dunstan CR, Kelley M, Chang MS, Luthy R, Nguyen HQ, Wooden S, Bennett L, Boone T, Shimamoto G, DeRose M, Elliott R, Colombero A, Tan HL, Trail G, Sullivan J, Davy E, Bucay N, Renshaw-Gegg L, Hughes TM, Hill D, Pattison W, Campbell P, Sander S, Van G, Tarpley J, Derby P, Lee R, & Boyle WJ (1997) Osteoprotegerin: a novel secreted protein involved in the regulation of bone density. *Cell* 89:309-319.

134. Bucay N, Sarosi I, Dunstan CR, Morony S, Tarpley J, Capparelli C, Scully S, Tan HL, Xu W, Lacey DL, Boyle WJ, & Simonet WS (1998) osteoprotegerin-deficient mice develop early onset osteoporosis and arterial calcification. *Genes Dev* 12:1260-1268.

135. Amieux PS, Cummings DE, Motamed K, Brandon EP, Wailes LA, Le K, Idzerda RL, & McKnight GS (1997) Compensatory regulation of RIalpha protein levels in protein kinase A mutant mice. *J Biol Chem* 272:3993-3998.

136. Griffin KJ, Kirschner LS, Matyakhina L, Stergiopoulos S, Robinson-White A, Lenherr S, Weinberg FD, Claflin E, Meoli E, Cho-Chung YS, & Stratakis CA (2004) Down-regulation of regulatory subunit type 1A of protein kinase A leads to endocrine and other tumors. *Cancer Res* 64:8811-8815.

137. Griffin KJ, Kirschner LS, Matyakhina L, Stergiopoulos S, Robinson-White A, Weinberg F, Meoli E, Bornstein SR, & Stratakis CA (2004) A mouse model for Carney complex. *Endocr Res* 30:903-911.

138. Griffin KJ, Kirschner LS, Matyakhina L, Stergiopoulos SG, Robinson-White A, Lenherr SM, Weinberg FD, Claflin ES, Batista D, Bourdeau I, Voutetakis A, Sandrini F, Meoli EM, Bauer AJ, Cho-Chung YS, Bornstein SR, Carney JA, & Stratakis CA (2004) A transgenic mouse bearing an antisense construct of regulatory subunit type 1A of protein kinase A develops endocrine and other tumours: comparison with Carney complex and other PRKAR1A induced lesions. *J Med Genet* 41:923-931.

139. Robinson-White A, Meoli E, Stergiopoulos S, Horvath A, Boikos S, Bossis I, & Stratakis CA (2006) PRKAR1A Mutations and protein kinase A interactions with other signaling pathways in the adrenal cortex. *J Clin Endocrinol Metab* 91:2380-2388.

140. Meoli E, Bossis I, Cazabat L, Mavrakis M, Horvath A, Stergiopoulos S, Shiferaw ML, Fumey G, Perlemoine K, Muchow M, Robinson-White A, Weinberg F, Nesterova M, Patronas Y, Groussin L, Bertherat J, & Stratakis CA (2008) Protein kinase A effects of an expressed PRKAR1A mutation associated with aggressive tumors. *Cancer Res* 68:3133-3141.

141. Herberg FW, Doyle ML, Cox S, & Taylor SS (1999) Dissection of the nucleotide and metal-phosphate binding sites in cAMP-dependent protein kinase. *Biochemistry* 38:6352-6360.

142. Kim C, Xuong NH, & Taylor SS (2005) Crystal structure of a complex between the catalytic and regulatory (RIalpha) subunits of PKA. *Science* 307:690-696.

143. Taylor SS, Kim C, Vigil D, Haste NM, Yang J, Wu J, & Anand GS (2005) Dynamics of signaling by PKA. *Biochim Biophys Acta* 1754:25-37.

144. Pavel E, Nadella K, Towns WH, 2nd, & Kirschner LS (2008) Mutation of Prkar1a causes osteoblast neoplasia driven by dysregulation of protein kinase A. *Mol Endocrinol* 22:430-440.

145. Bianco P, Kuznetsov SA, Riminucci M, Fisher LW, Spiegel AM, & Robey PG (1998) Reproduction of human fibrous dysplasia of bone in immunocompromised mice by transplanted mosaics of normal and Gsalpha-mutated skeletal progenitor cells. *J Clin Invest* 101:1737-1744.

146. Riminucci M, Liu B, Corsi A, Shenker A, Spiegel AM, Robey PG, & Bianco P (1999) The histopathology of fibrous dysplasia of bone in patients with

activating mutations of the Gs alpha gene: site-specific patterns and recurrent histological hallmarks. *J Pathol* 187:249-258.

147. Riminucci M, Saggio I, Robey PG, & Bianco P (2006) Fibrous dysplasia as a stem cell disease. *J Bone Miner Res* 21 Suppl 2:P125-131.

148. Cheadle C, Becker KG, Cho-Chung YS, Nesterova M, Watkins T, Wood W, 3rd, Prabhu V, & Barnes KC (2007) A rapid method for microarray cross platform comparisons using gene expression signatures. *Mol Cell Probes* 21:35-46.

149. Cheadle C, Nesterova M, Watkins T, Barnes KC, Hall JC, Rosen A, Becker KG, & Cho-Chung YS (2008) Regulatory subunits of PKA define an axis of cellular proliferation/differentiation in ovarian cancer cells. *BMC Med Genomics* 1:43.

150. Livak KJ & Schmittgen TD (2001) Analysis of relative gene expression data using real-time quantitative PCR and the 2(-Delta Delta C(T)) Method. *Methods* 25:402-408.

151. Saba E, Grivel JC, Vanpouille C, Brichacek B, Fitzgerald W, Margolis L, & Lisco A (HIV-1 sexual transmission: early events of HIV-1 infection of human cervico-vaginal tissue in an optimized ex vivo model. *Mucosal Immunol*.

152. Rohlff C, Clair T, & Cho-Chung YS (1993) 8-Cl-cAMP induces truncation and down-regulation of the RI alpha subunit and up-regulation of the RII beta subunit of cAMP-dependent protein kinase leading to type II

holoenzyme-dependent growth inhibition and differentiation of HL-60 leukemia cells. *J Biol Chem* 268:5774-5782.

153. Poch G (1971) Assay of phosphodiesterase with radioactively labeled cyclic 3',5'-AMP as substrate. *Naunyn Schmiedebergs Arch Pharmakol* 268:272-299.

154. Nesterova M, Yokozaki H, McDuffie E, & Cho-Chung YS (1996) Overexpression of RII beta regulatory subunit of protein kinase A in human colon carcinoma cell induces growth arrest and phenotypic changes that are abolished by site-directed mutation of RII beta. *Eur J Biochem* 235:486-494.

155. Kashima TG, Nishiyama T, Shimazu K, Shimazaki M, Kii I, Grigoriadis AE, Fukayama M, & Kudo A (2009) Periostin, a novel marker of intramembranous ossification, is expressed in fibrous dysplasia and in c-Fos-overexpressing bone lesions. *Hum Pathol* 40:226-237.

156. Dufresne T, Chmielewski P, Borah B, & Laib A (2004) Microcomputed Tomography and Its Applications eds Bowlin GL & Wnek G (Encyclopedia of Biomaterials and Biomedical Engineering), Vol 2, pp 994-1003.

157. Carden A & Morris MD (2000) Application of vibrational spectroscopy to the study of mineralized tissues (review). *J Biomed Opt* 5:259-268.

158. Robinson-White A, Hundley TR, Shiferaw M, Bertherat J, Sandrini F, & Stratakis CA (2003) Protein kinase-A activity in PRKAR1A-mutant cells, and regulation of mitogen-activated protein kinases ERK1/2. *Hum Mol Genet* 12:1475-1484.

159. Bertherat J, Groussin L, Sandrini F, Matyakhina L, Bei T, Stergiopoulos S, Papageorgiou T, Bourdeau I, Kirschner LS, Vincent-Dejean C, Perlemoine K, Gicquel C, Bertagna X, & Stratakis CA (2003) Molecular and functional analysis of PRKAR1A and its locus (17q22-24) in sporadic adrenocortical tumors: 17q losses, somatic mutations, and protein kinase A expression and activity. *Cancer Res* 63:5308-5319.

160. Pekkinen M, Ahlstrom ME, Riehle U, Huttunen MM, & Lamberg-Allardt CJ (2008) Effects of phosphodiesterase 7 inhibition by RNA interference on the gene expression and differentiation of human mesenchymal stem cell-derived osteoblasts. *Bone* 43:84-91.

161. Sandrini F, Matyakhina L, Sarlis NJ, Kirschner LS, Farmakidis C, Gimm O, & Stratakis CA (2002) Regulatory subunit type I-alpha of protein kinase A (PRKAR1A): a tumor-suppressor gene for sporadic thyroid cancer. *Genes Chromosomes Cancer* 35:182-192.

162. Bianco P, Kuznetsov SA, Riminucci M, & Gehron Robey P (2006) Postnatal skeletal stem cells. *Methods Enzymol* 419:117-148.

163. Edgar R, Domrachev M, & Lash AE (2002) Gene Expression Omnibus: NCBI gene expression and hybridization array data repository. *Nucleic Acids Res* 30:207-210.

164. Eisen MB, Spellman PT, Brown PO, & Botstein D (1998) Cluster analysis and display of genome-wide expression patterns. *Proc Natl Acad Sci U S A* 95:14863-14868.

165. Otten AD & McKnight GS (1989) Overexpression of the type II regulatory subunit of the cAMP-dependent protein kinase eliminates the type I holoenzyme in mouse cells. *J Biol Chem* 264:20255-20260.

166. Amieux PS & McKnight GS (2002) The essential role of RI alpha in the maintenance of regulated PKA activity. *Ann N Y Acad Sci* 968:75-95.

167. Lange-Carter CA, Fossli T, Jahnsen T, & Malkinson AM (1990) Decreased expression of the type I isozyme of cAMP-dependent protein kinase in tumor cell lines of lung epithelial origin. *J Biol Chem* 265:7814-7818.

168. Steinberg RA & Agard DA (1981) Turnover of regulatory subunit of cyclic AMP-dependent protein kinase in S49 mouse lymphoma cells. Regulation by catalytic subunit and analogs of cyclic AMP. *J Biol Chem* 256:10731-10734.

169. Weber W & Hilz H (1986) cAMP-dependent protein kinases I and II: divergent turnover of subunits. *Biochemistry* 25:5661-5667.

170. Collier LS, Suyama K, Anderson JH, & Scott MP (2004) Drosophila Costal1 mutations are alleles of protein kinase A that modulate hedgehog signaling. *Genetics* 167:783-796.

171. Clegg CH, Cadd GG, & McKnight GS (1988) Genetic characterization of a brain-specific form of the type I regulatory subunit of cAMP-dependent protein kinase. *Proc Natl Acad Sci U S A* 85:3703-3707.

172. San Agustin JT & Witman GB (2001) Differential expression of the C(s) and Calpha1 isoforms of the catalytic subunit of cyclic 3',5'-adenosine

monophosphate-dependent protein kinase testicular cells. *Biol Reprod* 65:151-164.

173. Desseyn JL, Burton KA, & McKnight GS (2000) Expression of a nonmyristylated variant of the catalytic subunit of protein kinase A during male germ-cell development. *Proc Natl Acad Sci U S A* 97:6433-6438.

174. Reinton N, Orstavik S, Haugen TB, Jahnsen T, Tasken K, & Skalhegg BS (2000) A novel isoform of human cyclic 3',5'-adenosine monophosphate-dependent protein kinase, c alpha-s, localizes to sperm midpiece. *Biol Reprod* 63:607-611.

175. San Agustin JT, Leszyk JD, Nuwaysir LM, & Witman GB (1998) The catalytic subunit of the cAMP-dependent protein kinase of ovine sperm flagella has a unique amino-terminal sequence. *J Biol Chem* 273:24874-24883.

176. Funderud A, Henanger HH, Hafte TT, Amieux PS, Orstavik S, & Skalhegg BS (2006) Identification, cloning and characterization of a novel 47 kDa murine PKA C subunit homologous to human and bovine Cbeta2. *BMC Biochem* 7:20.

177. Uhler MD, Chrivia JC, & McKnight GS (1986) Evidence for a second isoform of the catalytic subunit of cAMP-dependent protein kinase. *J Biol Chem* 261:15360-15363.

178. Yu SH, Chiang WC, Shih HM, & Wu KJ (2004) Stimulation of c-Rel transcriptional activity by PKA catalytic subunit beta. *J Mol Med* 82:621-628.

179. Beebe SJ, Oyen O, Sandberg M, Froysa A, Hansson V, & Jahnsen T (1990) Molecular cloning of a tissue-specific protein kinase (C gamma) from human testis--representing a third isoform for the catalytic subunit of cAMP-dependent protein kinase. *Mol Endocrinol* 4:465-475.

180. Morris RC, Morris GZ, Zhang W, Gellerman M, & Beebe SJ (2002) Differential transcriptional regulation by the alpha- and gamma-catalytic subunit isoforms of cAMP-dependent protein kinase. *Arch Biochem Biophys* 403:219-228.

181. Beebe SJ, Salomonsky P, Jahnsen T, & Li Y (1992) The C gamma subunit is a unique isozyme of the cAMP-dependent protein kinase. *J Biol Chem* 267:25505-25512.

182. Diskar M, Zenn HM, Kaupisch A, Prinz A, & Herberg FW (2007) Molecular basis for isoform-specific autoregulation of protein kinase A. *Cell Signal* 19:2024-2034.

183. Li W, Yu ZX, & Kotin RM (2005) Profiles of PrKX expression in developmental mouse embryo and human tissues. *J Histochem Cytochem* 53:1003-1009.

184. Zimmermann B, Chiorini JA, Ma Y, Kotin RM, & Herberg FW (1999) PrKX is a novel catalytic subunit of the cAMP-dependent protein kinase regulated by the regulatory subunit type I. *J Biol Chem* 274:5370-5378.

185. Manni S, Mauban JH, Ward CW, & Bond M (2008) Phosphorylation of the cAMP-dependent protein kinase (PKA) regulatory subunit modulates PKA-

AKAP interaction, substrate phosphorylation, and calcium signaling in cardiac cells. *J Biol Chem* 283:24145-24154.

186. Geahlen RL, Allen SM, & Krebs EG (1981) Effect of phosphorylation on the regulatory subunit of the type I cAMP-dependent protein kinase. *J Biol Chem* 256:4536-4540.

187. Scott CW & Mumby MC (1985) Phosphorylation of type II regulatory subunit of cAMP-dependent protein kinase in intact smooth muscle. *J Biol Chem* 260:2274-2280.

188. Carlson CR, Witczak O, Vossebein L, Labbe JC, Skalhegg BS, Keryer G, Herberg FW, Collas P, & Tasken K (2001) CDK1-mediated phosphorylation of the RIIalpha regulatory subunit of PKA works as a molecular switch that promotes dissociation of RIIalpha from centrosomes at mitosis. *J Cell Sci* 114:3243-3254.

189. Rubin CS (1994) A kinase anchor proteins and the intracellular targeting of signals carried by cyclic AMP. *Biochim Biophys Acta* 1224:467-479.

190. Dell'Acqua ML & Scott JD (1997) Protein kinase A anchoring. *J Biol Chem* 272:12881-12884.

191. Prinz A, Diskar M, Erlbruch A, & Herberg FW (2006) Novel, isotype-specific sensors for protein kinase A subunit interaction based on bioluminescence resonance energy transfer (BRET). *Cell Signal* 18:1616-1625.

192. Robinson-White AJ, Leitner WW, Aleem E, Kaldis P, Bossis I, & Stratakis CA (2006) PRKAR1A inactivation leads to increased proliferation and

decreased apoptosis in human B lymphocytes. *Cancer Res* 66:10603-10612.

193. Brandon EP, Logue SF, Adams MR, Qi M, Sullivan SP, Matsumoto AM, Dorsa DM, Wehner JM, McKnight GS, & Idzerda RL (1998) Defective motor behavior and neural gene expression in RIIbeta-protein kinase A mutant mice. *J Neurosci* 18:3639-3649.

194. Klein DC & Raisz LG (1971) Role of adenosine-3',5'-monophosphate in the hormonal regulation of bone resorption: studies with cultured fetal bone. *Endocrinology* 89:818-826.

195. Swarthout JT, D'Alonzo RC, Selvamurugan N, & Partridge NC (2002) Parathyroid hormone-dependent signaling pathways regulating genes in bone cells. *Gene* 282:1-17.

196. Luben RA, Wong GL, & Cohn DV (1976) Biochemical characterization with parathormone and calcitonin of isolated bone cells: provisional identification of osteoclasts and osteoblasts. *Endocrinology* 99:526-534.

197. Partridge NC, Alcorn D, Michelangeli VP, Kemp BE, Ryan GB, & Martin TJ (1981) Functional properties of hormonally responsive cultured normal and malignant rat osteoblastic cells. *Endocrinology* 108:213-219.

198. Majeska RJ & Rodan GA (1982) Alkaline phosphatase inhibition by parathyroid hormone and isoproterenol in a clonal rat osteosarcoma cell line. Possible mediation by cyclic AMP. *Calcif Tissue Int* 34:59-66.

199. Karaplis AC, Luz A, Glowacki J, Bronson RT, Tybulewicz VL, Kronenberg HM, & Mulligan RC (1994) Lethal skeletal dysplasia from targeted

disruption of the parathyroid hormone-related peptide gene. *Genes Dev* 8:277-289.

200. Lanske B, Karaplis AC, Lee K, Luz A, Vortkamp A, Pirro A, Karperien M, Defize LH, Ho C, Mulligan RC, Abou-Samra AB, Juppner H, Segre GV, & Kronenberg HM (1996) PTH/PTHrP receptor in early development and Indian hedgehog-regulated bone growth. *Science* 273:663-666.

201. Habener JF, Rosenblatt M, & Potts JT, Jr. (1984) Parathyroid hormone: biochemical aspects of biosynthesis, secretion, action, and metabolism. *Physiol Rev* 64:985-1053.

202. Brown EM (1993) Mechanisms underlying the regulation of parathyroid hormone secretion in vivo and in vitro. *Curr Opin Nephrol Hypertens* 2:541-551.

203. Teitelbaum SL (2000) Bone resorption by osteoclasts. *Science* 289:1504-1508.

204. Bastepe M, Weinstein LS, Ogata N, Kawaguchi H, Juppner H, Kronenberg HM, & Chung UI (2004) Stimulatory G protein directly regulates hypertrophic differentiation of growth plate cartilage in vivo. *Proc Natl Acad Sci U S A* 101:14794-14799.

205. Sakamoto A, Chen M, Kobayashi T, Kronenberg HM, & Weinstein LS (2005) Chondrocyte-specific knockout of the G protein G(s)alpha leads to epiphyseal and growth plate abnormalities and ectopic chondrocyte formation. *J Bone Miner Res* 20:663-671.

206. Candeliere GA, Glorieux FH, Prud'homme J, & St-Arnaud R (1995) Increased expression of the c-fos proto-oncogene in bone from patients with fibrous dysplasia. *N Engl J Med* 332:1546-1551.

207. Riminucci M, Fisher LW, Shenker A, Spiegel AM, Bianco P, & Gehron Robey P (1997) Fibrous dysplasia of bone in the McCune-Albright syndrome: abnormalities in bone formation. *Am J Pathol* 151:1587-1600.

208. Sette C, Iona S, & Conti M (1994) The short-term activation of a rolipram-sensitive, cAMP-specific phosphodiesterase by thyroid-stimulating hormone in thyroid FRTL-5 cells is mediated by a cAMP-dependent phosphorylation. *J Biol Chem* 269:9245-9252.

209. Sette C & Conti M (1996) Phosphorylation and activation of a cAMP-specific phosphodiesterase by the cAMP-dependent protein kinase. Involvement of serine 54 in the enzyme activation. *J Biol Chem* 271:16526-16534.

210. Rochais F, Vandecasteele G, Lefebvre F, Lugnier C, Lum H, Mazet JL, Cooper DM, & Fischmeister R (2004) Negative feedback exerted by cAMP-dependent protein kinase and cAMP phosphodiesterase on subsarcolemmal cAMP signals in intact cardiac myocytes: an in vivo study using adenovirus-mediated expression of CNG channels. *J Biol Chem* 279:52095-52105.

211. Oyen O, Sandberg M, Eskild W, Levy FO, Knutsen G, Beebe S, Hansson V, & Jahnsen T (1988) Differential regulation of messenger ribonucleic acids for specific subunits of cyclic adenosine 3',5'-monophosphate

(cAMP)-dependent protein kinase by cAMP in rat Sertoli cells. *Endocrinology* 122:2658-2666.

212. Tasken KA, Knutsen HK, Attramadal H, Tasken K, Jahnsen T, Hansson V, & Eskild W (1991) Different mechanisms are involved in cAMP-mediated induction of mRNAs for subunits of cAMP-dependent protein kinases. *Mol Endocrinol* 5:21-28.

213. Gaudin C, Ishikawa Y, Wight DC, Mahdavi V, Nadal-Ginard B, Wagner TE, Vatner DE, & Homcy CJ (1995) Overexpression of Gs alpha protein in the hearts of transgenic mice. *J Clin Invest* 95:1676-1683.

214. Huang XP, Song X, Wang HY, & Malbon CC (2002) Targeted expression of activated Q227L G(alpha)(s) in vivo. *Am J Physiol Cell Physiol* 283:C386-395.

215. Sakamoto A, Chen M, Nakamura T, Xie T, Karsenty G, & Weinstein LS (2005) Deficiency of the G-protein alpha-subunit G(s)alpha in osteoblasts leads to differential effects on trabecular and cortical bone. *J Biol Chem* 280:21369-21375.

216. Riminucci M, Kuznetsov SA, Cherman N, Corsi A, Bianco P, & Gehron Robey P (2003) Osteoclastogenesis in fibrous dysplasia of bone: in situ and in vitro analysis of IL-6 expression. *Bone* 33:434-442.

217. Geoffroy V, Kneissel M, Fournier B, Boyde A, & Matthias P (2002) High bone resorption in adult aging transgenic mice overexpressing cbfa1/runx2 in cells of the osteoblastic lineage. *Mol Cell Biol* 22:6222-6233.

218. Kitazawa R, Kitazawa S, & Maeda S (1999) Promoter structure of mouse RANKL/TRANCE/OPGL/ODF gene. *Biochim Biophys Acta* 1445:134-141.

219. Mori K, Kitazawa R, Kondo T, Maeda S, Yamaguchi A, & Kitazawa S (2006) Modulation of mouse RANKL gene expression by Runx2 and PKA pathway. *J Cell Biochem* 98:1629-1644.

220. Yang DC, Tsay HJ, Lin SY, Chiou SH, Li MJ, Chang TJ, & Hung SC (2008) cAMP/PKA regulates osteogenesis, adipogenesis and ratio of RANKL/OPG mRNA expression in mesenchymal stem cells by suppressing leptin. *PLoS One* 3:e1540.

221. Siddappa R, Mulder W, Steeghs I, van de Klundert C, Fernandes H, Liu J, Arends R, van Blitterswijk C, & de Boer J (2009) cAMP/PKA signaling inhibits osteogenic differentiation and bone formation in rodent models. *Tissue Eng Part A* 15:2135-2143.

222. Kvissel AK, Orstavik S, Oistad P, Rootwelt T, Jahnsen T, & Skalhegg BS (2004) Induction of Cbeta splice variants and formation of novel forms of protein kinase A type II holoenzymes during retinoic acid-induced differentiation of human NT2 cells. *Cell Signal* 16:577-587.

223. Liu S, Zhou J, Tang W, Jiang X, Rowe DW, & Quarles LD (2006) Pathogenic role of Fgf23 in Hyp mice. *Am J Physiol Endocrinol Metab* 291:E38-49.

224. Quarles LD (2008) Endocrine functions of bone in mineral metabolism regulation. *J Clin Invest* 118:3820-3828.

225. Riminucci M, Collins MT, Fedarko NS, Cherman N, Corsi A, White KE, Waguespack S, Gupta A, Hannon T, Econs MJ, Bianco P, & Gehron Robey P (2003) FGF-23 in fibrous dysplasia of bone and its relationship to renal phosphate wasting. *J Clin Invest* 112:683-692.

226. Kuznetsov SA, Cherman N, Riminucci M, Collins MT, Robey PG, & Bianco P (2008) Age-dependent demise of GNAS-mutated skeletal stem cells and "normalization" of fibrous dysplasia of bone. *J Bone Miner Res* 23:1731-1740.

227. Calvi LM, Sims NA, Hunzelman JL, Knight MC, Giovannetti A, Saxton JM, Kronenberg HM, Baron R, & Schipani E (2001) Activated parathyroid hormone/parathyroid hormone-related protein receptor in osteoblastic cells differentially affects cortical and trabecular bone. *J Clin Invest* 107:277-286.

228. Kuznetsov SA, Riminucci M, Ziran N, Tsutsui TW, Corsi A, Calvi L, Kronenberg HM, Schipani E, Robey PG, & Bianco P (2004) The interplay of osteogenesis and hematopoiesis: expression of a constitutively active PTH/PTHrP receptor in osteogenic cells perturbs the establishment of hematopoiesis in bone and of skeletal stem cells in the bone marrow. *J Cell Biol* 167:1113-1122.

229. Hilton MJ, Tu X, & Long F (2007) Tamoxifen-inducible gene deletion reveals a distinct cell type associated with trabecular bone, and direct regulation of PTHrP expression and chondrocyte morphology by Ihh in growth region cartilage. *Dev Biol* 308:93-105.

230. Kiuru M, Solomon J, Ghali B, van der Meulen M, Crystal RG, & Hidaka C (2009) Transient overexpression of sonic hedgehog alters the architecture and mechanical properties of trabecular bone. *J Bone Miner Res* 24:1598-1607.

231. Li Y, Lacerda DA, Warman ML, Beier DR, Yoshioka H, Ninomiya Y, Oxford JT, Morris NP, Andrikopoulos K, Ramirez F, & et al. (1995) A fibrillar collagen gene, Col11a1, is essential for skeletal morphogenesis. *Cell* 80:423-430.

232. Annunen S, Korkko J, Czarny M, Warman ML, Brunner HG, Kaariainen H, Mulliken JB, Tranebjaerg L, Brooks DG, Cox GF, Cruysberg JR, Curtis MA, Davenport SL, Friedrich CA, Kaitila I, Krawczynski MR, Latos-Bielenska A, Mukai S, Olsen BR, Shinno N, Somer M, Vikkula M, Zlotogora J, Prockop DJ, & Ala-Kokko L (1999) Splicing mutations of 54-bp exons in the COL11A1 gene cause Marshall syndrome, but other mutations cause overlapping Marshall/Stickler phenotypes. *Am J Hum Genet* 65:974-983.

233. Kaplan FS, Shen Q, Lounev V, Seemann P, Groppe J, Katagiri T, Pignolo RJ, & Shore EM (2008) Skeletal metamorphosis in fibrodysplasia ossificans progressiva (FOP). *J Bone Miner Metab* 26:521-530.

234. Feldman GJ, Billings PC, Patel RV, Caron RJ, Guenther C, Kingsley DM, Kaplan FS, & Shore EM (2007) Over-expression of BMP4 and BMP5 in a child with axial skeletal malformations and heterotopic ossification: a new syndrome. *Am J Med Genet A* 143:699-706.

235. Fukuda T, Kohda M, Kanomata K, Nojima J, Nakamura A, Kamizono J, Noguchi Y, Iwakiri K, Kondo T, Kurose J, Endo K, Awakura T, Fukushi J, Nakashima Y, Chiyonobu T, Kawara A, Nishida Y, Wada I, Akita M, Komori T, Nakayama K, Nanba A, Maruki Y, Yoda T, Tomoda H, Yu PB, Shore EM, Kaplan FS, Miyazono K, Matsuoka M, Ikebuchi K, Ohtake A, Oda H, Jimi E, Owan I, Okazaki Y, & Katagiri T (2009) Constitutively activated ALK2 and increased SMAD1/5 cooperatively induce bone morphogenetic protein signaling in fibrodysplasia ossificans progressiva. *J Biol Chem* 284:7149-7156.

236. Deirmengian GK, Hebela NM, O'Connell M, Glaser DL, Shore EM, & Kaplan FS (2008) Proximal tibial osteochondromas in patients with fibrodysplasia ossificans progressiva. *J Bone Joint Surg Am* 90:366-374.

237. Lounev VY, Ramachandran R, Wosczyna MN, Yamamoto M, Maidment AD, Shore EM, Glaser DL, Goldhamer DJ, & Kaplan FS (2009) Identification of progenitor cells that contribute to heterotopic skeletogenesis. *J Bone Joint Surg Am* 91:652-663.

238. Almeida MQ, Muchow M, Boikos S, Bauer AJ, Griffin KJ, Tsang KM, Cheadle C, Watkins T, Wen F, Starost MF, Bossis I, Nesterova M, & Stratakis CA (2010) Mouse Prkar1a haploinsufficiency leads to an increase in tumors in the Trp53+/- or Rb1+/- backgrounds and chemically induced skin papillomas by dysregulation of the cell cycle and Wnt signaling. *Hum Mol Genet*.

239. Iliopoulos D, Bimpaki EI, Nesterova M, & Stratakis CA (2009) MicroRNA signature of primary pigmented nodular adrenocortical disease: clinical correlations and regulation of Wnt signaling. *Cancer Res* 69:3278-3282.

240. Nadella KS, Jones GN, Trimboli A, Stratakis CA, Leone G, & Kirschner LS (2008) Targeted deletion of Prkar1a reveals a role for protein kinase A in mesenchymal-to-epithelial transition. *Cancer Res* 68:2671-2677.

241. Martin BL & Kimelman D (2008) Regulation of canonical Wnt signaling by Brachyury is essential for posterior mesoderm formation. *Dev Cell* 15:121-133.

242. Tirabosco R, Mangham DC, Rosenberg AE, Vujovic S, Bousdras K, Pizzolitto S, De Maglio G, den Bakker MA, Di Francesco L, Kalil RK, Athanasou NA, O'Donnell P, McCarthy EF, & Flanagan AM (2008) Brachyury expression in extra-axial skeletal and soft tissue chordomas: a marker that distinguishes chordoma from mixed tumor/myoepithelioma/parachordoma in soft tissue. *Am J Surg Pathol* 32:572-580.

243. Bousdras K, O'Donnell P, Vujovic S, Henderson S, Boshoff C, & Flanagan AM (2007) Chondroblastomas but not chondromyxoid fibromas express cytokeratins: an unusual presentation of a chondroblastoma in the metaphyseal cortex of the tibia. *Histopathology* 51:414-416.

244. Oakley GJ, Fuhrer K, & Seethala RR (2008) Brachyury, SOX-9, and podoplanin, new markers in the skull base chordoma vs chondrosarcoma

differential: a tissue microarray-based comparative analysis. *Mod Pathol* 21:1461-1469.

245. Yang XR, Ng D, Alcorta DA, Liebsch NJ, Sheridan E, Li S, Goldstein AM, Parry DM, & Kelley MJ (2009) T (brachyury) gene duplication confers major susceptibility to familial chordoma. *Nat Genet* 41:1176-1178.

246. Siddappa R, Martens A, Doorn J, Leusink A, Olivo C, Licht R, van Rijn L, Gaspar C, Fodde R, Janssen F, van Blitterswijk C, & de Boer J (2008) cAMP/PKA pathway activation in human mesenchymal stem cells in vitro results in robust bone formation in vivo. *Proc Natl Acad Sci U S A* 105:7281-7286.

247. Jukes JM, Both SK, Leusink A, Sterk LM, van Blitterswijk CA, & de Boer J (2008) Endochondral bone tissue engineering using embryonic stem cells. *Proc Natl Acad Sci U S A* 105:6840-6845.

248. Dahir GA, Cui Q, Anderson P, Simon C, Joyner C, Triffitt JT, & Balian G (2000) Pluripotential mesenchymal cells repopulate bone marrow and retain osteogenic properties. *Clin Orthop Relat Res*:S134-145.

249. Siddappa R, Doorn J, Liu J, Langerwerf E, Arends R, van Blitterswijk C, & de Boer J (2009) Timing, rather than the concentration of cyclic AMP, correlates to osteogenic differentiation of human mesenchymal stem cells. *J Tissue Eng Regen Med.*

250. Siddappa R, Fernandes H, Liu J, van Blitterswijk C, & de Boer J (2007) The response of human mesenchymal stem cells to osteogenic signals

and its impact on bone tissue engineering. *Curr Stem Cell Res Ther* 2:209-220.

251. Rosland GV, Svendsen A, Torsvik A, Sobala E, McCormack E, Immervoll H, Mysliwietz J, Tonn JC, Goldbrunner R, Lonning PE, Bjerkvig R, & Schichor C (2009) Long-term cultures of bone marrow-derived human mesenchymal stem cells frequently undergo spontaneous malignant transformation. *Cancer Res* 69:5331-5339.